

✓ m (1)

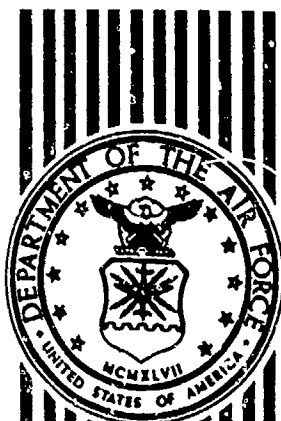
DTIC

SELECTE

DEC 1989

AD-A242 998

ESL-TR-88-06



MOBILE ATMOSPHERIC POLLUTANT MAPPING SYSTEM (MAPMS)

W.B. GRANT

JET PROPULSION LABORATORY
CALIFORNIA INSTITUTE OF TECHNOLOGY
4800 OAK GROVE DRIVE
PASADENA CA 91109

DECEMBER 1989

FINAL REPORT

AUGUST 1984 — APRIL 1988

APPROVED FOR PUBLIC RELEASE: DISTRIBUTION UNLIMITED

91-16566



1 1126 054

AIR FORCE ENGINEERING & SERVICES CENTER
ENGINEERING & SERVICES LABORATORY
TYNDALL AIR FORCE BASE, FLORIDA 32403

NOTICE

PLEASE DO NOT REQUEST COPIES OF THIS REPORT FROM
HQ AFESC/RD (ENGINEERING AND SERVICES LABORATORY).
ADDITIONAL COPIES MAY BE PURCHASED FROM:

NATIONAL TECHNICAL INFORMATION SERVICE
5285 PORT ROYAL ROAD
SPRINGFIELD, VIRGINIA 22161

FEDERAL GOVERNMENT AGENCIES AND THEIR CONTRACTORS
REGISTERED WITH DEFENSE TECHNICAL INFORMATION CENTER
SHOULD DIRECT REQUESTS FOR COPIES OF THIS REPORT TO:

DEFENSE TECHNICAL INFORMATION CENTER
CAMERON STATION
ALEXANDRIA, VIRGINIA 22314

REPORT DOCUMENTATION PAGE				Form Approved OMB No. 0704-0188	
1a. REPORT SECURITY CLASSIFICATION Unclassified		1b. RESTRICTIVE MARKINGS			
2a. SECURITY CLASSIFICATION AUTHORITY		3. DISTRIBUTION/AVAILABILITY OF REPORT Approved for Public Release Distribution Unlimited			
2b. DECLASSIFICATION/DOWNGRADING SCHEDULE		4. PERFORMING ORGANIZATION REPORT NUMBER(S) ESL-TR-88-06			
6a. NAME OF PERFORMING ORGANIZATION Jet Propulsion Laboratory California Institute of Technology		6b. OFFICE SYMBOL (if applicable)	7a. NAME OF MONITORING ORGANIZATION Air Force Engineering and Services Center		
6c. ADDRESS (City, State, and ZIP Code) 4800 Oak Grove Drive Pasadena CA 91109		7b. ADDRESS (City, State, and ZIP Code) HQ AFESC/RDVS Tyndall AFB FL 32403			
8a. NAME OF FUNDING, SPONSORING ORGANIZATION HQ AFESC	8b. OFFICE SYMBOL (if applicable) RDV	9. PROCUREMENT INSTRUMENT IDENTIFICATION NUMBER			
8c. ADDRESS (City, State, and ZIP Code) HQ AFESC/RDVS Tyndall AFB FL 32403-6001		10. SOURCE OF FUNDING NUMBERS			
	PROGRAM ELEMENT NO. 63723F	PROJECT NO. 2103	TASK NO. 70	WORK UNIT ACCESSION NO. 24	
11. TITLE (Include Security Classification) Mobile Atmospheric Pollutant Mapping System (Unclassified)					
12. PERSONAL AUTHOR(S) Grant, William B.					
13a. TYPE OF REPORT Final		13b. TIME COVERED FROM 84-08-01 TO 88-04-30	14. DATE OF REPORT (Year, Month, Day) December 1989		15. PAGE COUNT 87
16. SUPPLEMENTARY NOTATION Availability of this report is specified on reverse of front cover					
17. COSATI CODES			18. SUBJECT TERMS (Continue on reverse if necessary and identify by block number)		
FIELD	GROUP	SUB-GROUP	Lidar, Remote Sensing, Heterodyne Detection, Pollution Detection, Differential Absorption Lidar (DIAL), Water Vapor, Organic Solvents, CO ₂ Laser		
17	05				
20	06				
19. ABSTRACT (Continue on reverse if necessary and identify by block number) The Mobile Atmospheric Pollutant Mapping (MAPM) System is a dual CO ₂ laser, differential absorption lidar (DIAL) system designed and developed for the remote, range-resolved measurement of concentrations of trace molecular species and aerosols optical depths. In the DIAL technique, atmospheric aerosols provide the backscatter for a pulsed laser beam; one laser is tuned to an absorbing wavelength of the molecular species of interest; the other is tuned to a nearby non-absorbing wavelength. The derivative of the logarithm of the ratio of the two signals is used to determine the gas concentration. Heterodyne detection is employed with MAPM to enable long-range measurements. MAPM has been demonstrated with ambient water vapor, ozone, and aerosols, with a free release of ethylene, and with various organic solvent vapors in a sample chamber.					
20. DISTRIBUTION/AVAILABILITY OF ABSTRACT <input type="checkbox"/> UNCLASSIFIED/UNLIMITED <input type="checkbox"/> SAME AS RPT. <input type="checkbox"/> DTIC USERS			21. ABSTRACT SECURITY CLASSIFICATION UNCLASSIFIED		
22a. NAME OF RESPONSIBLE INDIVIDUAL Kenneth T. DenBleyker		22b. TELEPHONE (Include Area Code) 904-283-4298		22c. OFFICE SYMBOL HQ AFESC/RDVS	


PREFACE


This report was prepared by Dr William Grant, NASA-Jet Propulsion Laboratory, Pasadena CA, under Contract NAS7-100/918, Task Order RE182, Amendment A378, for the Air Force Engineering and Services Center, Engineering and Services Laboratory, Tyndall Air Force Base, Florida.

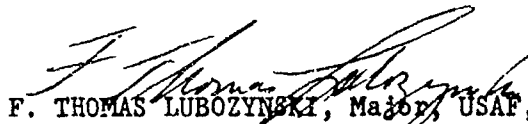
This technical report summarizes work done between 1 August 1984 and 30 April 1988. Major Kenneth T. DenBleyker was the HQ AFESC/RDVS project officer.

This report has been reviewed by the Public Affairs (PA) Office, and it may be released to the National Information Service (NTIS). At NTIS, this document will be available to the general public, including foreign nationals.

This technical report has been reviewed and is approved for publication.


KENNETH T. DENBLEYKER, Major, USAF
Chief, Environmental Sciences Branch


RICHARD M. HANES, Col, USAF
Director, Engineering
and Services Laboratory


F. THOMAS LUBOZYNSKI, Major, USAF, BSC
Chief, Environics Division

Accession For	
NTIS GRA&I	<input checked="" type="checkbox"/>
DTIC TAB	<input type="checkbox"/>
Unannounced	<input type="checkbox"/>
Justification	
By	
Distribution/	
Availability Codes	
Dist	Avail and/or Special
A-1	



TABLE OF CONTENTS

Section	Title	Page
I	INTRODUCTION	1
	A. OBJECTIVE	1
	B. BACKGROUND	1
	C. SCOPE	2
II	DESCRIPTION OF THE MAPM HARDWARE	3
	A. FUNCTIONAL REQUIREMENTS	3
	B. SEMITRAILER	3
	C. OPTICAL TABLE	5
	D. PULSED LASERS	5
	1. Operation	5
	2. Component Problems	8
	E. cw CO ₂ LASERS	12
	1. Operation	12
	2. Problems Encountered	12
	F. HELIUM-NEON LASERS	15
	G. OPTICS	15
	1. Transmitter Optics	15
	2. Local Oscillator Optics	18
	3. Receiver Optics	18
	4. Alignment Procedure	18
	H. DOME	19
	I. PHOTOMIXER	20
	J. SIGNAL CHAIN ELECTRONICS	20
	1. Photomixer Bias Box	20
	2. Trontech Pre-amplifier Model L30 APS	20
	3. In-Line Attenuators	20
	4. RHG Linear Amplifier, Model EST 3010LD	20
	5. 93-50 Ohm Impedance Matching Network	22
	6. Cir-Q-Tel Flat Phase Filter	22
	7. Flip-Flop Array	22
	8. RF Switches and RF Power Splitter	22
	9. RFI Shielding	22
	10. Transient Digitizer	23
	K. DIGITAL DELAY GENERATOR (DDG)	23
	L. MONITORING EQUIPMENT	23
	1. Storage Oscilloscope	25
	2. RF Spectrum Analyzer	25

TABLE OF CONTENTS
(Continued)

Section	Title	Page
	3. Room-Temperature HgCdTe Detector	24
	4. Boxcar Averager	24
	5. Spectrum Analyzer	26
	6. Laser Power Meters	26
	M. COMPUTER	26
	N. REMOTE SAMPLE CHAMBER	26
	O. ABSORPTION COEFFICIENT CELL	26
	P. LIST OF COMPONENTS	28
III	DATA PROCESSING CODES	32
IV	OPERATION	35
	A. TURN-OP PROCEDURE	35
	B. MAPM DATA LOG	38
V	MEASUREMENT RESULTS	42
	A. DIAL SIGNAL AVERAGING	42
	B. WATER VAPOR	42
	1. Water Vapor Absorption Coefficients	42
	2. DIAL Measurements	45
	C. OZONE MEASUREMENTS	48
	D. ETHYLENE FREE RELEASE	48
	E. ABSORPTION COEFFICIENT MEASUREMENTS	50
	F. REMOTE SAMPLE CHAMBER MEASUREMENTS	55
	G. RAPID PROCESSING OF DATA	57
	H. MAPM DIAL PERFORMANCE AND SCALING	59
VI	CONCLUSIONS AND RECOMMENDATIONS	62
	A. FINDINGS WITH MAPM	62
	1. Water Vapor	62
	2. Sample Chamber Measurements	62
	3. Ethylene Free Release	62
	B. PREPARATION OF MAPM FOR TRANSPORT	63
	1. Optics	63
	2. Equipment	63
	3. Electrical Generator	63
	4. Gas Cylinders	63
	5. Ancillary Equipment	63
	6. Photomixer	64

TABLE OF CONTENTS
(Concluded)

Section	Title	Page
	7. Lasers	64
	8. Data System	64
	9. Thermostats	64
	10. Spectral Data	64
	C. FUTURE USES OF MAPM	64
	1. SF ₆ Tracer Studies	65
	2. Water Vapor Measurements	65
	3. Aerosol Studies	65
	4. Ozone Studies	65
	5. Emissions of Toxic and Hazardous Gases	66
	6. Gas-to-Aerosol Conversion Studies	66
	D. CONSIDERATIONS FOR MAPM II	67
VII	REFERENCES	68
APPENDIX		
A	CO ₂ DIAL MEASUREMENTS OF WATER VAPOR	73
B	DIFFERENTIAL ABSORPTION LIDAR SIGNAL AVERAGING.	83

LIST OF FIGURES

Figure	Title	Page
1	A Plan View of the Semitrailer Housing MAPM, Showing the Location of the Major Components. . .	4
2	Various Views of the Optical Table with the Optics and Lasers	6
3	Plan View of the Optical Layout	16
4	Side View of the Optical Layout	17
5	Block Diagram of the Signal Chain Electronics . .	21
6	Photograph of the Electronic Rack Showing Both Diagnostic and Control Electronics.	25
7	Block Diagram of the Computer System.	27
8	Diagram of MAPM	31
9	Water Vapor DIAL Measurement Signals.	46
10	Free Release of Ethylene Looking Downwind	49
11	Values for the Squares of the Lidar Signals (Proportional to Backscattered Power) for Various Numbers of Signals Added before Squaring	58
12	Typical Values for the Standard Deviation of the Derivative of the Lidar Signal as a Function of Range for Several Thousand Pulse Pairs at a Time. .	60
13	Estimated Performance Levels for Molecular Species with Differential Absorption Coefficients for 5000 Pulse Pairs and 500-m Range Resolution .	61

LIST OF TABLES

Table	Title	Page
1	LASER SCIENCE INC. MODEL PRF-150S CO ₂ LASER SPECIFICATIONS	7
2	MAPM: "YELLOW" TRANSMITTER LASER TUNING CURVE	9
3	MAPM: "RED" TRANSMITTER LASER TUNING CURVE.	10
4	MAPM: "YELLOW" LOCAL OSCILLATOR TUNING CURVE.	13
5	MAPM: "RED" LOCAL OSCILLATOR TUNING CURVE	14
6	MAJOR MAPM COMPONENTS.	29
7	MAPM DATA LOG.	39
8	COMPARISON OF WATER VAPOR ABSORPTION COEFFICIENTS DETERMINED USING CO ₂ LASERS WITH THE VALUES ON THE AFGL SPECTRAL DATA TAPES FOR 10-TORR PARTIAL PRESSURE, 300 K, $\alpha(\text{C}_2\text{H}_6) = 35.0 \text{ atm}^{-1} \text{ cm}^{-1}$	44
9	CO ₂ LASER LINE PAIRS USEFUL FOR WATER VAPOR MEASUREMENTS	45
10	SUMMARY OF WATER VAPOR MEASUREMENTS.	47
11	OZONE MEASUREMENTS USING MAPM.	48
12	ABSORPTION COEFFICIENTS OF SEVERAL ORGANIC SOLVENT VAPORS AT CO ₂ LASER LINE FREQUENCIES	51
13	LINE PAIRS APPROPRIATE FOR SELECTED MOLECULAR SPECIES.	54
14	REMOTE SAMPLE CHAMBER DETERMINED ABSORPTION COEFFICIENTS	56

SECTION I

INTRODUCTION

A. OBJECTIVE

The original objective of this project was to develop a lidar system and use it to measure hydrogen chloride (HCl) concentrations and aerosol distributions following space shuttle launches at Vandenberg AFB. In addition to the CO₂ lidar, which was to be used for aerosols, a Co:MgF₂ laser source was to be supplied for the HCl measurements. Unfortunately, researchers at MIT Lincoln Laboratory could not develop a Co:MgF₂ laser with sufficient pulse energy to enable range resolved measurements to be made beyond ranges of 3 km (Reference 1), so that aspect of the project was postponed.

The revised objective of this project was to design, develop, test, and demonstrate a field-usable carbon dioxide (CO₂) lidar for the remote measurement of atmospheric gases and aerosols. The intended application was for the measurement of organic solvent vapors emitted from waste sites and industrial operations at U.S. Air Force bases.

B. BACKGROUND

Lidars have been used since 1963 for the remote measurement of atmospheric aerosols (Reference 2) and since 1966 for gases (Reference 3). The field has been well-reviewed in a number of journal articles and books (References 4-14).

CO₂ lidars are particularly useful for measuring atmospheric trace gases because of several factors:

1. many molecular species have absorption features in the 9-11 micron spectral region, where CO₂ lasers emit radiation,
2. the atmosphere is relatively transparent, in this spectral region;
3. CO₂ lasers are discretely tunable in this spectral region, and can generate sufficient pulse energy for measurements to ranges of several kilometers (Reference 9).

Indeed, CO₂ lidars have been applied to measuring a number of molecular species: water vapor (References 15-20), ethylene (References 21, 22), ozone (References 23, 24), ammonia (Reference 25), hydrazines (Reference 26), freons (Reference 27), methanol (Reference 28), and sulfur hexafluoride (SF₆) (Reference 29).

While most of this work has been with direct detection, some work has been reported using heterodyne detection (References 19, 20, 24, and 27). In direct detection, a receiver acts as a "light bucket," detecting photons in a wide bandwidth, typically tens to hundreds of wavenumbers (cm⁻¹ where 1 cm⁻¹ = 30 GHz). In heterodyne detection, the detection region is narrowed to a few MHz by use of a local oscillator laser and RF-detection electronics so that the thermal background radiation is kept to a minimum (References 30-32). Thus, in

direct detection, measurements are typically limited to ranges of 1-3 km, while in heterodyne detection, measurements can be made to ranges of 5-10 km.

In either approach, the Differential Absorption Lidar (DIAL) technique is employed. In this technique, two laser frequencies are transmitted: one, where the molecular species of interest has weak absorption of the laser radiation, is used as a reference line to calibrate the system and the atmosphere, and another, where the species has strong absorption, is used to measure the concentration distribution of that species. The pulsed laser radiation is reflected from atmospheric aerosols (and molecules where the irradiating radiation is in the UV and visible spectral regions) and the time-resolved signal is used to give a range-resolved measurement. The derivative of the logarithm with respect to distance of the ratio of the two range-resolved signals is used to give the concentration profile:

where

$$C = - \frac{1}{2\Delta\alpha} \frac{\partial}{\partial l} (\ln (I_{on} / I_{off})) \quad (1)$$

C is the concentration

$\Delta\alpha$ is the differential absorption coefficient

$\frac{\partial}{\partial l}$ is the partial derivative with respect to range

I_{on} is the normalized intensity of the backscattered power for the absorbed wavelength,

and I_{off} is the normalized intensity of the backscattered power for the reference wavelength.

For plumes, regions from both the front and back of the plume can be used to measure the differential spectral attenuation caused by the plume:

$$C = - \frac{1}{2\Delta\alpha} \left[\left[\ln \frac{I_{on}}{I_{off}} \right]_1 - \left[\ln \frac{I_{on}}{I_{off}} \right]_2 \right] \quad (2)$$

where the subscripts 1 and 2 denote regions before and after the plume.

C. SCOPE

In the sections that follow, the hardware for the Mobile Atmospheric Pollutant Mapping (MAPM) System is described, along with measurement results using it, the absorption coefficients and measurement sensitivities for a number of molecular species, and the factors that limit measurement accuracy and range.

SECTION II

DESCRIPTION OF THE MAPM HARDWARE

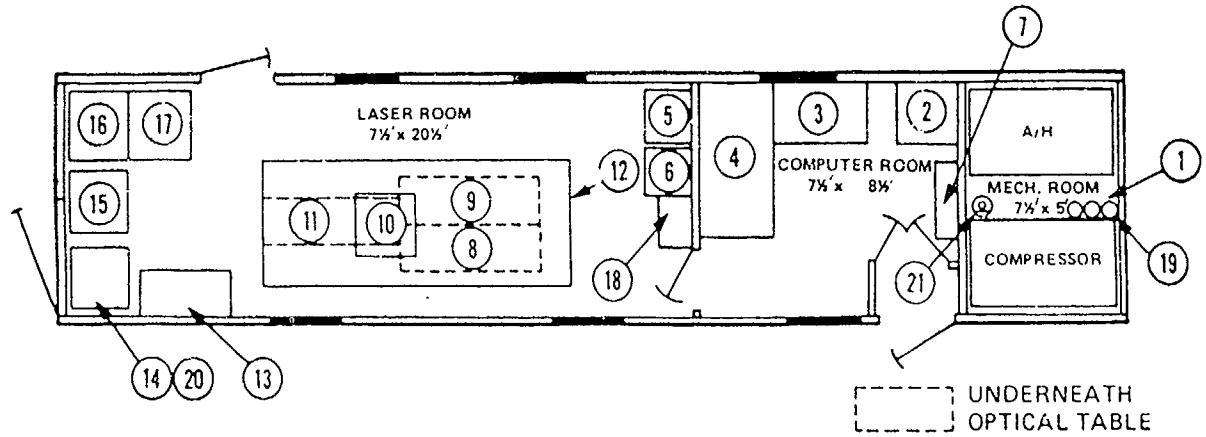
A. FUNCTIONAL REQUIREMENTS

The system was required to meet a number of functional requirements. These included transportability, the ability to operate in a variety of weather and atmospheric conditions, the capability of operating as a stand-alone system, the capability for making range-resolved measurements of atmospheric gases to ranges of 5 km, and of aerosols to 10 km, and the ability to scan 360 degrees in azimuth, and from -10 to +30 degrees in elevation. The scan requirements were dictated by the necessity for making measurements over a wide range of directions from a fixed location, since there would be a significant time delay in resuming data collection if MAPM were to be moved. The elevation angle limits are determined by the gimbals mount and the scan mirror dimensions. (If an additional mirror were placed on the roof of the semitrailer, full hemispherical coverage could be achieved.) Most of these requirements have been fulfilled; those that haven't, such as transportability and stand-alone operation, can be fulfilled with minor system upgrades when a field use for the system is identified. All of the work reported herein was performed with the system parked just east of Building 245 at the Jet Propulsion Laboratory, which houses other lidar activities, including the CO₂ lidar used to measure aerosol backscatter.

B. SEMITRAILER

The semitrailer accommodating the lidar system was designed by engineers at JPL and constructed by Diamond B. Corp. in Pico Rivera, CA. It was divided into three rooms -- the largest (20 feet by 8 feet by 7 feet), to house the laser portion; the middle one (10 feet by 8 feet by 7 feet) to house the transient digitizer and computer; and the smallest (5 feet by 8 feet by 7 feet) to contain the heating, ventilating, and air-conditioning (HVAC) plant, as well as the gas cylinders used to supply the pulsed CO₂ lasers. The locations of the various system components were determined in advance, so that structural supports, forced air, electrical outlets, lights, doors, windows, and the ceiling openings could be properly placed. A plan of the semitrailer, locating the major components, is shown in Figure 1. Note that the semitrailer has the maximum legal dimensions for transport on federal highways - a width of 8 feet, and a height of 13 feet 6 inches. The length of 35 feet was chosen to adequately house the system while still being relatively easily maneuverable.

The semitrailer has many special features. The walls, ceiling, and floor have polyurethane foam insulation to allow operation from near 0° C to above 100° C with the HVAC system in operation. The ceiling is covered with acoustical tile. There are six "belly boxes" below the floor where equipment can be stored. A Halon 1201 fire extinguisher system can be activated to extinguish any fire that might occur inside the laser and computer rooms. In addition to the rapid deployment feature, the halon system end products do not damage the optics or electronics. The rear axle is mounted on an air-ride suspension to keep vibrations to a minimum during transport. When the semitrailer is stationary, four jacks can be lowered to keep it level and relatively sturdy (the lidar pointing can change slightly if people move about inside the semitrailer).



COMPONENTS FOR TYNDALL - MAPM TRAILER

- | | |
|---------------------------------|--|
| 1. AIR CONDITIONER ROOM | 11. SOLID STATE LASER * |
| 2. PERSONNEL SUPPORT EQUIPMENT | 12. OPTICAL TABLE |
| 3. MINICOMPUTER/TABLE | 13. OPTICS TOOL CABINET |
| 4. COMPUTER/DISK | 14. CO ₂ LASER COOLER |
| 5. INSTRUMENT RACK, ELECTRONICS | 15. SOLID STATE LASER POWER SUPPLY |
| 6. INSTRUMENT RACK, ELECTRONICS | 16. CO ₂ LASER POWER SUPPLY |
| 7. ELECTRICAL PANEL | 17. CO ₂ LASER POWER SUPPLY |
| 8. CO ₂ LASER | 18. STORAGE CABINET |
| 9. CO ₂ LASER | 19. GAS CYLINDERS |
| 10. SCANNING MIRRORS | 20. SOLID STATE LASER COOLER * |
| | 21. HALON FIRE EXTINGUISHER |

* SPACE PROVIDED FOR PHASE II ADDITION

Figure 1. A Plan View of the Semitrailer Housing MAPM, Showing the Location of the Major Components

The HVAC system was supplied by Geary Pacific, Inc. The cooling uses Freon 27, monochlorodifluoromethane (CClF₂H), boiling point 90° F. When operating the air-conditioning the heaters must be turned on approximately 4 hours in advance to vaporize the freon so that the pumps are not damaged. The heating and cooling thermostats are both in the HVAC room, and are set about 5° C apart, with the heating point below the cooling point. The forced air enters the semitrailer through a manifold below the floor with the return manifold above the ceiling. While there are intake louvers to the outside in the HVAC room, they normally stay closed unless air escapes from the main two rooms of the semitrailer.

The roof has a skin of aluminum with an antiskid raised pattern. A guard chain and post structure, erected for personnel safety, can be removed for semitrailer transport.

C. OPTICAL TABLE

The optical table was designed to accommodate the CO₂ lidar system and possible additional lasers, using common optics and electronics. The top shelf is 4 feet by 10 feet by 1 foot; the bottom shelf is 3 feet 6 inches by 9 feet 6 inches by 4 inches. The upper shelf supports the continuous wave (cw) CO₂ lasers, most of the optics, including the scan mirror that extends beyond the roof line, and some of the electronics. The lower shelf supports the pulsed CO₂ laser heads and the cw CO₂ laser power supplies. The table is rigidly mounted to the frame of the semitrailer by three 10-inch diameter legs. The upper table has 1/4-20 tapped holes on a 1-inch grid. The top is made of magnetic steel. The bottom table is also made of magnetic steel and supports optics mounts with magnetic bases. The inner matrices of the tables are honeycomb aluminum. Figure 2 shows various views of the optical table with the optics and lasers.

D. PULSED LASERS

For use in a heterodyne lidar system, the desirable features of a CO₂ laser are high-pulse repetition frequency (prf), single longitudinal mode operation, low beam divergence, moderate pulse energy, short pulse width, and multiline tunability. At the time MAPM was designed, the laser that most nearly met these criteria was the Laser Science Inc. (LSI) Model PRF-150S. Its features are listed in Table 1.

1. Operation

The operation of the lasers is relatively routine. The electricity, gas, and water are turned on following procedures laid out by the manufacturer and enforced by a set of interlocks, including one for the high voltage with a 5-minute time delay. (A 10-minute delay is suggested if the lasers have not been operated for a few days.) To obtain lasing on a given line, the micrometer screw is used to tune the grating. The wavelength can be read nearly directly from the micrometer barrel. Fine tuning is achieved by using a power meter placed in the beam path while the grating is adjusted. The vertical tilt adjust on the output coupler can be used to peak the power. Single-longitudinal mode (SLM) operation is achieved by closing the output aperture while monitoring the pulse shape using a room-temperature mercury-cadmium-telluride (HgCdTe) detector and looking for a smooth envelope with no high-frequency components. The cavity

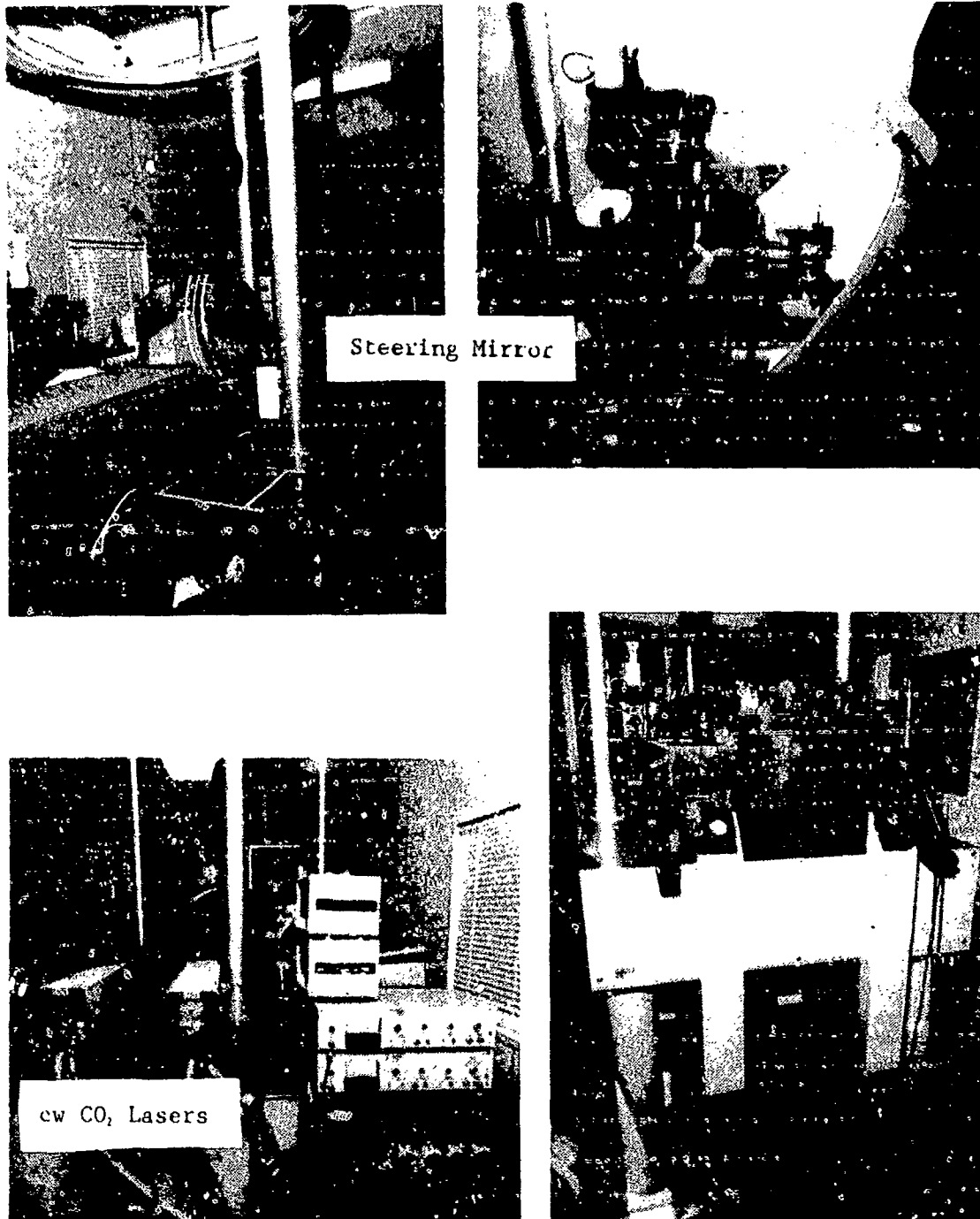


Figure 2. Various Views of the Optical Table with the Optics and Lasers.

TABLE 1. LASER SCIENCE INC., MODEL PRF-150S CO₂ LASER SPECIFICATIONS

Line tunability: Approximately 60 lines from 9.2 to 10.7 microns.

Energy per pulse, single longitudinal mode: 10-60 mJ

Pulse repetition frequency:

to 150 Hz at 80% of maximum voltage
to 100 Hz at 90% of maximum voltage
to 50 Hz at 100% of maximum voltage

Divergence: 2+ mrad

Pulse width: 270 ns in the gain switched spike; tail to 2 microseconds with N₂;
tail to 500 ns without N₂.

Cavity: Transversely excited atmospheric pressure (TEA) gain cell for power;
low pressure gain cell for mode selection; piezoelectric (PZT) mounts for grating
drive to control frequency.

Gas consumption rates for size K gas cylinders:

nitrogen: 80 hours
helium: 20 hours
carbon dioxide: 160 hours
mixed gas for low-pressure gain cell: years

length is adjusted using the piezoelectric device connected to the output coupler, and, if required, changing the pressure slightly in the main discharge tube. Care must be exercised to ensure that the smooth envelope is due to SLM operation controlled by the cavity length and not just due to other constraints for which the frequency is not adjustable, which can occur if the aperture is closed too far. Note that the laser is a hybrid Transverse Excited Atmospheric (TEA) pressure laser, meaning that there is a low-pressure gain cell with just enough gain to force the TEA section to lase on only one mode near line center. An alternative approach would be to mode select using seeding by injection from an external cw CO₂ laser (Reference 33). While injection seeding allows pulsed TEA lasers to operate at higher pulse energy levels, operation is much more complex than for the hybrid TEA. The partial tuning curves for the two pulsed lasers are given in Tables 2 and 3. The tuning curves were measured primarily for those lines which were thought to be useful for the molecular species of greatest interest, and for which the lasers operated in a single longitudinal mode manner. When the pulse energy was below some threshold value (approximately 13 mJ per pulse), SLM operation could not be achieved because there was not sufficient pulse energy to permit cavity control of the lasing properties using the intracavity aperture.

Near the end of the program, when the sample chamber measurements were being performed, it was realized that the laser pulse tail interfered with those measurements. Since the backscatter from the chamber windows is much stronger than from the atmosphere, the tail, which lasts to 2 microseconds in normal operation, prevented atmospheric data from being obtained from the zone within about 300 m beyond the chamber. The obvious step was to reduce the nitrogen flow rate to near zero. The UV preionizer sliding arc arrays in the "yellow" TEA Laser required replacement before this scheme could be successfully implemented, yielding 500-ns pulse lengths. The CO₂ flow rate also had to be reduced to eliminate arcing. The pulse energy was reduced to about 15-20 mJ with the short pulse.

2. Component Problems

After several months of operation, during which time several component problems were solved, in consultation with the manufacturer, the lasers were rendered operable in a reliable manner. On a typical day, more than 300,000 shots were fired during 4-5 hours. Some of the problems encountered and solved are discussed here.

a. Optics

The output couplers develop burn spots occasionally. The likely cause is that a speck of dust settles on the coupler and is heated by the intense radiation fields in the laser cavity. Replacement couplers were obtained from CVI Laser Corp. in Albuquerque, N.M.

The zinc selenide (ZnSe) Brewster windows on the low pressure gain cells also showed burn marks. All four of these windows were replaced after about 10 million shots.

TABLE 2. MAPM: "YELLOW" TRANSMITTER LASER TUNING CURVE

Line Assignment	mJ/SLM Shot	Drive Setting	Line Assignment	mJ/SLM Shot	Drive Setting
10P:	38	10.833	10R:	38	
	36	10.804		36	
	34	29		34	
	32	25		32	
	30			30	
	28			28	
	26			26	
	24	27		24	
	22			22	
	20			20	
	18	25		18	
	16			16	
	14	9		14	
	12	17		12	
	10	7		10	18 10.355
9P:	38	9.739	9R:	38	
	36	9.723		36	
	34	17		34	
	32	32		32	
	30	33		30	9.247
	28	29		28	9.256
	26	54		26	9.265
	24			24	9.272
	22			22	9.284
	20			20	9.293
	18			18	9.305
	16			16	9.314
	14	60		14	9.332
	12	31		12	12 9.332
	10			10	9.355

TABLE 3. MAPM: "RED" TRANSMITTER LASER TUNING CURVE

Line Assignment	mJ/SLM Shot	Drive Setting	Line Assignment	mJ/SLM Shot	Drive Setting
10P:	38	10.820	10R:	38	
	36	10.803		36	
	34	42		34	
	32	29		32	
	30			30	
	28			28	
	26			26	
	24	27		24	
	22	25		22	
	20			20	
	18	35		18	
	16			16	
	14	35		14	
	12	35		12	
	10	42		10	44 10.352
9P:	38		9R:	38	
	36			36	
	34	40		34	
	32	35		32	9.242
	30	42		30	9.251
	28	65		28	9.267
	26	54		26	9.271
	24			24	9.281
	22			22	
	20			20	9.309
	18			18	9.319
	16			16	9.329
	14	24		14	9.339
	12	24		12	
	10			10	

b. Micrometer Screws

One micrometer screw adjustment ground off some of the surface of a mating disk, causing line tuning to be jerky. The mating surfaces were cleaned and restored and have had reliable operation.

c. Electronics

One EG&G thyratron failed, and was replaced.

The Bakelite cover shielding a high voltage diode network arced to ground, due to carbon in the Bakelite. The cover was removed, along with some redundant electronics, eliminating the problem.

A loose fuse holder caused the laser coolant water flow solenoid to trip off several times. The holder was resoldered and now functions satisfactorily.

A spring in a relay socket lost resilience after the relay was changed and had to be replaced.

The divergence out of the laser is about 2 mrad. However, as the laser pulse energy increases, the divergence also increases. This can limit the amount of lidar signal for a tightly coupled heterodyne detection system. It appears that turning up the voltage allows more modes to lase, as is the case with other laser types.

e. Single-Mode Operation

Normally, one can achieve single-mode operation by adjusting the output aperture and PZT voltage. Sometimes the gas pressure in the cell (3 lbs/in²) must be adjusted to change the effective cavity length to where the PZT controller works in a convenient range. LSI now has a translation device with a greater operating range.

f. Arcing Between Electrodes

The Serial No. 11 laser started arcing between the nickel electrodes after about 10 million shots. At first, the voltage was reduced below 80 percent of maximum to permit operation without arcing. When this procedure limited operation on the weaker lines, the laser head was disassembled and the electrodes were sanded down using first 400, then 600 grit Emery cloth.

g. Cooler

A Neslab Model HX-75 cooler was used to provide cooling water to the lasers at a temperature of 15° C. The pressure relief valve on the cooler has been set to 30 psi so that when the water flow valve in the laser is closed, the Tygon tubing will not rupture.

h. Frequent Laser Shut-Off

One laser would turn off after about 10 minutes of operation. The problem was traced to the gain setting of the arc-detector electronics in the laser head. The gain was changed, and the problem disappeared.

i. Failure to Lase Without N₂

One laser did not lase when N₂ flow was interrupted in order to eliminate the 2-microsecond pulse tail. The UV-preionizer inside the laser head was replaced by a spare, and lasing in the absence of N₂ was achieved.

E cw CO₂ LASERS

The cw CO₂ lasers used as local oscillators are the Ultra Lasertech Model 3822 lasers. They are of the "open resonator" rather than waveguide configuration. The gas mixture at 30-40 torr is contained in a Pyrex tube with a water jacket and Brewster-angle ZnSe windows at each end. The output coupler is flat, while the grating is concave. While a confocal cavity design is required for stable operation, the use of a curved grating limits the number of lines per millimeter that can be ruled on the grating. This fact sometimes gives rise to lasing on two lines simultaneously, especially for the 9- and 10-micron R branches where the line spacing is about 1 cm⁻¹, which can be monitored on the RF spectrum analyzer. The tuning curves for the cw CO₂ lasers are given in Tables 4 and 5.

1. Operation

The laser tuning curves listed in Tables 4 and 5 are used to adjust the grating. Occasionally there is mechanical shift, perhaps of the grating mount, so that there is an additive shift in the wavelength vs micrometer setting. The power meters are used to monitor fine tuning of the lasers.

2. Problems Encountered

The primary problem encountered with the operation of the cw CO₂ lasers has been in the frequency-offset control. The optogalvanic technique is used. In this approach, the cavity length is modulated a small amount at a low frequency (100 Hz), which causes the laser power to vary; this, in turn, affects the current flowing through the discharge, which can be monitored electronically. This approach is not reliable, because (1) the electronics card supplied with one control unit generated some noise spikes on an AC voltage. The card was replaced, and the unit worked much better, and (2) a number of controls must be adjusted properly for optimal operation. It is generally impractical to implement this procedure each time the lasers are tuned to new lines. When the optogalvanic technique doesn't work well with a minimum of effort, the laser frequencies are offset manually. They maintain frequency stability reasonably well in free-running modes, but do require occasional adjustments.

The PZT stack in one laser failed, and was replaced under warranty. The repaired unit was subsequently used when a second stack failed.

After the lasers had been in operation for about a year, they were found to lase poorly in the 9-micron spectral region. At the suggestion of the manufacturer, the Brewster-angle windows were cleaned with ethanol, and the power was returned to about 1 W on the stronger 9R-branch lines.

TABLE 4. MAPM: "YELLOW" LOCAL OSCILLATOR TUNING CURVE

Line Assignment	Micrometer Drive Setting	Line Assignment	Micrometer Drive Setting
10P: 38	1.530	10R: 38	
36	1.562	36	
34	1.600	34	
32	1.635	32	
30		30	
28		28	
26		26	
24	1.750	24	
22	1.785	22	
20		20	
18	1.840	18	
16		16	
14	1.902	14	
12	1.930	12	
10	1.960	10	2.207
9P: 36	3.075	9R: 36	
34	3.100	34	
32	3.128	32	3.745
30	3.152	30	3.730
28	3.180	28	3.715
26	3.210	26	3.700
24	3.232	24	3.685
22	3.250	22	3.670
20	3.270	20	3.655
18		18	3.640
16		16	3.625
14	3.345	14	3.603
12	3.370	12	3.585

TABLE 5. MAPM: "RED" LOCAL OSCILLATOR TUNING CURVE

Line Assignment	Micrometer Drive Setting	Line Assignment	Micrometer Drive Setting
10P: 38	1.628	10R: 38	
36		36	
34	1.696	34	
32	1.733	32	
30		30	
28		28	
26		26	
24	1.873	24	
22	1.908	22	
20		20	
18	1.973	18	
16		16	
14	2.038	14	
12	2.071	12	
10	2.099	10	2.379
9P: 36	3.355	9R: 36	
34	3.306	34	
32	3.416	32	4.093
30	3.442	30	4.079
28	3.473	28	4.065
26	3.495	26	4.051
24	3.519	24	4.037
22	3.548	22	4.023
20	3.578	20	4.009
18		18	3.971
16		16	3.957
14	3.648	14	3.943
12	3.672	12	3.929

F. HELIUM-NEON (He-Ne) LASERS

Three He-Ne lasers (Melles Griot Model 05-LLP-83) were included with the optical system to aid in the alignment of the optics. One, which as a 20x beam expander attached to it, is used to help steer the pulsed CO₂ laser beams through the optical train into the atmosphere. Two others are coaligned with He-Ne lasers near the cw CO₂ lasers, and are used for aligning both the local oscillator optics and the receiver optics. Two have have failed and should be repaired.

G. OPTICS

The optics were designed to efficiently manage the laser beams, diagnostic equipment, and the atmospheric backscatter. The general optical layout was outlined at JPL; the details were carefully worked out by Frank Mitchell and Associates, in South Pasadena, who also designed those optics mounts that could not be easily procured. The optical layout is shown in Figures 3 and 4. The details are discussed for the optics and mounts arranged into three groups: transmitter optics; local oscillator optics; and receiver optics.

1. Transmitter Optics

Each transmitter beam is directed to a beam expander at the top level of the optical table by a pair of molybdenum metal mirrors (SPAWR Optical Research, Inc.). These mirrors can withstand relatively high powers, but nonetheless have suffered some burn damage arising from hot spots in the diffraction pattern when the beam is narrowed too much.

The 10x beam expanders, from Space Optics Research Laboratory, each have a 20-mm diameter, copper, convex secondary mirror and a 15-cm diameter, aluminum-coated-Pyrex, concave-ellipsoidal primary mirror. The secondary mirror has a radius of curvature of 7.029 inches, while the primary has a vertex radius of 70.0 inches, and a cone constant of -0.93314. The off-axis distance is 0.655 inch, while the optimal vertex separation is 31.50 inches. The secondary mirror is mounted to a stage which can be adjusted using a micrometer screw. The primary mirror has a vertical tilt adjustment.

A pair of octagonal beam-steering mirrors is placed after each beam expander. These mirrors allow the beams to be walked in two dimensions, and have their corners clipped so that the obscuration of the backscatter is minimized.

Following those beam-steering mirrors are a pair of 24-inch diameter, 1-5/8-inch thick, aluminized Pyrex mirrors with a magnesium fluoride (MgF₂) overcoat. These mirrors are used to transmit the beam up through the semitrailer roof, then out in any azimuthal direction, and from -10 degrees to +30 degrees in elevation. When necessary, a third 24-inch diameter mirror is placed on the roof, which enables full hemispherical coverage.

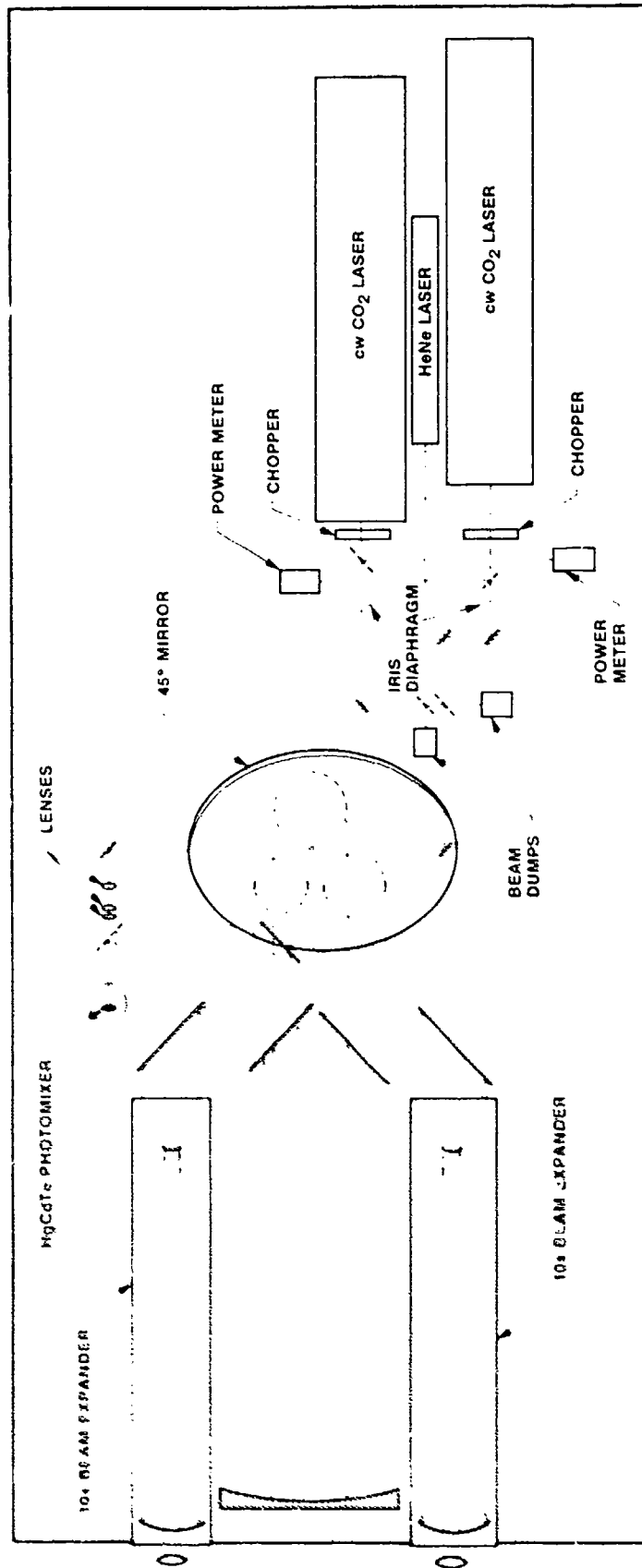


Figure 3. Plan View of the Optical Layout

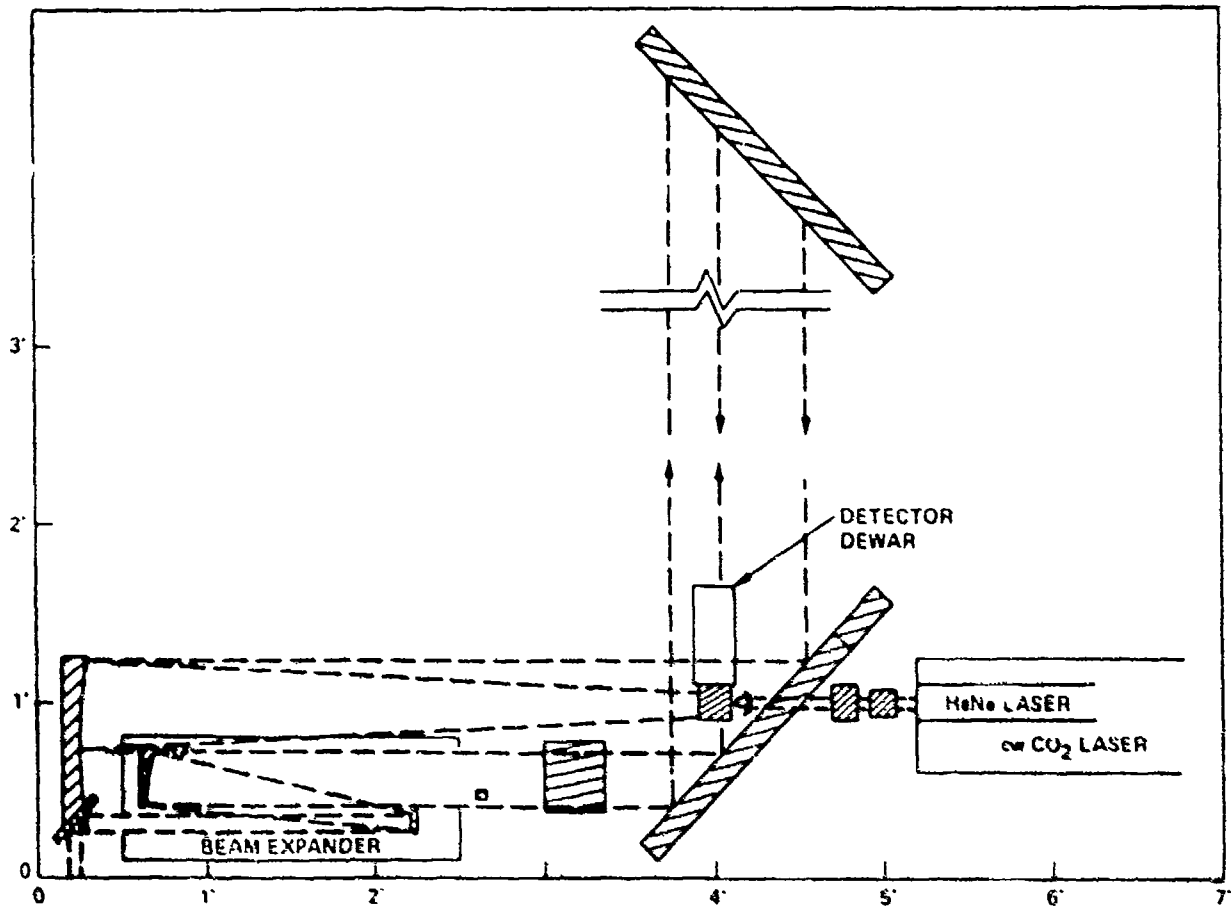


Figure 4. Side View of the Optical Layout

The upper mirror is mounted in an Aerotech mount, which can be manually scanned to nearly the desired direction, then controlled with the UNIDEX III scan controller over a ± 4 -degree range in azimuth and elevation (this gives a ± 8 degree beam pointing change in elevation). The maximum scan rate is 8 degrees in 72 seconds. While the UNIDEX III controller can be programmed internally or controlled externally, we have typically used the up/down and left/right buttons on its front panel to position the mirror in an appropriate orientation, then leave it stationary.

2. Local Oscillator (LO) Optics

The local oscillator optics comprise a set of aluminum coated mirrors, 50 percent reflective ZnSe beam splitters, one 90 percent reflective ZnSe beam splitter, three ZnSe lenses, and three iris diaphragms for controlling LO power. The optics are arranged to divert a portion of the laser power to a pair of laser power meters, to combine the two beams into one which is directed onto the photomixer. Since the lasers typically emit 1 watt of power, whereas only 0.5 mW is required at the photomixer, the iris diaphragms are used to control the power at the photomixer.

A pair of Rofin-Sinar optical chopper wheels were added to the LO beam paths in order to allow only one LO at a time to reach the photomixer. (When both LO's illuminate simultaneously, the power in each must be reduced by 50 percent, resulting in about a 50 percent reduction in signal-to-noise ratio (SNR).) The two chopper wheels can be synchronized so that one transmits 180 degrees out of phase with respect to the other. The chopper-wheel drive electronics are used to provide the master signal to the digital delay generators. A few-msec delay is used between firing the two lasers to eliminate the effects of chopper jitter.

3. Receiver Optics

Two additional pieces of optics are not included in either the transmitter or local oscillator optics - the primary and secondary telescope mirrors. The primary mirror has a diameter of 12-1/2 inches, a parabolic surface with a 59-inch focal length, and an off-axis radius of 5 inches. The substrate is 2-inches thick. It is coated with aluminum with a silicon dioxide (SiO_2) overcoat. This is acceptable in the 9-11 micron spectral region for near-normal incidence, but not for 45 degree incidence. The secondary mirror is an elliptical mirror with a 3-inch minor axis, and is aluminum coated with a MgF_2 overcoat.

4. Alignment Procedure

After the optics were placed in mounts located according to the engineering drawings, they were aligned. Wherever possible, the He-Ne beams were used. For the transmitter, the He-Ne beam is made coaxial with the pulsed CO₂ laser beam path by means of a small mirror in a kinematic mount, which can be returned to the same position each time. This allows the He-Ne beam to be steered properly into the beam expander and for the subsequent beam-steering mirrors to be aligned to first order (the position of the He-Ne beam on the door of the dome is used to some extent). A 5-inch diameter, corner-cube reflector

can be lowered into the path of the He-Ne beams and used to direct a portion of the beam into the receiver and into the photomixer to allow it to be positioned (Reference 34). The CO₂ laser beams are then transmitted into the atmosphere. For operation beyond 2 km, the beams are usually aimed at a hillside at a distance of 5 km. A boxcar averager is used to keep a running, few-shot average of the return from the hillside, and one of the beam steering mirrors after the beam expander is adjusted to maximize the signal in the boxcar averager. For operation at ranges less than 2 km, the mirrors are adjusted while looking at the atmospheric backscatter displayed on the oscilloscope. Both beam-steering mirrors should be adjusted to achieve full-transmitter/receiver alignment, but one usually suffices for distances beyond one kilometer.

Transport of the local oscillator beams through the optical system is verified, partly by using thermally sensitive paper, partly by using a laser power meter, and partly by using the He-Ne guide beams. The hardest task was focusing the LO beams tightly onto the photomixer. The successful procedure was to use a series of pinhole apertures to guide the focusing of the lenses while monitoring laser power with a power meter located above the pinhole. Successively smaller pinholes were used until the beam was tightly focused to about a 300-micron diameter.

In heterodyne detection, the local oscillator beams must be coaxial with the receiver field-of-view. (For optimal photomixing, the two beams must have matched phase fronts and the same polarization.) In order to align the receiver of MAPM, one of the He-Ne beams aligned with the cw CO₂ lasers was reflected backwards by a flat mirror in the detector focal plane. It was sent back through the beam splitter at the point where it first entered it. The reflected beam was then coaxial with the LO beam, and the portion reflected by the beam splitter was used to adjust both the secondary and primary mirrors in the receiver telescope.

H. DOME

To provide a cover for the mirror above the roof line, a fiberglass observatory dome was mounted on a rotating wooden platform or "Lazy Susan." The dome is of the type typically made for amateur astronomers. It is white, with a sliding 18-inch wide metal door. The dome was fastened to a 12-inch skirt mounted on the rotatable wooden platform. The upper deck of the Lazy Susan has 12 wheels held in casters, which slide in a groove in the lower deck, which is fastened securely to the lip of the opening in the roof. Sheet rubber is used to prevent water or air from entering the semitrailer through the region between the two decks.

A 0.4-mil polyethylene window, made from inexpensive painter's dropcloth, is used as the window on the dome. It is mounted in a frame which is tilted at a slight angle with respect to the normal of the transmitted laser beam in order to reduce the strength of the signal from the beam backscattered from the window. The window material was measured to have about a 10 percent one-way reflective loss, plus a few percent absorption loss in the region for a few wavenumbers around the 10P(14) CO₂ laser line, where ethylene has its strong absorption coefficient. Several sources and thicknesses of polyethylene were evaluated to find the optimal material.

I. PHOTOMIXER

The HgCdTe photomixer was chosen for high-frequency operation as required for use with heterodyne detection. The side dimension was specified as 0.25 mm to achieve the high-speed requirement and match the central diffraction or Airy spot of the receiver telescope. A photovoltaic, rather than photoconductive detector is used. One photomixer was mounted in the liquid nitrogen ($1N_2$) dewar with twisted leads, the other was mounted in a dewar supplied with the leads spread far apart. While the former method was better for high-speed response, both seemed to have equal response out to 80 MHz (they were used at 30 MHz). However, the dewar with the leads spread far apart seemed much more susceptible to radio frequency interference (RFI), to the point where it cannot be used.

It is extremely important to keep the LO power on the photomixer below 5-10 mW. Two photomixers were overheated and destroyed by failing to monitor the bias voltage while adjusting the LO beam on the photomixer. It was also observed that occasionally the secondary LO beam, caused by multiple reflections from the lenses or dewar window could be confused with the primary LO beam. If the bias voltage decreases by only a few mV, then it is probably the secondary beam.

J. SIGNAL CHAIN ELECTRONICS

The signal chain electronics was assembled to convert the electronic signal from the photomixer to a signal that the computer could accept. A block diagram of the signal chain electronics is shown in Figure 5.

1. Photomixer Bias Box

A 9-V battery with a resistor-capacitor network supplies a bias voltage to place the photomixer response in an optimal region. The bias voltage network includes a resistive voltage divider that limits the total current to the photomixer to less than 1 mA, and provides a voltage level for the no-radiation level in the linear region of the back-biased I-V curve. Typically, one resistor is 15K ohms, while the other is 400 to 800 ohms. A small inductor is also added in order to isolate high frequency signals from the voltage meter.

2. Trontech Preamplifier Model L30 APS

This is a narrow bandwidth (25-35 MHz) preamplifier with 45-dB amplification. It is located approximately 2 meters from the photomixer.

3. In-line Attenuators

An approximately 6 decibels of attenuation is added between the Trontech preamplifier and the RHG linear amplifier to reduce the probability of saturation and nonlinear effects.

4. RHG Linear Amplifier, Model EST 3010LD

This unit has two outputs - one is the intermediate frequency (IF) output, which gives the signal in the 25-35 MHz region, while the other is the linear envelope detector output. The IF output is used to monitor the frequency

SIGNAL CHAIN

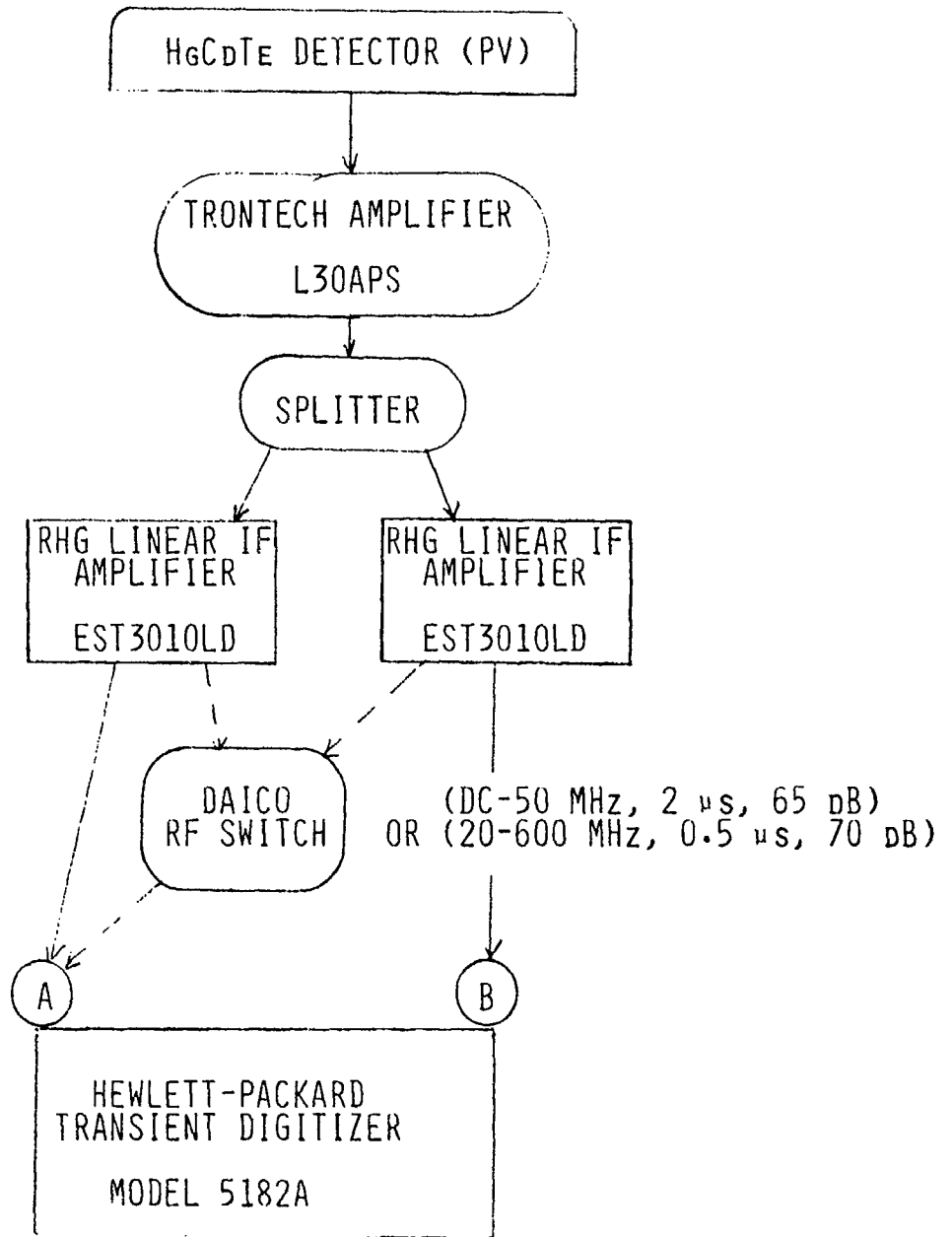


Figure 5. Block Diagram of the Signal-Chain Electronics

separation between the local oscillator and the pulsed CO₂ laser. When the separation is within the passband of the filter, a highspeed oscillation is observed on the oscilloscope. The envelope detector measures a signal proportional to the square root of the backscattered laser radiation, due to the photomixing with the the local oscillator. The fact that it is proportional to the square root of the backscattered power increases the dynamic range of the signal-chain electronics.

5. 93-50 Ohm Impedence Matching Network

This component is added to match the impedances of the RHG linear amplifier and the filter.

6. Cir-Q-Tel Flat Phase Filter

The electronic filter was carefully chosen to have the proper frequency response with minimal pulse distortion. The frequency range is from 2.4 MHz (to accommodate a 300-ns pulse width) to 400 kHz (375-m range resolution). (The relationship between frequency and range resolution can be understood by recalling that light travels a round-trip kilometer in 6.67 microseconds.) The transient digitizer has a 50-ns window, necessitating some pulse stretching for the 5-MHz sampling rate typically employed with MAPM. The type of filter chosen was Bessel because it has the flattest response of the three basic filter types (Chebyshev and Butterworth were also evaluated). The number of poles ordered was 7, selected to given an optimal roll-off rate (6 dB/octave/ pole). The filter is removed for 10- and 20-MHz operation.

7. Flip-Flop Array

A flip-flop array circuit was designed and fabricated by Carlos Esproles at JPL. The purpose of the circuit is to use timing information from the digital delay generator to turn on and off the Daico RF switch which can be used to send the heterodyne signal to either the low- or high-gain RHG linear amplifier. This feature would be useful if the dynamic range of the signal were too large to be accommodated by the transient digitizer. To date, this feature has not been required.

8. RF Switches and RF Power Splitter

Daico Model 100C1562 RF switches and an RF power splitter provide up to 65 decibels of isolation in switching RF from one port to another.

9. RFI Shielding

The electronics responded to the high-voltage discharges associated with firing the pulsed lasers. Especially prominent was a large feature about 1.5 microseconds before the laser radiation was emitted, but there were also RFI spikes that occurred at later times. Several things were done to reduce the post-laser-firing RFI noise. First, braided shielding was placed over the BNC cable from the signal chain electronics to the transient digitizer and oscilloscope. Second, the same was done to the SMA cables from the photomixer to the electronics enclosure, from the enclosure to the bias box, and from the

bias box to the Trontech preamplifiers. One cable was grounded at the enclosure but not at the photomixer. Third, a small aluminum chassis box was placed over the photomixer bias box. Fourth, an RFI-shielded enclosure was made for the signal chain electronics from solid metal with isolated feedthroughs and "freezer" contacts between the lid and the side walls. Occasionally, RFI still invaded the data. The cause was traced to loose SMA connectors, or, for one particular case, to the wiring inside one photomixer dewar where the lead wires were not coaxial (the preferred arrangement) or pigtailed but entirely separate and passing through separate case feedthroughs. Near the end of the project, considerable RFI associated with the yellow transmitter laser developed. The exact source has not been identified.

10. Transient Digitizer

The Hewlett-Packard (HP) Waveform Recorder Model 5182A was chosen as the transient digitizer. While it nominally has 10-bit resolution at low data rates, at high speeds, this drops to 7.8 effective bits, which is higher than the approximately 7.0 effective bits for comparable transient digitizers. In addition, Hewlett-Packard had already developed the software required to transfer the data from the transient digitizer to the HP computer disk at a 300-kbps rate.

The 5182A has a number of features that permit the data to be recorded in an optimal manner. There are 1024 channels, which allow the signals from each of two laser pulses to be recorded for 100 microseconds (15 km) each at a 5-MHz rate. This is usually sufficient for the backscatter signal from one laser to recede into the noise before the other laser is fired. However, after the optical choppers were added in the LO beam paths, the transient digitizer was operated in the "toggle mode" in which a few millisecond interval can be placed between the two 100-microsecond intervals used for the lidar signals. In the toggle mode, the highest prf at which the data system has been operated is about 30 Hz. However, the use of external pulse inputs should permit operation at 100 Hz or more to be realized. Among the settings that can be controlled from the front panel are sampling rate (to 20 MHz), voltage range, offset voltage and pretrigger sampling region. The panel can be set manually or from the computer. Once it is set, the computer can read the settings and place the transient digitizer in the "direct memory access" transfer mode for data acquisition and transfer.

When the 5182A was delivered, it was noted that the output for a linear ramp input had some nonlinear features, even at low sampling rates where it was expected to perform to 10-bit resolution. It was returned to HP, where a defective chip was replaced and the instrument readjusted.

K. DIGITAL DELAY GENERATOR (DDG)

A California Avionics Model 103DR Digital Delay Generator was included to control the time delay between firing the two pulsed lasers, and to control the gain switching using the Daico RF switch, should it be necessary. The DDG is triggered by either a pulse or by the positive edge of a square wave. It has three TTL outputs, and can generate time delays from 1 microsecond to 10 seconds.

L. MONITORING EQUIPMENT

Several pieces of equipment were purchased for use in monitoring or diagnosing various components of the lidar system. These include both electronics and optical instruments. They are described, along with their application, in the following paragraphs. Many of these components are shown in Figure 6.

1. Storage Oscilloscope

A Tektronix Model 7834 Mainframe Storage Oscilloscope with four plug-in units (Dual Trace Amplifier, Model 7A26, Differential Amplifier, Model 7A22, Real Time Base, Model 7B53A, and Delaying Time Base, Model 7B85) was purchased for use in monitoring the pulsed laser pulse shape, frequency offset from the local oscillators, and lidar signals. It has a storage mode of operation, so that fast waveforms can be examined carefully. It responds to frequencies up to 400 MHz, which is important for monitoring frequency offsets from the IF output of the RHG linear amplifier and pulse shape using a room-temperature HgCdTe detector.

2. RF Spectrum Analyzer

The Hewlett Packard RF Spectrum Analyzer with three plug-in units (Display Section, Model 141T, RF Section Model 8554B, and IF Section, Model 8552A) is used occasionally to monitor frequency offsets between the two cw CO₂ lasers (when they are being observed for frequency stability), to verify single frequency operation of the cw CO₂ lasers, and to check for ground loop problems. In doing so, care must be taken to ensure that the amount of power incident on the photomixer does not drive the photomixer and electronics into saturation. If it does, many additional frequencies appear as harmonics and sums and differences.

3. Room-Temperature HgCdTe Detector

A 1-mm diameter HgCdTe detector, manufactured in Poland and sold in the US by Boston Electronics, is used to monitor the pulse shape of the pulsed CO₂ lasers when they are being adjusted for single longitudinal mode (SLM) operation. The output is observed on the storage scope. When SLM operation is achieved, the pulse will have a smooth envelope; when SLM operation is not achieved, high-frequency hash will be observed inside the envelope. An attempt was made to use this detector as a photomixer in order to monitor the beat frequency between pulses and cw CO₂ lasers, but the sensitivity was not high enough for this application.

4. Boxcar Averager

A Princeton Applied Research Model 162 Boxcar Averager was incorporated into the system to speed the alignment procedure for the transmitters with the receiver. Typically, a hillside at a distance of 5 km is used as a target. Alignment at this distance should imply alignment from about 1.5 km to 15 km. The boxcar averager is adjusted to monitor the backscatter from the hillside, and to display a signal proportional to the average value of the signal for the preceding few seconds, with an update several times a second.

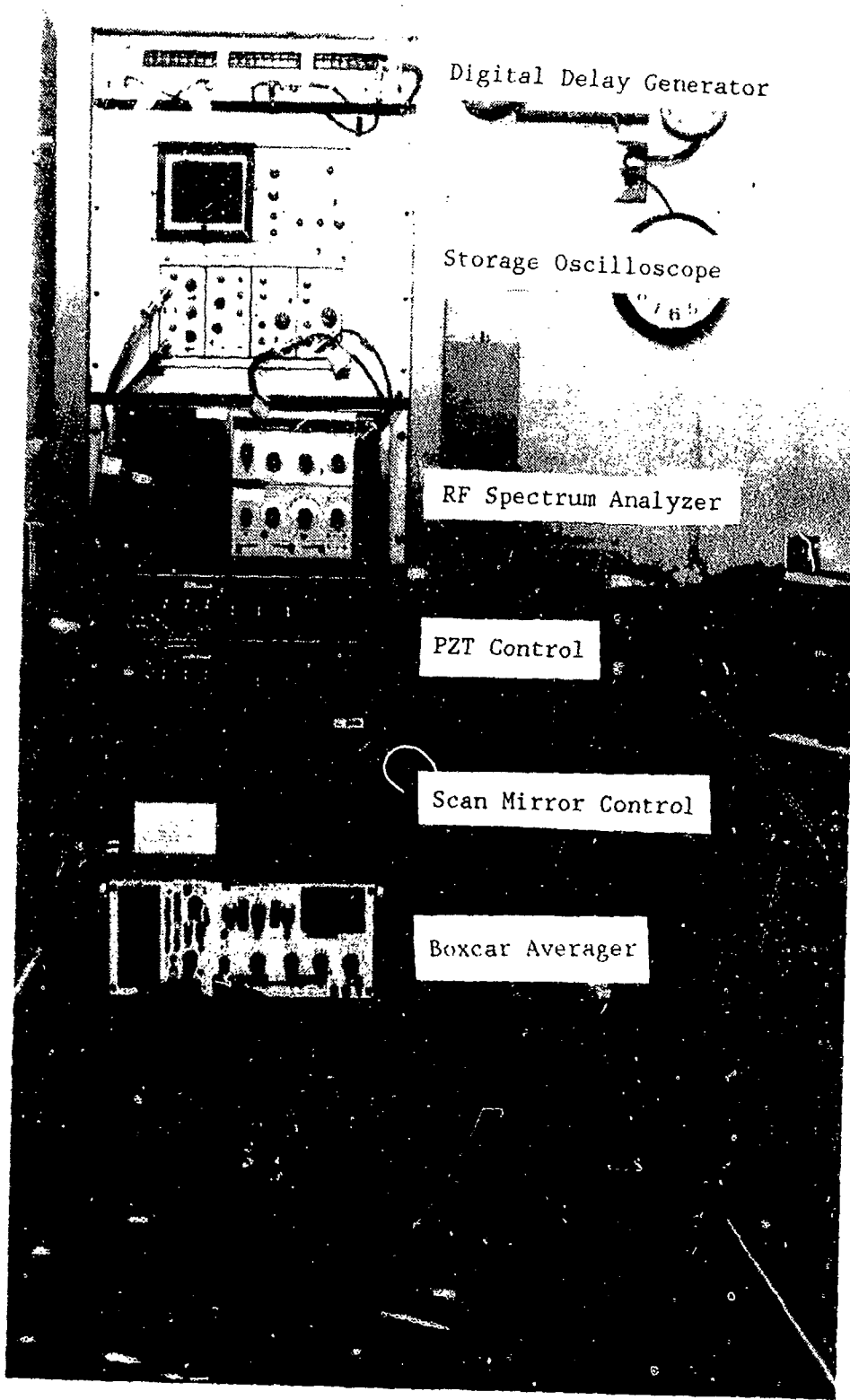


Figure 6. Photograph of the Electronics Rack Showing Both Diagnostic and Control Electronics

After the beams are aligned, atmospheric backscatter signals are stored and analyzed on the computer, and the process is repeated, if necessary. The boxcar averager must be disconnected from the signal cable before data is stored in the computer; failure to do so results in a long tail added to the data.

5. Spectrum Analyzer

A grating spectrograph with a graphite or fluorescent screen from Optical Engineering is used to determine the lines on which the CO₂ lasers are operating. The scale above the screen gives the laser line designations; the scale below gives the wavelength in microns. The graphite screen is better for pulsed laser radiation (it emits a bright flash) while the fluorescent screen is better for cw laser operation (it gives a dark line where the laser radiation quenches the UV-excited fluorescence).

6. Laser Power Meters

Three laser power meters are used to monitor the laser powers. Two are permanently installed in the system for monitoring the cw CO₂ laser power, while one can be placed in front of either pulsed laser to monitor pulsed laser power. Those for the cw CO₂ lasers are Scientech, Model 365, with digital readout, the other is Coherent Inc., Model 302. The Model 365 can read up to 20 watts, and have a 5-10 s time constant, while the Model 302 can read up to 100 watts, and has a 1-s time constant.

M. COMPUTER

The Hewlett-Packard System 1000, Model A900, Micro 29 Minicomputer was chosen primarily for its ability to acquire data rapidly and process them at a moderate rate. In addition, the computer is convenient to operate. A block diagram of the computer system is shown in Figure 7.

N. REMOTE SAMPLE CHAMBER

The sample chamber for remote use was designed and fabricated at JPL. The chamber was used to contain a known concentration of gases to calibrate the lidar for each particular gas. The cell length is 60 cm, the diameter 1 m. The walls are made of Teflon sheet rolled into a cylinder, and held in place by means of a wooden frame. The windows are made of 0.4-mil thick polyethylene. A muffin fan is placed near the bottom of the cell to mix the injected gas. Liquids and gases can be injected using graduated syringes. Laboratory tests indicated that absorption of CO₂ laser radiation by methanol stayed constant over a period of 10 minutes, indicating that the vapor was neither adsorbing onto the walls nor escaping through leaks in the chamber at a perceptible rate.

O. ABSORPTION COEFFICIENT CELL

A small cell was fabricated for use in the laboratory for making CO₂ laser measurements of absorption coefficients of various gases. The cell walls are stainless steel, coated with Teflon to reduce adsorption of molecular species onto the walls. The windows are ZnSe with antireflective coating. The cell length is 19 cm; the diameter, 5 cm. Two inlet-outlet ports that can be

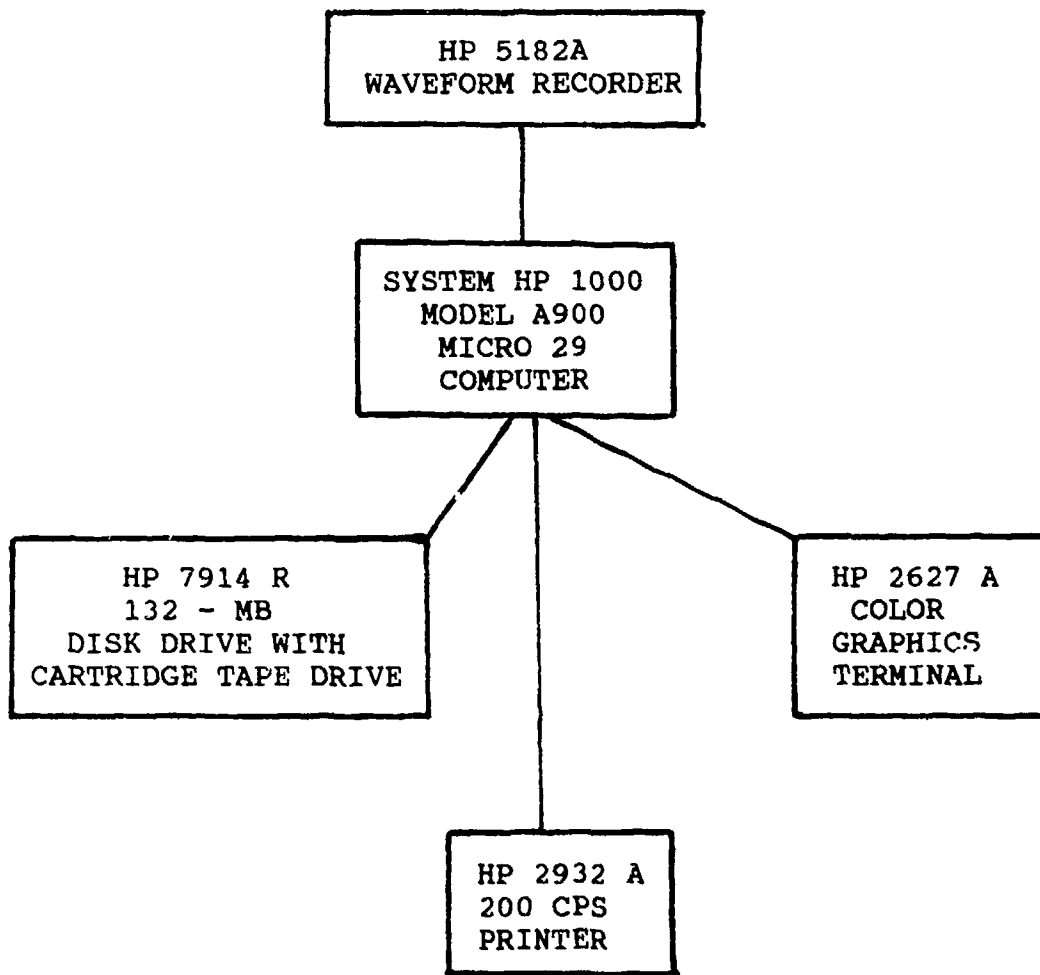


Figure 7. Block Diagram of the Computer System

connected to vacuum equipment. The design is similar to that of a cell successfully used for hydrazine fuel gas measurements (Reference 35).

P. LIST OF COMPONENTS

A list of the major MAPM components, their suppliers, model numbers, and specifications, is given in Table 6. Their layout in the system is shown in Figure 8.

TABLE 6 MAJOR MAPM COMPONENTS

Item	Supplier*	Model No.	Specifications
Semitrailer	Diamond B. Co.		35' long
Pulsed CO ₂ Lasers	Laser Science, Inc.	PRF 150S	150 Hz, SLM
cw CO ₂ Lasers	Ultra Lasertech	3822	1-2 W
Laser Coolers	Neslab	RTE-4, HX-75	
HgCdTe Detector-Signal	New England Research Center		0.25mmx0.25mm 77K
HgCdTe Detector	Boston Electronics	R005A	1 mmx1 mm 300K
Transient Digitizer	Hewlett-Packard	5182A	20 MHz, 7.7 eff. bits
Data Computer	Hewlett-Packard	1000, Micro 29	
Scan Mirror Mount, Controller	Aerotech	AOM 130-24M UNIDEX III	24" aperture
Optical Table	Modern Optics		4'x10'x1' & lower shelf
Beam-expanding Telescope	S.O.R.L.	COAR 10X15	10X, 15-cm diam.
Optical Chopper	Kofin-Sinar	7505	10-200 Hz
Linear Phase Filter	Cir-Q-Tel	FLI/2IL-4-7/ 50-3A/3A	0.2 to 2.5 MHz

*Mention of the supplier's name does not constitute an endorsement of the supplier by the Air Force, NASA, JPL, or CalTech.

TABLE 6 MAJOR MAPM COMPONENTS (CONCLUDED)

Item	Supplier*	Model No.	Specifications
Off-Axis Parabolic Receiver Mirror	J. L. Wood Optical		4" off axis, 12" diam.
Flat Mirrors	Prisms Unlimited		24" dia, 1-5/8" thick
Window	Hardware store		0.4-mil polyethylene
Dome	B. E. Meyers & Co.		2-m diam. fiberglass
Linear IF Amplifier	RHG Electronics	EST 301OLD	f= 30 MHz, Δf = 10 MHz
Digital Delay Generator	California Avionics	103 CR	resolution 100 ns to 10 s

*Mention of the supplier's name does not constitute an endorsement of the supplier by the Air Force, NASA, JPL, or CalTech.

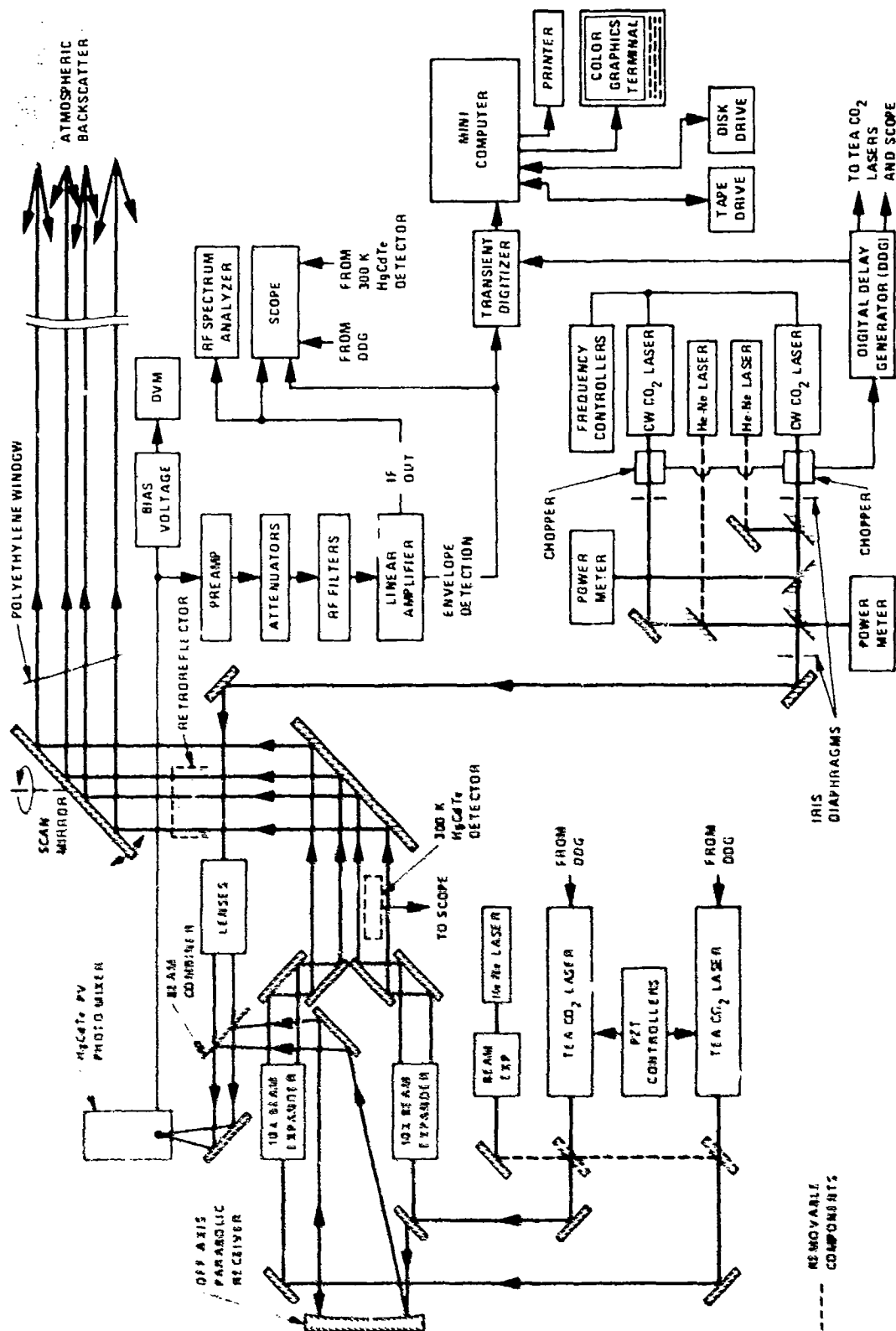


Figure 8. Diagram of MAPM

SECTION III

DATA PROCESSING CODES

A number of data processing codes were used for MAPM. Some were adapted from the Winds Measurement Assessment task (Reference 36), while others were developed especially for MAPM. This section describes the most important codes.

CRUMS7 is the primary code used for processing the lidar data. As the "7" indicates, it is the seventh version developed. Earlier versions employed different algorithms for subtracting background noise, and had less capability to manipulate the data. CRUMS7 does the following:

1. Reads all inputs from a disk file.
2. Reads pulse-pair data from the disk (LU 19). The pulse-pair data is in the form of 1024 channels containing two pulses: pulse A and pulse B (thus, the term pulse-pair).
3. Discriminates pulse-pair data (according to input parameters) so that only "good" pulse-pairs are used.
4. Adds a number of pulse pairs (typically (30-100)) together.
5. Subtracts pre- or post-pulse background level from the sum of the pulse pair set.
6. Squares the pulse-pairs (and multiplies by the range**2 if needed).
7. Calculates and subtracts the background of the squares (using a range of channels which are inputs) and subtracted -- this changes the baseline of the squares.
8. Adds the pulse-pair squares.
9. Takes the ratio of pulse A to pulse B (or vice versa) when a specified (by an input) number of squares are used.
10. Takes different sets of ratios -- each set corresponding to a different number of squares used before the ratio is taken.
11. Calculates the natural logarithm of these ratios.
12. Calculates the derivative of these log ratios with respect to distance.
13. Does Step 11 on all the sets of ratios, and Step 12 can be done on any ratio set desired.
14. Calculates means and standard deviations of all the sets of ratios -- this entails going through the data a second time.

15. Plots squares, ratios, derivatives, etc. The squares can be saved in a disk file for archiving and future further processing.

The previous version, CRUMS6, was used in analyzing data up through July 1987 (for example, Reference 20). CRUMS6 is similar to CRUMS7 except that Steps (4) and (5) involve calculating and subtracting the minimum values of each laser pulse before proceeding. The rationale for this was to avoid squaring negative numbers. It was finally realized that this approach introduces a range-dependent bias into the calculations in that cross-terms between the offset between the minimum value and the background level with noise and backscattered signal values that cannot be corrected for. While both CRUMS6 and 7 give similar results for strong signals, CRUMS6 gave larger values for weaker signals at long range.

More recently, another data analysis code, CRUMS8, was developed. It processes the data in much the same way as does CRUMS7, but is intended for use in displaying a large number of sequential measurements. A given data set is divided into a number of subsets, and each subset is processed and stored. After these calculations, the data can be displayed using either a color graphics package or a three-dimensional overlay code. In the color graphics package, the horizontal axis is used to display time (up to 50 traces can be displayed), the vertical axis is used to display distance, and color is used to display the derivative of the natural logarithm of the ratio of the signal at the two laser lines. In the 3-D overlay code, each derivative is placed diagonally on the screen, with a small separation between successive traces. One disadvantage of this code is that peaks for some traces can obscure later data. The presentation of the data can be inverted so that later data is shown first.

Another useful program is "ATTEN," developed by Michael Kavaya for the NASA Winds Measurement Assessment task (Reference 36). This program calculates the atmospheric attenuation due to carbon dioxide and water vapor continuum as a function of laser line frequency, and atmospheric temperature, pressure, and relative humidity. Data on atmospheric CO₂ absorption lines includes the ground state energy levels and line widths from the HITRAN data base (Reference 37). The water vapor continuum uses the temperature and wavelength dependence in HITRAN.

A third data analysis program is "BETA," originally developed by Kavaya and Menzies for the NASA Winds Measurement Assessment task (Reference 36). This program takes the multipulse averaged lidar signal, generally stored after processing the data from any run, and calculates a relative backscatter coefficient, as well as the signal noise level. The input parameters include a calculated transmitter/receiver overlap function, the laser line used, the lidar vertical pointing angle, the total and molecular extinction coefficients in the boundary layer, and the height of the inversion layer. This program has proven useful in highlighting aerosol structure along the lidar path and estimating the total extinction coefficient which, with the molecular extinction coefficient calculated using "ATTEN," can be used to estimate the aerosol extinction coefficient or molecular line extinction coefficients.

The transmitter/receiver overlap function code was developed for the Winds Measurement Assessment task, primarily for the annular output beam of an unstable resonator laser (Reference 38). MAPM, on the other hand, has a truncated Gaussian beam, so the calculations with this code are not fully appropriate for MAPM. The incorporation of the truncated Gaussian case is planned.

SECTION IV

OPERATION

A. TURN-ON PROCEDURE

MAPM has been operated for a sufficient period of time such that its operation is reasonably well understood, and it can be made fully operational within one hour from initial turn on. A large portion of the delay is due to the lasers which must reach a thermal equilibrium before becoming stable. Some of the time is also spent making sure that the transmitters are properly aligned with the receiver.

A turn-on and check-out procedure protocol has been developed and can be referred to as required. If the pulsed lasers return to their pointing direction of the previous run, very little adjustment will be required of the beam steering mirrors. It is best to wait five to ten minutes after turning the lasers on before making any adjustments of the output coupler. The procedure is as follows:

1. Put on safety goggles
2. Turn on electronics
3. Turn on cw laser
 - a. close output port
 - b. turn water on
 - c. turn power supply on
 - d. turn stabilization off
 - e. turn Lansing controller on
 - f. turn Scientech on
4. Optics
 - a. remove dust covers
 - b. blow off dust with bottled gas
5. Turn on pulsed lasers
 - a. turn gas cylinder on (check gas pressures - 20 lbs on regulators, several hundred pounds in cylinders)
 - b. turn power supply on
 - c. set gas flow to laser (5-10 min)
 - d. turn laser head on

- e. turn water on
 - f. set Coherent power meter in front of laser
 - g. set prf
 - h. turn high voltage on - 70 to 100 percent, depending on PRF, etc.
 - i. turn on gain cell - 6 mA
 - j. fire
 - k. adjust grating, if required
 - l. adjust output coupler (vertical only) if required - after thermal equilibrium is reached
6. Check alignment between He-Ne and pulsed CO₂ in the center of beam expander using liquid crystal film
7. Single longitudinal mode (SLM) operation
- a. place 300K HgCdTe detector after beam expander
 - b. observe signal on scope
 - c. close output iris 4.5 to 8 turns (until SLM observed)
 - d. adjust Burleigh bias to get single mode
 - e. adjust gas pressure (if required) to change effective cavity length
8. Photomixer
- a. cool detector with liquid nitrogen
 - b. turn on bias box
 - c. check that local oscillator is centered on photomixer and not too powerful using digital voltmeter (DVM); replenish 1N₂ dewar periodically.
9. Transmitter/Receiver
- a. align, using He-Ne lasers
 - b. note settings (H and V) for first octagonal mirror after beam splitter
 - c. adjust octagonal mirror while watching scope and boxcar averager.

10. Frequency-offset setting
 - a. place mask with small hole over output of beam expander
 - b. lower retroreflector to couple pulsed CO₂ laser radiation into photomixer
 - c. observe IF output from RHG on scope
 - d. stabilize cw CO₂ laser with offset control on shelf
 - e. find setting for maximum IF signal
 - f. if large signal not found, verify that lasers are on the same line
 - g. vary bias setting on the PZT of the pulsed laser, but check with the 300K detector that single-mode operation is achieved
 - h. check photomixer dewar for LN₂
 - i. flip retroreflector out of beam
11. Transmission into atmosphere
 - a. install polyethylene window
 - b. ensure retroreflector is out of beam path
 - c. aim at a hard target 5 km away
 - d. adjust octagonal mirror in a range of 2-10 small micrometer divisions from the original setting, searching for a signal, watching scope and boxcar averager
 - e. optimize the signal with mirror, Burleigh, L.O., diaphragms
12. Recovering signal
 - a. check Scientech power reading - if low, restabilize
 - b. check pulsed laser for single mode operation
 - c. possibly adjust bias of Burleigh box
 - d. check photomixer dewar for LN₂
13. Transient digitizer
 - a. reset until ready to receive commands
 - b. set range (500 mV)
 - c. set offset (-400 mV)
 - d. set time base (50 ns to 200 ns)

- f. set delay step to 1 ms
- g. set delay to approximately -10 ms
- h. set arm to normal
- i. set trigger to external
- j. set trigger level to 2.5 V or 99%

14. HP 1000

On the terminal, enter the following commands:

COMD

FM1

X

INDAT

number of digitized pulses to sum before storing on disk, number 1024 word sums to store on disk, location of first sum on disk.

B. MAPM DATA LOG

Table 7 provides a list of the days MAPM was operated during the project, the measurement objective, and any comments on the system performance or measurement objective that seem important.

TABLE 7 MAPM DATA LOG

Date	Measurement	Comments
9-15-86	10P(22)	
9-16	WATER VAPOR	
9-26	ALIGNMENT	
10-3	10P(20)-10P(10)	N ^{1/2} DATA
11-3	VERTICAL AEROSOLS	
11-7	VERTICAL AEROSOLS	CIRRUS CLOUD
11-10	VERTICAL AEROSOLS	
11-11	VERTICAL AEROSOLS	
11-12	WATER VAPOR 10 MICRONS	
11-17	WATER VAPOR 10 MICRONS	
11-19	WATER VAPOR 10 MICRONS	
12-4	WATER VAPOR 9 MICRONS	
12-8	SYSTEM TESTS	
12-10	SYSTEM TESTS	RFI PROBLEM TRACED
12-11	WATER VAPOR 9 MICRONS	
12-31	WATER VAPOR 9 MICRONS	
2-6-87	AEROSOLS - 10P(20)	FOR PROJECT WITH ANCELLET
2-26	VARIOUS LINE PAIRS: 10P(24)/10P(22) 10P(32)/10P(22) 10P(10)/10P(22)	FIRST USE OF CHOPPERS
2-27	10P(22)/10P(24) 10P(22)/10R(12)	BOXCAR INTEGRATOR IN CIRCUIT
3-2	10P(24)/10P(22)	WITH AND WITHOUT CHOPPER

TABLE 7 MAPM DATA LOG (CONTINUED)

Date	Measurement	Comments
3-3-87	10P(14)/10P(12)	NEW GAIN CELL IN "RED" LASER
3-4	9R(12)/9P(24) 9R(12)/9R(22)	
3-23	9P(20)/9P(20)	RECALIBRATED PULSED LASER LINES
5-6	9P(14)/9P(22)	OZONE, SMALL PHOTOMIXER
5-12	9P(14)/9P(22)	OZONE, SMALL PHOTOMIXER
5-14	9P(14)/9P(22)	OZONE, SMALL PHOTOMIXER
5-15	9P(14)/9P(22)	OZONE, SMALL PHOTOMIXER
7-10	10P(20)	REPLACEMENT PHOTOMIXER
7-13	10P(20)	
7-20	10P(14)/10P(20)	ETHYLENE
7-22	10P(14)/10P(20)	SAMPLE CHAMBER - ETHYLENE
10-7	30-Hz OPERATION	
10-8	TEST	
10-9	TEST	
10-13	TEST	
10-16	TEST	
10-21	TEST	
10-27	TEST	YELLOW LASER OUTPUT COUPLER BURNED. ELECTRONIC SENSITIVITY TO ARCING REDUCED IN YELLOW LASER.
10-30	TEST	

TABLE 7 MAPM DATA LOG (CONCLUDED)

Date	Measurement	Comments
11-12-87	TEST	AIMED AT MESA, OPTIMIZED FOR MEASUREMENTS FROM 0.5 TO 1 KM
11-13	ETHYLENE FREE RELEASE	
11-16	ETHYLENE FREE RELEASE	
11-18	ETHYLENE FREE RELEASE	
11-29	PULSE WIDTH STUDIES	
12-1	TEST	REPLACE UV PREIONIZER IN RED LASER
12-2	TEST	
12-7	GROUND CLOUD MEASUREMENTS	
12-11	TEST	
12-14	SIGNAL AVERAGING MEASUREMENTS	
12-15	SAMPLE CHAMBER MEASUREMENTS	NOT ENOUGH MATERIAL INJECTED
12-21	SAMPLE CHAMBER MEASUREMENTS	MOSTLY SUCCESSFUL
12-22	SAMPLE CHAMBER MEASUREMENTS	COMPLETED THE MEASUREMENTS

SECTION V
MEASUREMENT RESULTS

A. DIAL SIGNAL AVERAGING

MAPM was used to help determine when DIAL signal averaging could be expected to result in an improvement of the signal-to-noise ratio (SNR) that varies as $N^{1/2}$, where N is the number of lidar pulse pairs averaged, and when it cannot. A series of measurements reported by researchers at Massachusetts Institute of Technology (MIT) Lincoln Laboratories had shown that it was seemingly impossible to obtain $N^{1/2}$ improvement when a stationary hard target was used (References 26, 32, 39, and 40). Recent MAPM data was analyzed to show that for N at least out to 2000, $N^{1/2}$ behavior could be expected for atmospheric backscatter in a stationary atmosphere (Reference 41). These results are consistent with results reported for a UV DIAL system using atmospheric backscatter (Reference 42). In general, such results are expected because the atmospheric aerosols decorrelate in a few microseconds or less (Reference 43), and because the atmosphere is relatively stationary over short periods of time. However, if the ratio of the two lidar signals changes during the measurement, due to changes in absorption or scattering, then there will be deviations from $N^{1/2}$ behavior. Such was demonstrated with MAPM by processing together two sequential data sets - one for the laser lines tuned to be sensitive to water vapor, and the other tuned to be insensitive to water vapor. A further limitation to $N^{1/2}$ behavior with atmospheric backscatter was found to be background noise. It appears to provide a limit at about 1000 pulse pairs if the atmosphere has not changed in the meantime.

The results given in References 26, 32, 39, and 40, where deviations from $N^{1/2}$ behavior were evident even for $N = 10$, and even if both lasers were tuned to the same line, are thought to be due primarily to the limited change in intensity distribution on the receiver from pulse to pulse when a fixed hard target is used. Atmospheric turbulence causes only a small modulation from pulse to pulse (see, for example, References 28 and 44).

B. WATER VAPOR

MAPM was used early in the measurement program to measure atmospheric water vapor. This effort was motivated in part by the occurrence of water vapor in the atmosphere at various concentrations, and in part by the importance of water vapor in weather, climate, and remote sensing. To aid in the interpretation of the data, considerable effort was expended to review and revise the values of the absorption coefficients appearing in the literature. It was demonstrated that MAPM could measure water vapor concentrations to an accuracy of about ± 1 torr-km at ranges from 2 to 6 km.

1. Water Vapor Absorption Coefficients

There have been six comparable sets of water vapor absorption coefficient data measured using CO₂ lasers, usually with an optoacoustic cell or spectrophone for detecting the weak absorptions (References 46-50). However, the published values differed considerably, primarily due to assuming different values for the ethylene absorption at the 10P(14) CO₂ laser line, which was used for transfer calibration of the optoacoustic cells as well as whether nitrogen or synthetic air was used as the buffer gas, and to the amount of care that went into the experiment. Thus, the first task was to determine the best current estimate of this absorption coefficient, then adjust the published water vapor absorption coefficients accordingly. Using seven reported values of the ethylene absorption coefficient, an average value of $35.0 \pm 2.2 \text{ atm}^{-1} \text{ cm}^{-1}$ at 300 K, 760-torr total pressure, was determined. When the water vapor values were then revised to reflect this value, as well as corrections to the continuum absorption for suspected impurities in the measurement cells, all of the strong water vapor absorption coefficients for 300 K, 10 torr of water vapor in 760-torr total pressure with synthetic air as the buffer gas showed relative agreement between laboratories of ± 16 percent or better; the values are given in Table 8 (see also Reference 51). Note that the values in Table 8 differ from the values given in Reference 20. Values measured with N₂ buffer gas could not be used in this analysis because the O₂ pressure broadening coefficient is about 75 percent of that for N₂, so that a few percent error is introduced.

Measurements of the water vapor continuum were also carefully analyzed. The spectrophone measurements with air as the buffer gas (References 45, 48, and 49) gave values generally 40 to 70 percent higher than for the measurements made using nitrogen as the buffer gas (References 46, 47, and 50). In Reference 46, it was shown that air gives a slightly smaller value for the water vapor continuum absorption than does nitrogen. In Reference 51 it was argued that the best value for water vapor continuum absorption is about the same as in References 47 and 53, and the 10-micron band of Reference 50, and that the values reported in References 45, 48, and 49, and the 9-micron band in Reference 50 were higher due to impurities arising either from the water vapor or from the sample cell. It was suggested that further measurements are required to fully resolve this controversy.

Values useful for DIAL measurements are given in Table 9, together with the temperature dependences. Note that there is an order of magnitude difference in the water vapor differential absorption coefficients, $\Delta\alpha_C$, at various laser lines and that there is a strong temperature dependence (1.9 to 3.7 percent per degree C). The large variation in the absorption coefficients is useful as the concentration (C) and measurement range, R, changes, since optimal measurements are made when the exponential factor, $2 \Delta\alpha_C R$, is approximately equal to unity.

TABLE 8 COMPARISON OF WATER VAPOR ABSORPTION COEFFICIENTS α DETERMINED USING CO₂ LASERS WITH THE VALUES ON THE AIR FORCE GEOPHYSICS LABORATORY (AFGL) SPECTRAL DATA TAPES FOR 10-TORR PARTIAL PRESSURE, 300 K, $\alpha(\text{C}_2\text{H}_6) = 35.0 \text{ atm}^{-1} \text{ cm}^{-1}$

	CO ₂ Laser Line Frequency ^a	CO ₂ Laser Value ^b	AFGL Value ^c
Designation	(cm ⁻¹)	(10 ⁻⁶ cm ⁻¹)	(10 ⁻⁶ cm ⁻¹)
10P(40)	924.9740	12.4 ± 1.5	20.5
10P(20)	944.1940	0.93 ± 0.15	0.88
10P(16)	947.7420	1.05 ± 0.05	1.05
10R(12)	970.5472	2.11 ± 0.06	2.03
10R(14)	971.9303	1.72 ± 0.06	0.88
10R(16)	973.2885	1.37 ± 0.17	1.08
10R(18)	974.6219	0.95 ± 0.08	0.79
10R(20)	975.9304	11.3 ± 1.3	10.4
10R(22)	977.2139	1.35 ± 0.15	1.04
9P(28)	1039.3693	2.93 ± 0.17	1.63
9P(10)	1055.6251	2.67 ± 0.22	2.28
9R(12)	1073.2785	0.98 ± 0.16	1.57
9P(14)	1074.6465	3.56 ± 0.07	1.87
9R(16)	1075.9878	0.89 ± 0.05	1.00
9R(30)	1084.6351	2.78 ± 0.19	0.62
9R(32)	1085.7654	1.05 ± 0.08	0.75

^a Bradley et al., 1986 (Reference 52).

^b Includes 6.24 percent uncertainty due to the uncertainty in determining the value of the ethylene absorption coefficient for the 10P(14) CO₂ laser line.

^c Rothman et al., 1987 (Reference 37).

TABLE 9 CO, LASER LINE PAIRS USEFUL FOR WATER VAPOR MEASUREMENTS

CO, Laser Lines		$\Delta\alpha C^*$ for 10-Torr, 300K	$\Delta\alpha C^*$ Uncertainty	Temperature Dependence	Differential Absorption Coefficient for CO,
Signal	Reference	(10^{-4} cm^{-1})	(10^{-4} cm^{-1})	(%/°C)	($\text{atm}^{-1} \text{ cm}^{-1}$) ^b
10R(20)	10R(18)	10.6	1.6	2.1	-1.5E-4
9R(14)	9R(18)	3.02	0.25	1.9	-3.0E-5
9R(14)	9R(12)	3.01	0.25	2.4	+2.1E-4
10R(12)	10R(10)	1.37	0.20	3.4	+2.6E-4
10R(12)	10R(18)	1.38	0.20	3.7	-1.5E-4

* for 10-Torr partial pressure of water vapor.

^b Reference 21.

2. DIAL Measurements

A set of data using the 10R(20)/10R(18) CO₂ laser line pair is shown in Figure 9. The signal for the 10R(20) line drops below the noise level beyond 6 km due to strong attenuation by water vapor. The psychrometer-determined value near the lidar was 3.9 ± 0.7 torr, while the MAPN-determined value from 1.5 to 5 km was 3.3 ± 0.8 torr (see Table 10). Note that the water vapor concentration appears to be uniform over this range while some variation in the water vapor concentration is to be expected, it should be fairly uniform in the planetary boundary layer or "mixing" layer. The measurement time, approximately five minutes, may also tend to average out concentration fluctuations.

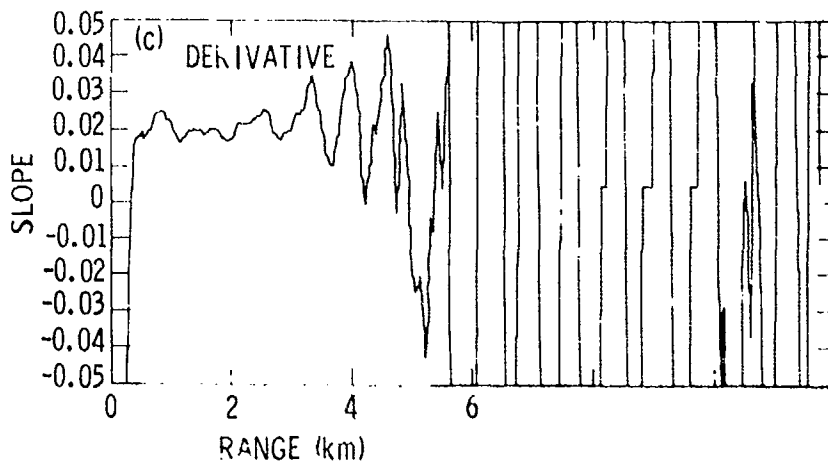
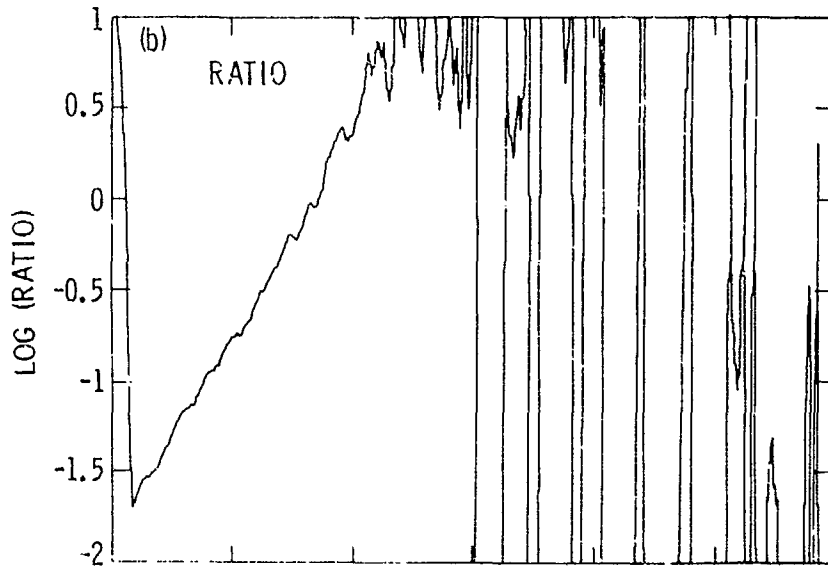
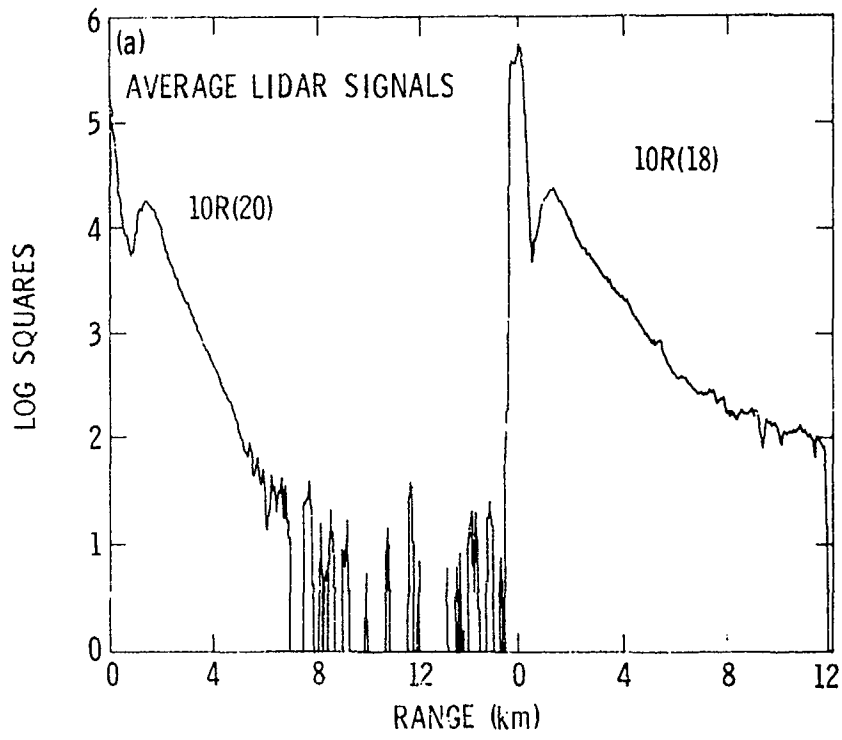


Figure 9. Water Vapor DIAL Measurement Signals

TABLE 10 SUMMARY OF WATER VAPOR MEASUREMENTS

Date (1986)	Temperature (°C)	Psychrometer Water Vapor Concentrat. (Torr)	CO ₂ Laser Line Pair	$\Delta\alpha C$ (10 ⁻⁶ cm ⁻¹)	Number of Pulse Pairs	MAPM Water Vapor Concentrat. (Torr)**	Measure- ment Range (km)
Nov. 12	26.5	3.9±0.7	10R(20) 10R(18)	10.6	1836	3.3±0.8	1.5-5
Nov. 12	26.5	3.9±0.7	10R(12) 10R(18)	1.3	2567	6.2±5.6	1.7-6
Nov. 19	15	10.2±0.5	10R(20) 10R(18)	7.9	1452	11.7±1.5	1.5-2.4
Nov. 19	16.5	10.2±0.5	10R(12) 10R(18)	0.8	4397	17.0±6.0	2.3-6
Dec. 31	15.5	3.3±0.2	9R(14) 9R(18)	2.4	5839	4.7±2.0	1-4.3

* For a water vapor partial pressure of 10 torr.

** This value includes both the lidar random measurement error and the absorption coefficient uncertainty.

C. OZONE MEASUREMENTS

During the time that only the small (0.15 mm square) backup photomixer was available, MAPM was used to measure ambient ozone. The lasers were tuned to the 9P(14)/9P(22) line pair where the differential absorption coefficient is $11 \text{ atm}^{-1}\text{cm}^{-1}$. A Dasibi ozone monitor was used to make point measurements near the lidar system. Results are listed in Table 11.

TABLE 11 OZONE MEASUREMENTS USING MAPM

Date (1987)	Time	Number of Pulse Pairs	MAPM O ₃ (ppb)	Dasibi O ₃ (ppb)
May 12	5:35 p.m.	7,000	140	90-95
May 14	4:38 p.m.	7,000	114	120
May 15	2:38 p.m.	7,000	120	100-110
May 15	2:47 p.m.	7,000	120	100-110
May 15	4:44 p.m.	7,000	60	65-70

D. ETHYLENE FREE RELEASE

In order to demonstrate that MAPM could be used to measure concentrations of molecular species in plumes, an ethylene free release experiment was designed and carried out. A cylinder of ethylene was taken to a site on a hillside 500 m east of the lidar site. The lidar was aimed at a point either above or downwind of the release point, and was tuned to the 10P(14)/10P(12) CO₂ laser lines where the differential absorption coefficient was about $31 \text{ atm}^{-1} \text{ cm}^{-1}$. The pulse-stretching filter was removed from the signal-chain electronics in order to allow measurements to be made with a 40-m range resolution, given by the laser pulsewidth. (The actual resolution may be somewhat lower due to averaging required with the DIAL technique.) The lidar was turned on and used to make measurements before, during, and after the cylinder was vented to the atmosphere. (The technician controlling the release could hear the popping sound caused by the laser beam hitting the ethylene and causing it to expand.) The data were processed and displayed in color on the CRT (see Figure 10). Concentrations up to 3 ppm were measured. In one case, the wind was blowing along the lidar pointing direction, and the ethylene plume did not appear until about 200 m downwind of the release site, where it was blown into the lidar path due to the local topography. In the other case, when the wind was blowing perpendicular to the lidar pointing direction, the plume appeared near the release site.

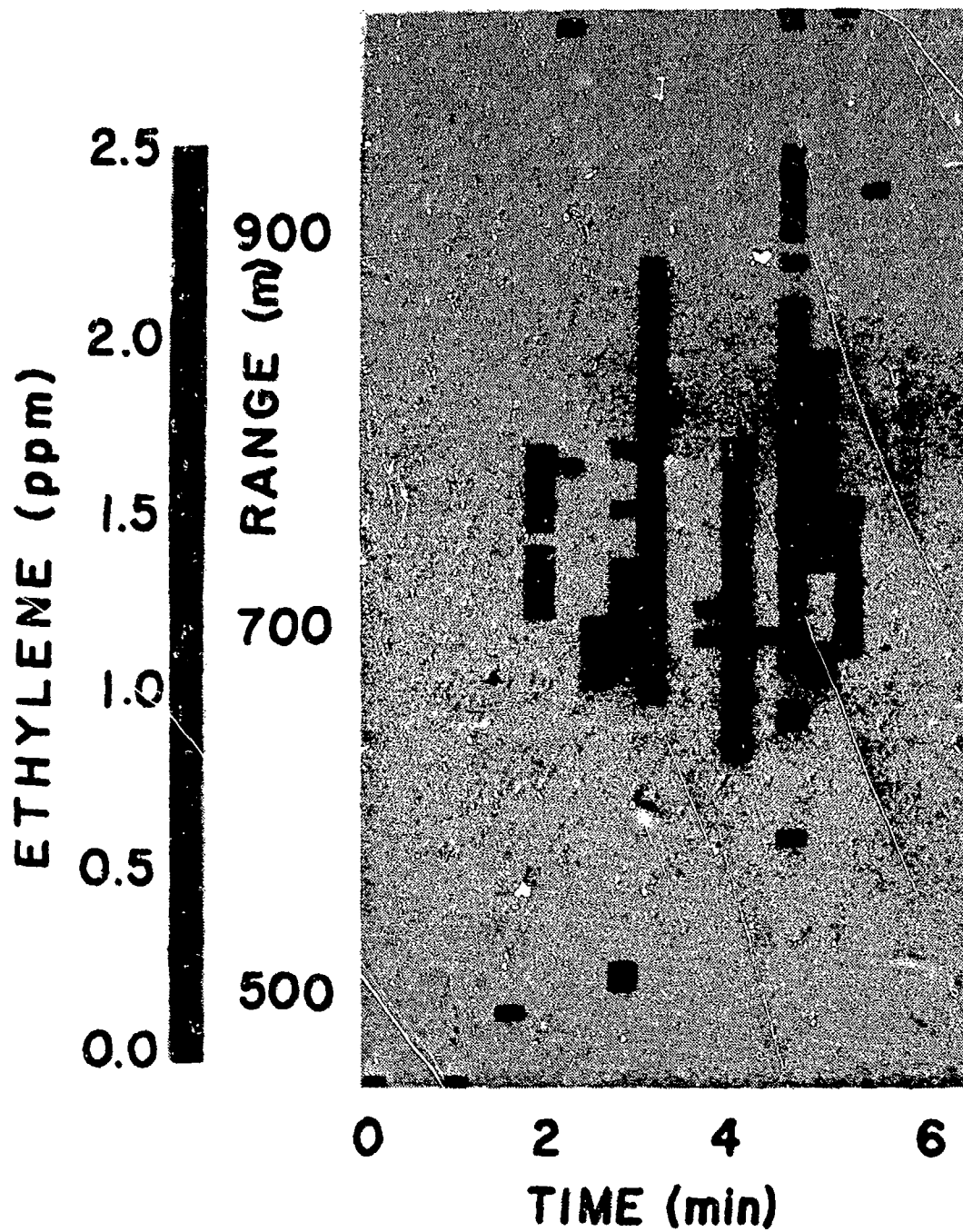


Figure 10. Free Release of Ethylene Looking Downwind

E. ABSORPTION COEFFICIENT MEASUREMENTS

The absorption coefficients for eight molecular species were measured at about 60 CO₂ laser line frequencies. Those chosen were from the list provided by AFESC after elimination of the rest of those molecular species on the list for various reasons:

1. Those that were measured elsewhere using CO₂ lasers;
2. Those with weak absorption features as indicated in the Dynamac, Inc. report (Reference 52);
3. Those with low vapor pressures;
4. Those which are expensive.

The remaining eight, along with their partial pressures in air to a total pressure of 760 torr are:

2-butanone (15 torr)
chlorobenzene (4.9 torr)
O-dichlorobenzene (1.35 torr)
1,1-dichloroethylene (7.4 torr)
trans 1,2 dichloroethylene (16 torr)
P-dioxane (9.6 torr)
1,1,1-trichloroethane (2.23 torr)
1,1,2-trichlorotrifluoroethane (1.3 torr).

The samples were prepared by placing the liquid form of the material in a glass evacuable container, pumping off all of the air, before and after freezing the sample, then filling the Teflon-coated sample cell with 1-20 torr of the vapor, followed by sufficient air to bring the total pressure to 760-torr. Measurements were made at only some of the CO₂ laser lines where the absorption was small. Measurement reproducibility was checked by making the measurements of each material on at least two days. For two species, o-dichlorobenzene and p-dioxane, the measurements repeated to ± 15 percent, while for the other six, the measurements repeated to ± 5 percent. Chlorobenzene was measured near 1 torr, and has a maximum vapor pressure at 20° C of about 2 torr; p-dioxane was measured near 10 torr. The averaged measured values are given in Table 12. They do not agree well with the values given in the Dynamac, Inc. report (Reference 55), which were as much as an order of magnitude smaller, probably because the values in that report were determined at 200° C, and with a FTIR with 4-cm⁻¹ resolution. The Dynamac values also did not agree well with published values at CO₂ laser line frequencies for those vapors which had been reported. The values in Table 13 were used to determine the CO₂ laser lines useful for DIAL measurements.

TABLE 12 ABSORPTION COEFFICIENTS OF SEVERAL ORGANIC SOLVENT VAPORS AT CO₂ LASER LINE FREQUENCIES.

	2-BUTANONE	CHLOROBENZENE	o-DICHLOROBENZENE	1,1-DICHLOROETHYLENE	TRANS 1,2-DICHLOROETHYLENE	P-DIOXANE	1,1,2-TRICHLOROTRIFLUOROETHANE	1,1,1 TRICHLOROETHANE
10R(38)	0.41							
10R(36)								
10R(34)								
10R(32)	0.30	0.2			0.18		0.3	
10R(30)								
10R(28)					0.20			
10R(26)	0.39				0.20			
10R(24)					0.17			
10R(22)	0.33				0.11			
10R(20)	0.32	0.	0.1		0.15	0.1	0.3	
10R(18)	0.37				0.19			
10R(16)					0.14	0.		
10R(14)	0.37				0.28			
10R(12)					0.11			
10R(10)	0.37				0.24			
10R(8)					0.28			
10R(6)	0.38				0.27			
10R(4)					0.20			

TABLE 12 ABSORPTION COEFFICIENTS OF SEVERAL ORGANIC
 SOLVENT VAPORS AT CO₂ LASER LINE FREQUENCIES
 (CONTINUED)

	2-BUTANONE	CHLOROBENZENE	o-DICHLOROBENZENE	1,1-DICHLOROETHYLENE	TRANS 1,2-DICHLOROETHYLENE	P-DIOXANE	1,1,2-TRICHLOROTRIFLUOROETHANE	1,1,1-TRICHLOROETHANE
10P(6)					0.41			
10P(8)	0.94				0.32			
10P(10)	0.96				0.48			
10P(12)	1.02				0.58			
10P(14)	1.01				0.52	0.1		
10P(16)	1.03				1.09			
10P(18)	1.04				0.64			
10P(20)	1.05	0.2			0.77		0.3	
10P(22)	1.11				0.75			
10P(24)	1.08				0.82			
10P(26)	1.05				2.42			
10P(28)	0.98		0.3		0.95	0.1		
10P(30)	1.00	0.2			1.29			
10P(32)	0.95				1.23			
10P(34)	0.84				1.16			
10P(36)	0.78				2.63			
10P(38)	0.68				1.38			
10P(40)	0.57				1.47			

TABLE 12 ABSORPTION COEFFICIENTS OF SEVERAL ORGANIC SOLVENT VAPORS AT CO₂ LASER LINE FREQUENCIES (CONCLUDED)

	2-BUTANONE	CHLOROBENZENE	o-DICHLOROBENZENE	1,1-DICHLOROETHYLENE	TRANS 1,2-DICHLOROETHYLENE	P-DIOXANE	1,1,2-TRICHLOROTRIFLUOROETHANE	1,1,1 TRICHLOROETHANE
9R(34)	0.36	5.1	0.3	7.7		1.0		15.9
9R(32)		4.7		6.6		2.2		13.3
9R(30)	0.31	4.5	0.	6.8		1.2	0.7	13.0
9R(28)		3.7		5.7		1.1		10.5
9R(26)	0.41	3.2		5.5		1.1		9.4
9R(24)		3.2		5.4		1.1		9.0
9R(22)	0.36	2.7		5.6		1.0		7.7
9R(20)	0.28	2.2		5.0		0.9		6.5
9R(18)	0.29	1.6		4.3		0.9		4.6
9R(16)		1.6		4.4		0.9		4.1
9R(14)	0.23	1.3		4.0		0.8	0.4	5.3
9R(12)								5.1
9P(10)	0.14	0.2	0.4			0.5	10.1	
9P(12)		0.	1.0	0.2		0.9	11.	0.31
9P(14)	0.14	0.2	1.5			2.1	13.7	
9P(16)		0.	3.3			0.9	15.7	
9P(18)	0.1	0.	3.4			0.7	15.9	
9P(20)		0.	4.0			0.7	16.6	
9P(22)	0.1	0.	5.3			0.7	15.3	
9P(24)	0.06	0.	4.1			0.6	16.4	
9P(26)	0.1		3.9			0.6	16.5	
9P(28)		0.	4.4			0.5	14.0	
9P(30)	0.03	0.1	4.6			0.4	13.3	
9P(32)		1.2	3.1			0.3	7.6	
9P(34)	0.0	1.44	2.8			0.3	7.6	
9P(36)	0.08	2.1	2.3			0.3	7.4	
9P(38)	0.07	1.9	0.7			0.3	3.5	
9P(40)								

The absorption coefficients thus measured, along with others published in the literature (References 35, 55-63), can be used to choose appropriate line pairs for various molecular species and to estimate the measurement accuracy or minimum detectable concentration. Values for 18 molecular species are listed in Table 13.

TABLE 13 LINE PAIRS APPROPRIATE FOR SELECTED MOLECULAR SPECIES

Molecular Species	Absorbing Line	Reference Line	Separation (cm ⁻¹)	(atm ⁻¹ cm ⁻¹)	MDC* (ppb)	References
Unsymmetrical dimethyl hydrazine	10P(34)	10P(22)	11.38	1.8	55	35, 60
Hydrazine	10P(32)	10P(34)	1.96	3.3	30	35, 60
Trans-1, 2-dichloroethylene	10P(26)	10P(24)	1.86	1.6	63	this work
2-Butanone	10P(24)	10R(10)	28.59	1.0	100	this work
Vinyl chloride	10P(22)	10P(20)	1.81	6.5	16	55, 58
Trichloroethylene	10P(20)	10P(10)	8.69	11.5	9	58, 61
Sulfur hexafluoride	10P(16)	10P(10)	5.14	620	0.16	29
Ethylene	10P(14)	10P(12)	1.73	30.7	3.3	20
Monomethyl hydrazine	10R(8)	10R(6)	1.46	3.4	30	35, 60
Methanol	9P(34)	9P(32)	1.98	21.6	47	35
Benzene	9P(30)	9P(26)	3.85	1.6	63	55, 58
1,1,1-Trichloroethane	9P(26)	9R(18)	4.39	4.8	21	this work
o-Dichlorobenzene	9P(22)	9P(12)	8.90	4.3	24	
1,1,2-Trichlorotrifluoroethane	9P(20)	9R(18)	30.45	16.2	6	this work
Ozone	9P(14)	9P(22)	7.17	11.1	9	57
p-dioxane	9P(14)	9P(18)	3.54	1.4	70	this work
Chlorobenzene	9R(26)	9P(12)	9.02	1.9	53	this work

*MDC - Minimum detectable concentration for R = 100 m, 1 percent differential absorptance, appropriate for ranges up to 1 km.

F. REMOTE SAMPLE CHAMBER MEASUREMENTS

The sample chamber was originally positioned on Devil's Gate Dam, about 2 km from the lidar, with a 24-inch diameter mirror placed behind it to provide atmospheric backscattered signals. Unfortunately, the frame holding the mirror produced such a large backscattered signal that it swamped any atmospheric backscattered signal after the sample chamber.

The sample chamber was then moved to the top of JPL Building 272 on the Mesa east of the lidar location. The distance between the two locations is 500 meters, and the elevation angle, 11 degrees. The nearest hill in the line-of-sight behind the sample chamber on Building 272 is 6 km away, affording ample clear air return from behind the sample chamber.

The lidar transmitter/receiver overlap function was adjusted for optimal operation at just beyond 500 meters, in order to reduce the signal from the sample chamber windows and enhance that from the atmosphere. It was found for weak atmospheric returns that the 2-microsecond laser pulse tail reflected from the windows was stronger than for the atmosphere. While some effort was devoted to reducing the length of the tail by reducing the N₂ flow rate (which also reduced the total pulse energy by a factor of three), the final measurements were made with the long tail, and with the transmitter pointing optimized for atmospheric backscatter.

Measurements of the absorption coefficients for five molecular species were successfully made on December 21 and 22, 1987. Known measured concentrations of each gas was injected into the chamber. Earlier tests had shown that the measurement error was approximately 5 percent, so sufficient material was injected to yield approximately a 20 percent differential absorptance, four times for each material. In making the measurements, the lidar was operated at 30 Hz for about 11 minutes. For each molecular species, material was injected every two minutes, starting at the 2-minute mark ending with the fifth injection. It took about 15 min to change wavelengths for the different species. The chamber was purged only after several materials had been injected, but since the absorption regions of the various species did not strongly overlap, and since the species were not expected to chemically react with each other, this was not expected to affect the results. Unfortunately, the yellow laser channel was too contaminated with RFI to be useful. Consequently, only the red laser channel was used in the analysis. This procedure relies on a constancy of the relative atmospheric backscatter from in front of and behind the sample chamber, which seems to be acceptable for these two days.

The data were processed sets taken over 2-minute intervals. This procedure may tend to give an underestimate of the absorption coefficient since it takes awhile for the muffin fan to thoroughly mix the material in the chamber, especially for those introduced as liquids. Data for each 2-minute interval was referenced to the initial 2-minute interval with no material present. An absorption coefficient was determined for each interval, and the standard deviation of the four determination was taken to be the measurement uncertainty.

The measurement results are tabulated in Table 14. For four of the materials, ethylene, trichloroethylene, trans -1,2 dichloroethylene and chlorobenzene, the laboratory and lidar measurements agree to within the limits of experimental error. For benzene, however, there is a considerable discrepancy. A line with only weak absorption for benzene was used because an earlier version of Reference 57 was used, in which the lines were mislabeled by one (9P(30) has an absorption coefficient of $2.0 \text{ atm}^{-1} \text{ cm}^{-1}$). The published value may be in error, but the values reported in that paper for other materials compare well with measurements reported elsewhere. The 9P(28) line also overlaps with a water vapor absorption line, and if the water vapor concentration were changing during the measurement, that could explain the discrepancy. Also, if the aerosol content were changing in an unusual manner, the results could be explained. Since the project has come to an end, this question will remain unresolved for the time being.

TABLE 14. REMOTE SAMPLE CHAMBER DETERMINED ABSORPTION COEFFICIENTS

Material	CO, Laser Line	Laboratory* Value α ($\text{atm}^{-1} \text{ cm}^{-1}$)	Quantity** Injected (cc)	Sample Chamber Value α ($\text{atm}^{-1} \text{ cm}^{-1}$)
Ethylene	10P(14)	35 ± 2 (Reference 20)	5	32 ± 2
Trichloroethylene	10P(18)	13.1 ± 0.8 (References 58, 61)	0.25	14.5 ± 1.1
Trans -1,2 dichloroethylene	10P(26)	2.42 ± 0.1	1.7	2.6 ± 0.2
Benzene	9P(28)	1.0 (References 55, 58)	2	3.3 ± 0.2
Chlorobenzene	9R(24)	3.2 ± 0.2	3	2.71 ± 0.6

*This study unless noted

**Ethylene was injected as a gas; the others were injected as liquids.

G. RAPID PROCESSING OF DATA

Rapid processing of the lidar data is sometimes more important than accuracy of the results, for example, when MAPM is being used in a field situation and one wants to know whether the molecular species of interest is being detected. The most time-consuming portion of the data analysis is that where the minimum signal is subtracted from the raw data, the resulting values are squared, and the background is subtracted from the squares; the second most time consuming portion is printing the graphs (1-1/2 minutes per graph). The data are usually processed on an individual pulse basis because this approach was considered most accurate. However, there is some question about the validity of this assumption because the electronic noise is convolved with the lidar signal. To determine the impacts on processing speed and measurement accuracy, a set of 4000 pulse pairs was analyzed several times, with the individual pulse pairs taken 1, 3, 10, 30, 100, 300 or 1000 at a time before the squaring step. The processing time decreased from over an hour for the data taken one pulse at a time to about one minute for the data taken 1000 pulses at a time. The family of curves for the averaged squared values is shown for CRUMS7 in Figure 11. Note that as the number of pulses squared at a time increased, the average value at longer ranges decreased. It is thought that the explanation for this result is that the average "background" determined from the pre- or post-lidar signal region using fewer than thirty pulses is not a good average for the entire pulse.

Similar results were obtained with CRUMS6. For CRUMS6,

$$Q = S + n + k \quad (3)$$

where

Q is the total signal

S is the backscattered signal

n is the background noise

and

k is the offset between the minimum value of Q and the average background noise

In the algorithm used in CRUMS6, k is introduced so that there are no negative numbers squared. In CRUMS6, Q is squared, and k^2 is subtracted, giving:

$$Q^2 - k^2 = S^2 + 2S(n+k) + n^2 + 2nk \quad (4)$$

Note that the data presented in Reference 20 were processed one signal at a time using CRUMS6. Since the strong signal results are relatively unaffected by the number of lidar signals added before squaring, the results presented in those papers are still generally sound. However, the backscatter signal beyond 5 or 6 km is exaggerated.

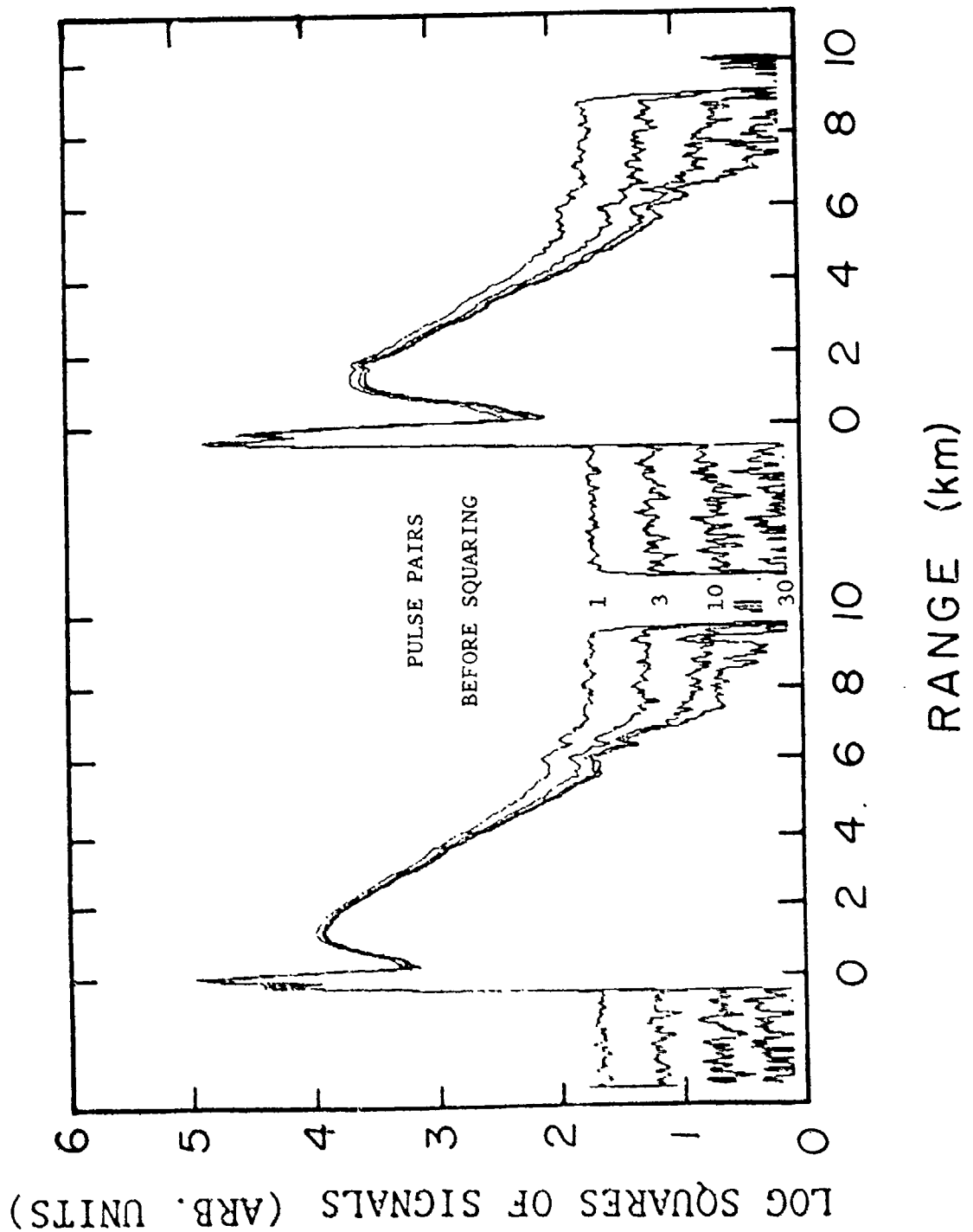


Figure 11.

Values for the Squares of the Lidar Signals (Proportional to Backscattered Power) for Various Numbers of Signals Added before Squaring, (1, 3, 10, 30).

H. MAPM DIAL PERFORMANCE AND SCALING

Data collected were used to determine the concentration uncertainty vs range performance of MAPM. Data from 5 days (November 19, 1986 to March 4, 1987) were used in the analysis, with only those data used where only one local oscillator was incident on the photomixer at a time. This permitted use of earlier data where both pulsed lasers were tuned to the same line, as well as later data when the choppers were in use so that two laser lines could be used. The data chosen were for 4000 to 7000 pulse pairs, and an interval for the derivative, of 510 m. The fluctuations of the derivative for each kilometer from 2 to 10 or 11 km were measured, and converted to a standard deviation by dividing the fluctuations by 2.8. Since data were chosen for which ambient gases, such as water vapor and ozone, did not contribute significantly to the atmospheric extinction, the results are most useful for small amounts of trace gases.

The results of this analysis are shown in Figure 12. For each day, one to three curves were generated, which were averaged for the curves shown in Figure 11. Thus, at intermediate range (2 km), the MAPM measurement uncertainty is reasonably good. However, at greater ranges, the uncertainty increases at a rate given approximately by $R \exp(-0.5R)$, where R is the range (km). What appears to be happening is that at near range, the signal-to-noise ratio (SNR), as calculated from the carrier-to-noise ratio (CNR), is greater than 0.9 (see Reference 64). At greater ranges, the CNR drops, (the atmospheric extinction during the measurement was typically 0.25 km^{-1} due primarily to scattering by aerosols and absorption by water vapor and CO_2).

The small differences in the range dependence of uncertainty for the five data sets have not been analyzed carefully to see whether these are significant effects due to atmospheric extinction and backscatter.

The results from Figure 12 can be scaled up and down to give estimates of system performance for various gases with various differential absorption coefficients. The slope of the curves in Figure 12 have been changed to reflect an atmospheric attenuation of 0.25 km^{-1} and processing by CRUMS7. These results are shown in Figure 13. Typical differential absorption coefficients are given: $1 \text{ atm}^{-1} \text{ cm}^{-1}$ for benzene; $3 \text{ atm}^{-1} \text{ cm}^{-1}$ for hydrazine; $10 \text{ atm}^{-1} \text{ cm}^{-1}$ for ozone; $30 \text{ atm}^{-1} \text{ cm}^{-1}$ for ethylene; $100 \text{ atm}^{-1} \text{ cm}^{-1}$ for chemical agents; and $600 \text{ atm}^{-1} \text{ cm}^{-1}$ for sulfur hexafluoride.

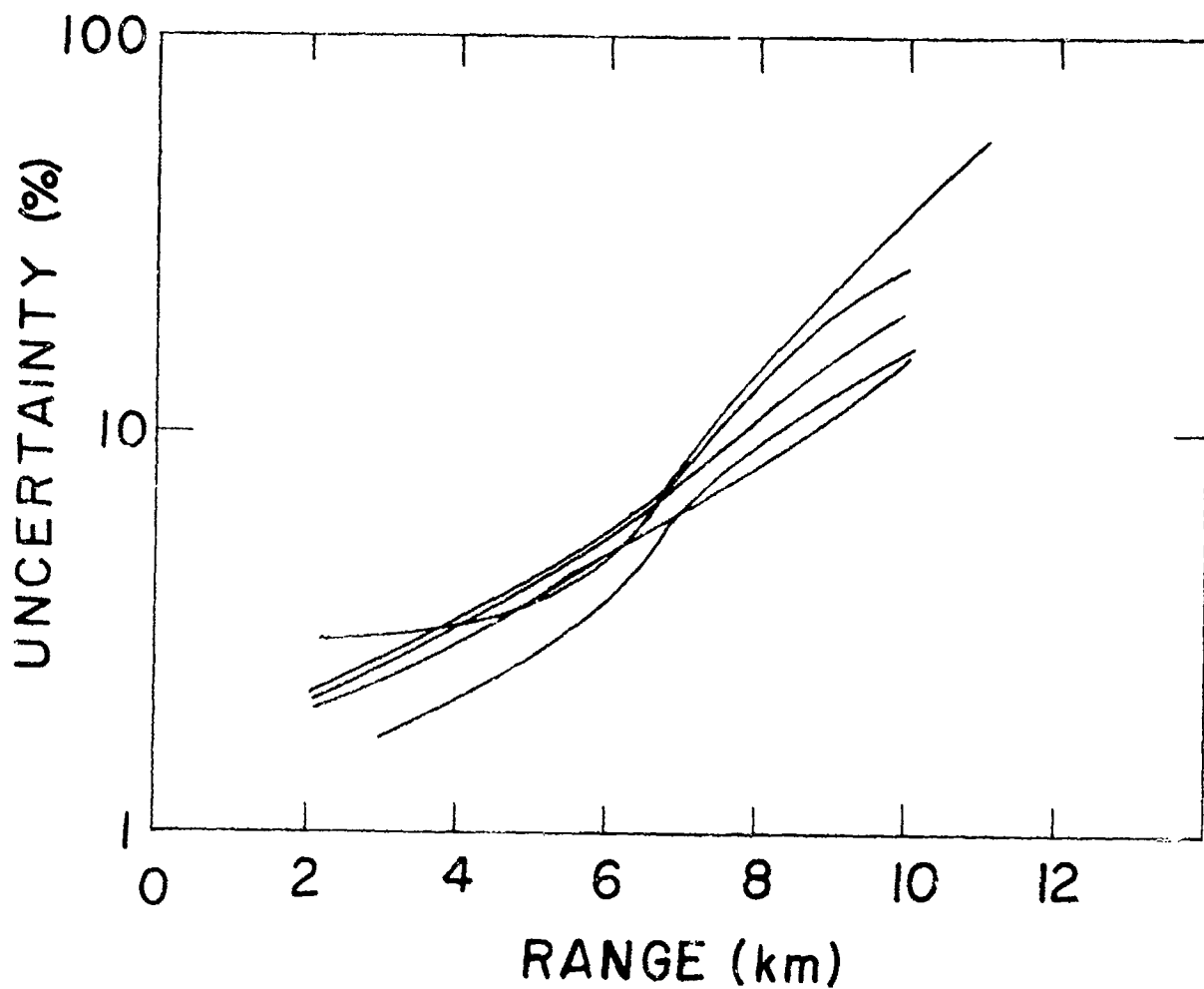


Figure 12. Typical Values for the Standard Deviation of the Derivative of the Lidar Signal as a Function of Range for Several Thousand Pulse Pairs at a Time. (Each Curve is for a Separate Day.)

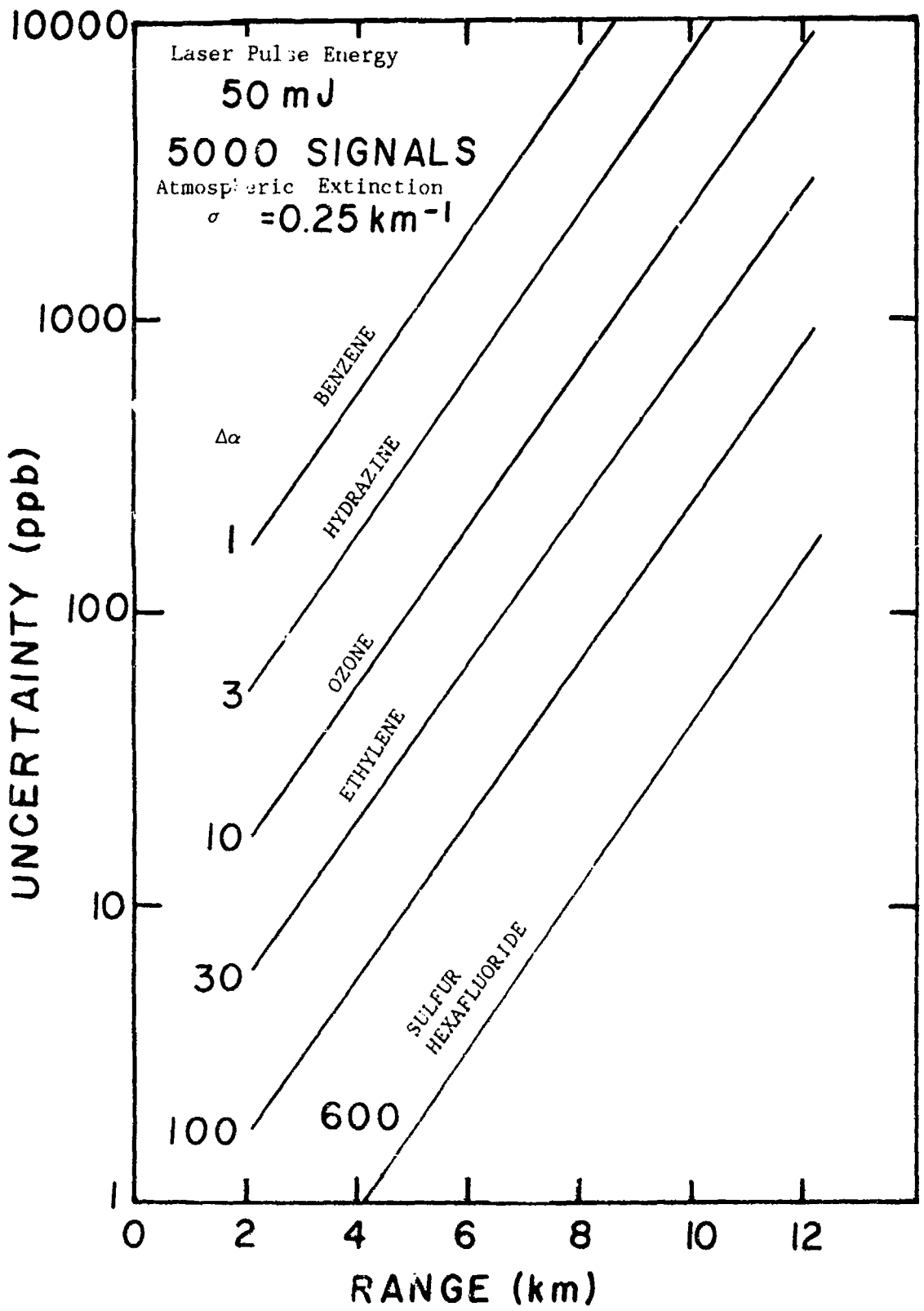


Figure 13. Estimated Performance Levels for Molecular Species with Differential Absorption Coefficients for 5000 Pulse Pairs, 500-m Range Resolution, and Laser Pulsed Energy 50mJ.

SECTION VI

CONCLUSIONS AND RECOMMENDATIONS

A. FINDINGS WITH MAPM

1. Water Vapor

MAPM is able to measure water vapor concentrations in the planetary boundary layer. The measurement results presented were obtained as a first demonstration of MAPM's capabilities, and do not represent the ultimate performance level possible using MAPM. Improved measurements would result from increasing the laser prf and somewhat restricting the measurement range. The choice of laser lines depends on the water vapor concentration and the range of interest. The optimum sensitivity for DIAL measurements occurs when the round-trip differential absorption to the range is equal to unity. For low water vapor concentrations and short ranges, the 10R(20)/10R(18) laser line pair is appropriate; for higher concentrations and/or longer ranges another pair from Table 9 is appropriate.

2. Sample Chamber Measurements

The sample chamber can be used successfully to verify absorption coefficients measured in the laboratory and to verify that the lasers are tuned to the appropriate lines. Four out of five comparisons of absorption coefficients agreed within about 10 percent, which was the combined experimental error of the laboratory and sample chamber measurements. The reason for the discrepancy in the fifth case was not investigated experimentally after the discrepancy was noted, but it is not considered a failing of the approach. The sample chamber is a bit difficult to use with the lidar because the polyethylene windows reflect the laser energy much better than does the atmosphere. When the laser pulse has a long tail, as the LSI lasers generally do, the reflected signal can be larger than the atmospheric backscatter signal for 100 to 200 m beyond the chamber. Two ways around this problem were found; either shorten the laser pulse by reducing the nitrogen content of the laser gas mixture or converge the transmitter and receiver some distance beyond the chamber so that signals due to window reflection are minimized, while still having some return from in front of the chamber.

3. Ethylene Free Release

MAPM was able to adequately map the free release of ethylene out to 1 km over a concentration range from a fraction of a part per million (ppm) over the 75-m path average to the maximum values encountered of 3 ppm in times of ten seconds per measurement. The minimum detectible concentration was not tested in these measurements, but could have been if the processed signal in the absence of ethylene were subtracted from the signals in the presence of ethylene. MAPM was not scanned during the release, relying instead on the wind blowing the gas into and out of the beam. It has been noticed that when the Aerotech mirror mount is scanned, sometimes RFI from the UNIDEX III controller enters the signal chain. This problem would have to be investigated in more detail before using

MAPM to routinely scan. Also, there were no aerosols associated with the plume, which would have increased the measurement error due to interference.

If the molecular species being emitted were unknown or if there were two or more species that had overlapping absorption bands, the DIAL approach would be more difficult to implement. In those cases, it would take longer to perform the measurement, and there might be more ambiguity in the results. An alternative approach is to use a Fourier transform spectrometer (see Ref. 9).

B. PREPARATION OF MAPM FOR TRANSPORT

While MAPM was designed for field use, it has not been fully prepared for transport because the decision was made early in the program to keep MAPM at JPL through the completion of the project funded by the AFESC. The modifications required to make MAPM field operable are relatively minor, and are outlined here.

1. Optics

The optics and optics mounts should be made more secure. Some optics can be better fastened into their mounts or, perhaps, temporarily stowed during transport. The mounts can be made more stable by, for example, adding opposing or locking screws for each adjustment screw or micrometer. Spare components should be obtained for rapid replacement in the field.

2. Equipment

Some of the equipment, such as the transient digitizer and the minicomputer, can be tied down securely to the semitrailer, or packed in boxes for transport.

3. Electrical Generator

An electrical generator should be rented or purchased for field use. The requirements are: voltage - 208-3 phase, power - 30 kVA; regulation - 1-2 percent.

4. Gas Cylinders

A moderate number of size K gas cylinders are required for field operation. At the present gas flow rate settings, a 2000-lb/in² K cylinder with nitrogen lasts 40 hours, with helium - 10 hours, and with carbon dioxide - 80 hours. The premixed gas cylinder for the low pressure gain cell has not been changed in over a year of operation. The present settings were determined by LSI for 150-Hz operation. The flow rates could be reduced for 40 Hz operation, but would require a series of measurements to optimize the settings.

5. Ancillary Equipment

Meteorological parameter monitoring equipment would be useful for temperature, relative humidity, and wind speed.

6. Photomixer

Currently, there are two sizes of photomixer: $0.15 \times 0.15 \text{ mm}^2$ and $0.25 \times 0.25 \text{ mm}^2$. It was found that when the smaller one was used, the signal strength was reduced by about 60 percent, the same as the ratio of the areas of the two photomixers. While the larger size was chosen to be optimal for the receiver optics, it could be that slight optical imperfections on atmospheric turbulence give a somewhat larger Airy spot size in the receiver focal plane. New England Research Center (NERC) can manufacture a $0.35 \times 0.35 \text{ mm}^2$ and a $0.50 \times 0.50 \text{ mm}^2$ photomixer on the same chip, so one should be ordered to determine the optimal photomixer size.

7. Lasers

Spare components should be obtained to avoid costly delays in the field. Components to consider procuring include output couplers, gratings, gas cells, Brewster-angle windows, thyratrons, electronics components, piezoelectric output coupler translators, and other items judged by the manufacturers as likely to fail in the near future.

8. Data System

A color graphics plotter or printer would facilitate obtaining hard copies of the color data displays.

9. Thermostats

The thermostats should be placed in the lidar room so that the temperature can be better regulated. Currently, the temperature is influenced too much by outside temperatures. When it is warm outside, it tends to be below 70° F in the semitrailer, when it is cold outside, it tends to be above 70° F in the semitrailer. Constant semitrailer temperature is important because the optics in and after the laser change position with temperature.

10. Spectral Data

While some information is stored on MAPM for water vapor, and carbon dioxide (from the AFGL spectral data tapes), it would be useful both to upgrade that data set, especially for water vapor, as well as add the available data for absorption coefficients at CO_2 laser line frequencies for other atmospheric trace species.

C. FUTURE USES OF MAPM

Now that MAPM has been developed and demonstrated, but not found to be immediately useful by the Air Force, it is important to try to find uses for MAPM which take advantage of its unique capabilities as well as maintain it in an operating condition. Several ideas have surfaced from ideas at JPL as well as discussions with potential project sponsors. Several of these ideas are outlined here.

1. SF₆ Tracer Studies

MAPM could be used to obtain three dimensional measurements of sulfur hexafluoride (SF₆) released in studies of atmospheric transport and plume dispersion. SF₆ has an extremely high absorption coefficient at the 10P(16) CO₂ laser line (620 atm⁻¹ cm⁻¹, Reference 29), so that concentrations as low as 1-2 ppb can be measured over path lengths of 500 m. SF₆ does not occur naturally, so all SF₆ measured is due to man-supervised releases. SF₆ has been successfully used for atmospheric transport studies at the parts per trillion levels, (for example, Reference 64) and these studies could be extended for higher concentrations, either closer to the source of SF₆ or for higher release rates.

2. Water Vapor Measurements

The ability of MAPM to measure water vapor to an accuracy of about one torr-km for several thousand pulse pairs has been demonstrated at long range. This accuracy can be improved by longer measurement times and the addition of the optical choppers in the local oscillator beam paths, completed subsequent to the bulk of the water vapor measurements. Some of the potential applications include measurement of water vapor in support of atmospheric index-of-refraction determinations for microwave and radiowave propagation studies of water vapor/cloud dynamics, water vapor dispersion in power plant plumes, etc.

3. Aerosol Studies

One type of aerosol study is of aerosol backscatter in the free troposphere in support of the winds measurement from a space-based platform. One set of measurements could be to extend the measurement of the wavelength dependence of aerosol backscatter (Menzies et al., Reference 65) by using the two lasers simultaneously, one at 10.6 micron, the other at 9.25 micron, using ¹³C¹⁸O, or 9.11 micron using ¹³C¹⁶O. Another set of measurements that could be performed simultaneously is to study the time dependence of the aerosol backscatter in a column above the lidar as the atmosphere advects by the lidar site, or the spatial inhomogeneties by using the azimuth scanning capability. Many of the measurements taken of free tropospheric backscatter have been made over periods of 15- 60 minutes, during which time there can be significant variations in the backscatter.

4. Ozone Studies

Ozone is becoming of increasing concern because regions such as the Los Angeles Basin will not be able to meet the U.S. EPA ozone standards. One question in particular that MAPM might be able to address is, "What are the diurnal variations in the concentrations of ozone aloft?" Typically, at night, ozone concentrations near the ground drop to very low values (20- 40 ppb) due to scavenging by NO and lack of photolysis. However, if the concentrations of ozone aloft remain high overnight, when mixing of the atmosphere in the morning brings that layer down to the ground, ozone levels can increase rapidly. If MAPM could be located near where elevated ozone levels occur at night, it might be used to show how the entrainment and remixing occurs.

5. Emissions of Toxic and Hazardous Gases

One of the ideas behind developing MAPM was the desire to measure emissions of toxic and hazardous gases from a variety of sources, including aircraft cleaning, industrial manufacturing, and hazardous waste disposal sites. The absorption coefficients for many gas species have been measured at CO₂ laser line frequencies, and the sensitivity of MAPM to these species can be estimated.

6. Gas-to-Aerosol Conversion Studies

Ammonia reacts with sulfates and nitrates to form aerosols. There are current sources of ammonia such as cattle feed lots, and potential sources, such as doped power plant plumes, with ammonia added to neutralize the sulfur oxides. MAPM, with its potential for measuring ammonia concentrations to long ranges and aerosols simultaneously, as well as water vapor with a short interlude, might be useful in clarifying the ammonia to ammonium conversion process.

D. CONSIDERATIONS FOR MAPM II

If a second-generation version of MAPM were to be constructed, some features might be changed to improve the ease of operation and performance of the system. Several ideas for improvements are outlined here.

The semitrailer could be constructed so that the scan mirror could be in place when the system arrives at a new location. It should be possible to lower the floor by about two feet, and to reduce the floor to ceiling height by about a foot. These changes would allow the dome to be permanently mounted on the roof and still be under the 13 feet 6 inches minimum clearance through underpasses on federal highways. Alternatively, the semitrailer height could be lowered a little and provision made for raising and lowering the scan mirror from inside the trailer, such as with a hydraulic lift. The dome might be segmented so that it could be easily stored.

The entire system should be placed under more automatic control. MAPM presently requires a considerable amount of attention from a skilled operator. Such things as locking the local oscillator to 30 MHz from line center of the pulsed laser, aligning the transmitters with the receiver, using motor drives on the mirror adjustments, and even tuning the lasers to various lines for different molecular species, could be done using control electronics or computers.

The new version should be designed to operate at a much higher prf. MAPM was operated at prf up to 30 Hz, apparently limited by the data acquisition rate and the chopper wheel jitter when a pair of chopper wheels was used to chop the L.O. beams on the photomixer. (It was calculated that the data system should operate at rates up to 45 Hz with the choppers.) Higher prf operation (to 150 Hz with the present lasers or 300 Hz with new lasers from LSI) would allow 10,000 pulse pairs to be collected in about a minute. This is a short time compared with many atmospheric changes of interest, and the amount of data collected would allow fairly accurate measurements of the parameters of interest.

The optics and signal chain electronics could be improved. There are some indications that the $0.25 \times 0.25 \text{ mm}^2$ photomixer is smaller than the Airy spot of the receiver. Also, the electronic noise in the receiver chain seems high, compared with the weak signal at far range. It might be possible to use a cooled preamplifier placed near the photomixer to reduce the electronic noise.

REFERENCES

1. N. Menyuk and D.K. Killinger, "Atmospheric Remote Sensing of Water Vapor, HCl and CH₄ Using a Continuously Tunable Co:MgF₂ Laser," Appl. Opt. **26**, 3061 (1987).
2. G. Fiocco and L.D. Smullin, "Detection of Scattering Layers in the Upper Atmosphere (60-140 km) by Optical Radar," Nature **199**, 1275 (1963).
3. R.M. Schotland, "Some Observations of the Vertical Profile of Water Vapor by a Laser Optical Radar, in Proc. 4th Symp. Remote Sensing of Environ., Univ. of Michigan, Ann Arbor, Mich., 273 (1966).
4. R.L. Byer, "Review (of) Remote Air Pollution Measurement," Opt. and Quantum Electron **7**, 147 (1975).
5. E.D. Hinkley, ed, Laser Monitoring of the Atmosphere, Springer-Verlag, Berlin (1976).
6. V.E. Zuev, Laser Beams in the Atmosphere, Consultants Bureau, New York, NY (1982).
7. D.K. Killinger and A. Mooradian, eds, Optical and Laser Remote Sensing, Springer-Verlag, Berlin (1983).
8. A.I. Carswell, "Lidar Measurements of the Atmosphere," Can. J. Phys. **61**, 378 (1983).
9. W.B. Grant and R.T. Menzies, "A Survey of Laser and Selected Optical Systems for Remote Measurement of Pollutant Gas Considerations," J. Air Poll. Cont. Assoc. **33**, 187 (1983).
10. R.M. Measures, Laser Remote Sensing: Fundamentals and Applications, Wiley, New York, NY (1984).
11. W.B. Grant, "Laser Remote Sensing Techniques," Ch. 8 in Laser Spectroscopy and Its Applications, L.J. Radziemski, R.W. Solarz, and J.A. Paisner, eds, Marcel Dekker, New York, NY, 565 (1987).
12. D.K. Killinger and N. Menyuk, "Laser Remote Sensing of the Atmosphere," Science **235**, 37 (1987).
13. T. Kobayashi, "Techniques for Laser Remote Sensing of the Environment," Remote Sensing Review, **3**, 1 (1987).
14. R.M. Measures, ed, Remote Chemical Analysis, J. Wiley & Sons, New York, NY (1987).
15. E.R. Murray, "Remote Measurement of Gases Using Differential Absorption Lidar," Opt. Engineering **17**, 30 (1978).

16. K.W. Rothe, "Monitoring of Various Atmospheric Constituents Using a cw Chemical Hydrogen/Deuterium Laser and a Pulsed Carbon Dioxide Laser," Radio and Electronic Engineer 50, 567 (1980).
17. P.W. Baker, "Atmospheric Water Vapor Differential Absorption Measurements on Vertical Paths with a CO₂ Lidar," Appl. Opt. 22, 2257 (1983).
18. W. Englisch, W. Wiesemann, J. Boscher, and M. Rother, "Laser Remote Sensing Measurements of Atmospheric Species and Natural Target Reflectivities," in Optical and Laser Remote Sensing, D.K. Killinger and A. Mooradian, eds., Springer-Verlag, Berlin, 38 (1983).
19. R.M. Hardesty, "Coherent DIAL Measurement of Range-Resolved Water Vapor Concentration," Appl. Opt. 23, 2545 (1984).
20. W.B. Grant, J.S. Margolis, A.M. Brothers, and D.M. Tratt, "CO₂ DIAL Measurements of Water Vapor," Appl. Opt. 26, 3033 (1987).
21. E.R. Murray and J.E. van der Laan, "Remote Measurement of Ethylene Using a CO₂ Differential-Absorption Lidar," Appl. Opt. 17, 814 (1978).
22. U. Persson, J. Johansson, B. Marthinsson, and S.T. Eng, "Ethylene Mass Flow Measurements with an Automatic CO₂ Laser Long-Path Absorption System," Appl. Opt. 21, 4417 (1982).
23. R. Asai, T. Itabe, and T. Igarashi, "Range Resolved Measurements of Atmospheric Ozone Using a Differential-Absorption CO₂ Laser Radar," Appl. Phys. Lett. 35, 60 (1979).
24. M.S. Shumate, W.B. Grant, and R.T. Menzies, "Remote Measurement of Trace Gases with the JPL Laser Absorption Spectrometer," in Optical and Laser Remote Sensing, D.K. Killinger and A. Mooradian, eds, Springer-Verlag, Berlin (1983).
25. A.P. Force, D.K. Killinger, W.E. DeFeo, and N. Menyuk, "Laser Remote Sensing of Atmospheric Ammonia Using a CO₂ Lidar System," Appl. Opt. 24, 2837 (1985).
26. N. Menyuk, D.K. Killinger, and W.E. DeFeo, "Laser Remote Sensing of Hydrazine, MMM, and UDMH Using a Differential-Absorption CO₂ Lidar," Appl. Opt. 21, 2275 (1982).
27. T. Fukuda, Y. Matsuura, and T. Mori, "Sensitivity of Coherent Range-Resolved Differential Absorption Lidar," Appl. Opt. 23, 2026 (1984).
28. W.B. Grant, "He-Ne and cw CO₂ Laser Long-Path Systems for Gas Detection," Appl. Opt. 25, 709 (1986).
29. E.E. Uthe, "Airborne CO₂ DIAL Measurement of Atmospheric Tracer Gas Concentration," Appl. Opt. 25, 2492 (1986).

30. R.T. Menzies, "Laser Heterodyne Detection Techniques," in Laser Monitoring of the Atmosphere, E.D. Hinkley, ed., Springer-Verlag, Berlin (1976).
31. J.H. Shapiro, B.A. Capron, and R.C. Harney, "Imaging and Target Detection with a Heterodyne-Reception Optical Radar," Appl. Opt. **20**, 3292 (1981).
32. D.K. Killinger, N. Menyuk, and W.B. DeFeo, "Experimental Comparison of Heterodyne and Direct Detection for Pulsed Differential Absorption CO₂ Lidar," Appl. Opt. **22**, 682 (1983).
33. D.M. Tratt, A.K. Kar, and R.G. Harrison, "Spectral Control of Gain-Switched Lasers by Injection Seeding: Application to TEA CO₂ Systems," Progress in Quantum Electronics **10**, 229 (1985).
34. U.P. Oppenheim and R.T. Menzies, "Aligning the Transmitter and Receiver Telescopes of an Infrared Lidar: a Novel Method," Appl. Opt. **21**, 174 (1982).
35. L.T. Molina and W.B. Grant, "FTIR Spectrometer Determined Absorption Coefficients of Seven Hydrazine Fuel Gases: Implications for Laser Remote Sensing," Appl. Opt. **23**, 3893 (1984).
36. R.T. Menzies, M.J. Kavaya, P.H. Flamant, and D.A. Haner, "Atmospheric Aerosol Backscatter Measurements using a Tunable Coherent CO₂ Lidar," Appl. Opt. **23**, 2510 (1984).
37. L.S. Rothman et al., "The HITRAN Databases: 1986 Edition," Appl. Opt. **26**, 4058 (1987).
38. G. M. Ancellet, M. J. Kavaya, R. T. Menzies, and A. M. Brothers, "Lidar Telescope Overlaps Function and Effects of Misalignment for Unstable Resonator Transmitter and Coherent Receiver," Appl. Opt. **25**, 2886 (1986).
39. D.K. Killinger and N. Menyuk, "Effect of Turbulence-Induced Correlation on Laser Remote Sensing Errors," Appl. Phys. Lett. **38**, 968 (1981).
40. N. Menyuk, D. K. Killinger, and C. R. Menyuk, "Error Reduction in Laser Remote Sensing: Combined Effects of Cross Correlation and Signal Averaging," Appl. Opt. **24**, 118 (1985).
41. W.B. Grant, A.M. Brothers and J.R. Bogan, "Differential Absorption Lidar Signal Averaging," Appl. Opt. **27**, 1934 (1988).
42. M.J.T. Milton and P.T. Woods, "Pulse Averaging Methods for a Laser Remote Monitoring System Using Atmospheric Backscatter," Appl. Opt. **26**, 2598 (1987).
43. G. Ancellet and R.T. Menzies "Atmospheric Correlation-Time Measurements and Effects on Coherent Doppler Lidar," J.O.S.A. **A4**, 367 (1987).

44. J.H. Shapiro, "Correlation Scales of Laser Speckle in Heterodyne Detection," Appl. Opt., 24, 1883 (1985).
45. M. S. Shumate, R. T. Menzies, J. S. Margolis, and L.-G. Rosengren, "Water Vapor Absorption of Carbon Dioxide Laser Radiation," Appl. Opt., 15, 2480 (1976).
46. R. J. Nordstrom, M. E. Thomas, J. C. Peterson, E. K. Damon, and R. K. Long, "Effects of Oxygen Addition on Pressure-Broadened Water-Vapor Absorption in the 10-micron Region," Appl. Opt., 17, 2724 (1978).
47. J. C. Peterson, M. E. Thomas, R. J. Nordstrom, E. K. Damon, and R. K. Long, "Water Vapor-Nitrogen Absorption at CO₂ Laser Frequencies," Appl. Opt., 18, 834 (1979).
48. J. Ryan, M. H. Hubert, and R. A. Crane, "Water-Vapor Absorption at Isotopic CO₂ Laser Wavelengths," Appl. Opt., 22, 711 (1983); Erratum, Appl. Opt., 23, 1302 (1984).
49. G. L. Loper, M. A. O'Neill, and J. A. Gelbwachs, "Water-Vapor Continuum CO₂ Laser Absorption Spectra Between 27° C and -10° C," Appl. Opt., 22, 3701 (1983).
50. J. Hinderling, M. W. Sigrist, and F. K. Kneubuhl, "Laser-Photoacoustic Spectroscopy of Water-Vapor Continuum and Line Absorption in the 8 to 14 Micron Atmospheric Window," Infrared Phys., 27, 63 (1987): private communication.
51. W. B. Grant, "A Critical Review of Measurements of Water Vapor Absorption in the 840 to 1100 cm⁻¹ Spectral Region," JPL Technical Publication No. 87-34, (1987).
52. L. C. Bradley, K. L. SooHoo, and C. Freed, "Absolute Frequencies of Lasing Transitions in Nine CO₂ Isotopic Species," IEEE J. Quantum Electron., QE-22, 234 (1986).
53. D. E. Burch and R. L. Alt, "Continuum Absorption by H₂O in the 700-1200 cm⁻¹ and 2400-2800 cm⁻¹ Windows," Report AFGL-TR-84-0128 to the Air Force Geophysics Laboratory (1984).
54. V. L. Kowalski, "Active Remote Sensing at Hazardous Waste Site," Draft Final Report by Dynamac Corp., to AFESC, Jan. 15, 1987.
55. B. D. Green and J. I. Steinfeld, "Absorption Coefficients for Fourteen Gases at CO₂ Laser Frequencies," Appl. Opt., 15, 1688 (1976).
56. R. J. Brewer and C. W. Bruce, "Photoacoustic Spectroscopy of NH₃ at the 9- and 10-micron ¹³C₁₈O₂ Laser Wavelengths," Appl. Opt., 17, 3746 (1978).
57. J. Boscher, G. Schafer, and W. Wieseemann, "Gasfernalyse mit CO₂-Laser," Battelle Institut e. V., D-6000 Frankfurt am Main, W. Germany (1979).

58. A. Mayer, J. Comera, H. Charpentier, and C. Jaussaud, "Absorption Coefficients of Various Pollutant Gases at CO₂ Laser Wavelengths; Application to the Remote Sensing of those Pollutants," Appl. Opt. 17, 391 (1978); Erratum, Appl. Opt. 19, 1572 (1980).
59. U. Persson, B. Marthinsson, J. Johansson, and S. T. Eng, "Temperature and Pressure Dependence of NH₃ and C₂H₆ Absorption Cross Sections at CO₂ Laser Wavelengths," Appl. Opt. 19, 1711 (1980).
60. G. L. Loper, A. R. Calloway, M. A. Stamps, and J. A. Gelwachs, "Carbon Dioxide Laser Absorption Spectra and Low ppb Photoacoustic Detection of Hydrazine Fuels," Appl. Opt. 19, 2726 (1980).
61. G. L. Loper, and G. R. Sasaki, and M. A. Stamps, "Carbon Dioxide Laser Absorption Spectra of Toxic Industrial Compounds," Appl. Opt. 21, 1648 (1982).
62. R. J. Brewer, C. W. Bruce, and J. L. Mater, "Optoacoustic Spectroscopy of C₂H₂ at the 9- and 10-micron ¹²C¹⁶O₂ Laser Wavelengths," Appl. Opt. 21, 4092 (1982).
63. P. Andersson and U. Persson, "Absorption Coefficients at CO₂ Laser Wavelengths for Toluene, m-xylene, o-xylene, and p-xylene," Appl. Opt. 23, 192 (1984).
64. R. Willson, F. Shair, B. Reynolds, and W. Greene, "Characterization of the Transport and Dispersion of Pollutants in a Narrow Mountain Valley Region by Means of an Atmospheric Tracer," Atmos. Environ. 17, 1633 (1983).
65. R. T. Menzies, M. Kavaya, P. H. Flamant, and D. A. Haner, "Atmospheric Aerosol Backscatter Measurements Using a Tunable Coherent CO₂ Lidar," Appl. Opt. 15, 2510 (1984).

CO₂ DIAL measurements of water vapor

William B. Grant, Jack S. Margolis, Alan M. Brothers, and David M. Tratt

CO₂ lidars have heretofore been used to measure water vapor concentrations primarily using the 10R(20) line at 10.247 μm , which has a strong overlap with a water vapor absorption line. This paper discusses the use of that line as well as other CO₂ laser lines for which the absorption coefficients are weaker. The literature on measurement of water vapor absorption coefficients using CO₂ lasers is reviewed, and the results from four laboratories are shown to be generally consistent with each other after they are normalized to the same partial pressure, temperature, and ethylene absorption coefficient for the 10P(14) CO₂ laser line; however, the agreement with the Air Force Geophysics Laboratory's HITRAN and FASCOD 2 spectral data tapes is not good either for the water vapor absorption lines or for the water vapor continuum. Demonstration measurements of atmospheric water vapor have been conducted using the Mobile Atmospheric Pollutant Mapping System, a dual CO₂ lidar system using heterodyne detection. Results are discussed for measurements using three sets of laser line pairs covering a wide range of water vapor partial pressures.

I. Introduction

There is an interest in measuring atmospheric water vapor concentrations for a variety of reasons, primarily, (1) the hydrological cycle is very important to life and the climate/weather on earth; (2) water vapor interferes with optical measurements of the earth's surface or of other atmospheric constituents, and its measurement is important to compensate for the problem; (3) water vapor affects the index of refraction of the atmosphere, thereby affecting the phase of radio waves; (4) water vapor affects aerosol size distribution and thus visibility, especially for relative humidities above 85%.

Carbon dioxide differential absorption lidar (DIAL) systems have been applied to the study of atmospheric water vapor in several configurations, using atmospheric backscatter and direct detection^{1,2} or heterodyne detection³; topographic backscatter and heterodyne detection⁴; or a retroreflector and direct detection⁵. Note that the use of direct detection with atmospheric backscatter usually limits the measurement range to ≤ 2 km, while heterodyne detection allows the range to be extended to 3–8 km. It should also be noted that the measurements reported hereto-

fore using atmospheric backscatter were made using one laser, which was tuned to the second (reference) line after a large number of measurements were made using the first line. Since atmospheric water vapor and aerosols can change in a few seconds or minutes (see, e.g., Ref. 7), measurement error is introduced using this method. Most of this work was performed using the 10R(20) CO₂ line at 10.25 μm , which has a strong overlap with a water vapor absorption line paired with the 10R(18) line at 10.26 μm as the reference line. Both lines are affected approximately the same by the water vapor continuum.

While other types of lidar system have been used successfully to make range-resolved measurements of water vapor concentrations (notably Nd:YAG-pumped dye lidar,^{8,9} frequency tripled Nd:YAG Raman lidar,⁷ and ruby lidar,¹⁰ CO₂ lidar does have some advantages compared with these lidar systems: measurements can be taken equally well day or night; eye safety is less of a problem; the laser line frequencies are well known; the water vapor absorption coefficients for several CO₂ laser lines are reasonably well known (as will be shown in this paper); and the water vapor absorption coefficients span a large range, permitting measurement of water vapor for various concentrations and distances. All the aforementioned are reasons for the consideration of CO₂ lidar in this particular application.

II. Absorption Coefficients

Before DIAL measurements of water vapor could be made using the Mobile Atmospheric Pollution & Mapping System (MAPMS), we felt that it was important to review the water vapor absorption coefficients in the

1. This work was supported by the Institute of Technology, Jet Propulsion Laboratory, Pasadena, California.

Received February 1987.

0896-6460/87/0203033-05\$01.00/0.

© 1987 The Optical Society of America.

literature and sort out the inconsistencies that existed. The literature was inconsistent because (1) the measurements reported in Refs. 11–15 were not all taken in the same temperature and water vapor partial pressure conditions; (2) the absorption coefficient for ethylene for the 10P(14) CO₂ laser line, which is used to calibrate the spectrophone measurements,^{11,13–15} has not been assumed to have the same value; (3) the first report of the measurements in Ref. 13 gave values that were underestimated because the partial pressure had not been properly determined; and (4) the values reported in Ref. 15 were measured using 100% nitrogen as the buffer gas. The first problem can be mostly overcome by comparing data for 300 K and 10-Torr partial pressure measurements. The data reported in Refs. 11 and 14 were measured in those conditions, while the data reported in Refs. 13 and 15 were measured at 296 K. The results in Ref. 13 could be converted to values at 300 K by using the temperature dependences reported in Ref. 14. The third problem has already been dealt with in the form of an erratum, and revised sets of values are available from the authors of Ref. 13. The fourth problem cannot be dealt with easily, as shown in Ref. 16, since the oxygen-broadening coefficient is ~75% of the nitrogen-broadening coefficient, which can work to make the pure-nitrogen buffer gas values for strong line absorption either higher or lower than air buffer-gas values by ~10%. Thus the values in Ref. 15 are not included in the analysis for line absorption but are included for analysis of the continuum.

The second problem can be overcome by using an average value for the ethylene absorption coefficient at the 10P(14) CO₂ laser line of $35.0 \pm 2.2 \text{ atm}^{-1} \text{ cm}^{-1}$ determined from Refs. 14, 17, and 19–23, as shown in Table I. This excludes the value from Ref. 18, which differs by 2.7σ from the mean for the other seven values. (The authors of Ref. 18 noted that their measurements of ethylene absorption coefficients were consistently lower than those reported in Ref. 17. Also, their values for ammonia absorption coefficients for five strong lines are, on average, 90% of the average values from Refs. 20, 22, 24, and 25.) The values from Ref. 19 were from data reported at 360 Torr, converted to a value at 760 Torr using the pressure dependence measured in Ref. 21. Values reported in Refs. 19, 20, 22, and 23 were corrected to 300 K by multiplying them by a factor that accounted for the temperature dependence of the ethylene absorption measured in Ref. 22 (–5% for a 30 K increase in temperature). Otherwise, the values were accepted as reported. (Some measurements were made using N₂ as the buffer gas, while others were made using synthetic air. While the choice of buffer gas may affect the value, it is not apparent from the data.) This implies an underlying systematic uncertainty of 6.24% in the absolute determination of the water vapor absorption coefficients at CO₂ laser line frequencies, since most experimenters calibrated their measurement apparatus using ethylene as the reference gas. Values from four laboratories^{11–14} were compared for eight ¹²C¹⁶O₂ laser lines.

Table I. Absorption Coefficients for C₂H₄ for 760 Torr, 300 K, at the 10P(14) CO₂ Laser Line

Published value (atm ⁻¹ cm ⁻¹)	Temperature (K)	Adjusted value ^a (atm ⁻¹ cm ⁻¹)	Ref.
35		35	17
29.10	300	29.10	19
33 ^b	293	35.54	13
32.14	292	31.71	20
36.5	300	36.5	21
38.99	297	38.79	22
34.76	300	34.76	14
33.47	285	32.63	23
Average		34.25 ± 2.82	
Average without Ref. 18		34.99 ± 2.18	

^a Adjusted to 760 Torr, 300 K.

^b At 360 Torr, converted to 35.96 atm⁻¹ cm⁻¹ at 760 Torr.

The results of the comparison are shown in Table II. Since the average value for the ethylene absorption coefficient for the 10P(14) CO₂ laser line ($35.0 \text{ atm}^{-1} \text{ cm}^{-1}$) is nearly the same as the value used for calibrating the measurement apparatus in Ref. 14 ($34.76 \text{ atm}^{-1} \text{ cm}^{-1}$), this latter value was used in preparing Table II. The values in Ref. 13 were increased by 0.67% to account for a change in the absorption coefficient of ethylene due to a different temperature.

It is noted that for eleven of thirteen CO₂ laser lines for which there is significant water vapor line absorption, the agreement between the laboratories for the values of the absorption coefficients is better than or equal to 8%. Four of the lines for which the agreement is not so good are lines for which the authors of Ref. 11 reported contamination by ammonia used to clean the glassware (see Ref. 24 for the absorption coefficients). Contamination by ammonia has also been discussed in Refs. 15 and 26. However, aside from the ammonia interference, the four sets of data show satisfactory agreement.

At this point, it is worthwhile to compare the values in Table II with the line values from the 1986 version of the AFGL HITRAN data base²⁷ and the continuum from the AFGL FASCOD 2.²⁸ To make the comparison, computer simulations were made at JPL and AFGL²⁹ of atmospheric transmission for 300 K 10-Torr partial pressure with a 3-MHz bandwidth centered at the laser line frequencies.³⁰ The results of the comparison are shown in Table III, where the CO₂-laser determined values have been adjusted for the current best estimate of the CO₂ 10P(14) laser line ethylene absorption coefficient, $\alpha = 35.0 \pm 2.0 \text{ atm}^{-1} \text{ cm}^{-1}$. Note that the agreement for the water vapor line absorption coefficients is not good. (The discrepancy between the laser-measured values and those calculated using the tape was pointed out previously in Ref. 15 for several CO₂ laser lines.) The significant H₂O line absorptions in this spectral region are mainly pure rotational or ν_2 vibrational band transitions with large values of ΔK_a . The positions and strengths for these, according to Rothman *et al.*²⁷ have been computed using molecular parameters determined from measurements of lines outside this spectral region. The accuracy of these is

Table II. Water Vapor Absorption Coefficients at 300 K, 10-Torr Partial Pressure, and α C₂H₄ = 34.76 atm⁻¹ cm⁻¹, for Selected CO₂ Laser Lines (10⁻⁶ cm⁻¹) for 10 Torr, 300 K

CO ₂ laser line	Shumate ¹¹	Nordstrom ¹²	Ryan ¹³	Loper ¹⁴	Average	Relative uncertainty (%)
10P(40)			13.04		13.04	
10R(20)	13.14		12.03	9.56	11.58 ± 1.45	13
9R(14)	4.19		4.05		4.11 ± 0.09	2
9P(28)	3.25		3.55		3.40 ± 0.15	4
9P(10)	3.37	3.4	3.09		3.29 ± 0.14	4
10R(12) ^a	2.47		2.66	2.51	2.55 ± 0.08	3
9R(30) ^a	1.97	1.8	2.98		2.25 ± 0.52	23
10R(14) ^a	2.09		1.47	2.10	1.89 ± 0.29	16
10R(16)	2.03		1.72	1.70	1.82 ± 0.15	8
10R(22)	1.98		1.68	1.72	1.79 ± 0.13	7
9R(16) ^a	1.91		1.24		1.58 ± 0.34	21
9R(32)	1.52		1.56		1.54 ± 0.02	1
10P(16) ^a	1.41		1.61	1.44	1.49 ± 0.09	6
9R(12)	1.40		1.56		1.48 ± 0.08	5
10R(18)	1.46		1.38	1.35	1.40 ± 0.05	3
10P(20)	1.37		1.17	1.25	1.26 ± 0.08	7
9R(18)	1.18		0.70		0.97 ± 0.25	25
10R(10) ^a	0.88		0.87	1.13	0.96 ± 0.12	12

^a Ammonia interference possible for this CO₂ laser line.

Table III. Comparison of Water Vapor Absorption Coefficients Determined Using CO₂ Lasers with the Values on the AFGL Spectral Data Tapes for 10-Torr Partial Pressure, 300 K, α C₂H₄ = 35.0 atm⁻¹ cm⁻¹

Designation	CO ₂ laser line frequency ^a (cm ⁻¹)	CO ₂ laser value ^b (10 ⁻⁶ cm ⁻¹)	AFGL value ^c (10 ⁻⁶ cm ⁻¹)
10P(40)	924.9740	13.13 ± 1.7	20.5
10R(20)	975.9304	11.65 ± 1.68	10.4
9R(14)	1074.6465	4.14 ± 0.22	1.87
9P(28)	1039.3693	3.42 ± 0.25	1.63
9P(10)	1055.6251	3.31 ± 0.25	2.28
10R(12)	970.5472	2.56 ± 0.18	2.03
9R(30)	1084.6351	2.27 ± 0.54	0.62
10R(14)	971.9303	1.90 ± 0.33	0.88
10R(16)	973.2885	1.83 ± 0.19	1.08
10R(2)	977.2139	1.80 ± 0.17	1.04
9R(16)	1075.9878	1.59 ± 0.35	1.00
9R(32)	1085.7654	1.55 ± 0.10	0.75
10P(16)	947.7420	1.50 ± 0.13	1.05
9R(12)	1073.2785	1.49 ± 0.12	1.57
10R(18)	974.6219	1.41 ± 0.10	0.79
10P(20)	944.1940	1.37 ± 0.12	0.88
9R(18)	1077.3025	0.95 ± 0.26	0.55
10R(10)	969.1395	0.91 ± 0.12	0.72

^a Ref. 30.

^b Includes 6.24% uncertainty due to the uncertainty in determining the value of the ethylene absorption coefficient for the 10P(14) CO₂ laser line.

^c JPL and AFGL²⁹ determinations estimated to be accurate to 10%.

claimed to be 20% for the line strengths and 0.002 cm⁻¹ for their positions. The disagreement between the measurements and the AFGL predictions seems too large, in many cases, to be accounted for with this level of uncertainty. One contributing factor may be the difference in the values of the continuum absorption, which is discussed below. However, the major cause of the discrepancy is probably that the water vapor spectral line data on the AFGL tape was determined

using theoretical calculations with a sparse amount of experimental data from spectral regions outside the 9–11- μ m region. In any case, it seems clear that accurate spectroscopic measurements of the H₂O line absorptions in this spectral region are needed.

It is also interesting to see whether the CO₂ laser determined values of water vapor absorption coefficients can be used to provide input in trying to understand the continuum absorption. Following Clough *et al.*^{31,32} we define the continuum as the unstructured portion of the water vapor absorption spectrum, excluding calculable contributions from the wings of lines within ~ 25 cm⁻¹. (Note that this definition is not unique, since a different interval could be used, and that it depends on the line data, which seems to be in error.) To select laser frequencies for this effort, the first step was to choose laser lines for which low-absorption coefficient data are available from at least three laboratories, so that the statistical reliability of the data can be assessed. The second step was to check using HITRAN^{27,29} whether there is appreciable absorption from water vapor lines out to 25 cm⁻¹, rejecting any lines for which the wings contributed more than 3% of the strength. These two screening steps left twelve frequencies for evaluation.

A comparison of the CO₂ data along with the results of the computer calculations, all for 300 K and 10 Torr of water vapor in a total pressure of 760 Torr, is given in Table IV. There are some problems apparent with the CO₂ laser data: only the data by Ryan *et al.*¹³ show a strong frequency dependence; also, the statistical and systematic standard deviation averages $\sim 16\%$, which is not as good as for the stronger line absorption data. Nonetheless, there is a reasonable degree of agreement among the data.

However, the AFGL values are significantly lower than the CO₂ laser values— 0.3×10^{-6} cm⁻¹ or $\sim 25\%$ in the 10- μ m band and 40% in the 9- μ m band.

Table IV. CO₂-Laser Determined Values for the Water Vapor Continuum Absorption for 300 K, 10-Torr Partial Pressure, 760-Torr Total Pressure

CO ₂ Laser line	Frequency (cm ⁻¹)	Shumate ¹¹ (10 ⁻⁶ cm ⁻¹)	Nordstrom ¹² (10 ⁻⁶ cm ⁻¹)	Ryan ¹³ (10 ⁻⁶ cm ⁻¹)	Loper ¹⁴ (10 ⁻⁶ cm ⁻¹)	Hinderling ¹⁵ (10 ⁻⁶ cm ⁻¹)	Average ^a	AFGL ^b
10P(28)	936 804	1.05		1.20	1.30	0.88	1.11 ± 0.17	0.82
10P(26)	938 688	1.07		0.92	1.21	0.86	1.02 ± 0.15	0.81
10P(22)	942 383	1.13		1.34	1.17	0.97	1.15 ± 0.15	0.80
10P(18)	945 980	1.20		0.94	1.17	0.88	1.05 ± 0.15	0.81
10R(10)	969 139	0.89		0.88	1.13	0.72	0.91 ± 0.16	0.73
9P(30)	1037 434	0.93		0.86		0.95	0.91 ± 0.09	0.61
9P(26)	1041 279	0.93		1.14		0.88	0.98 ± 0.13	0.60
9R(18)	1077 303	1.19		0.71		0.99	0.96 ± 0.21	0.58
9R(20)	1078 501	1.12		0.78		0.97	0.96 ± 0.15	0.58
9R(22)	1079 852	1.09		0.62		0.97	0.88 ± 0.21	0.57
9R(26)	1082 296	1.01	0.99	0.65		0.96	0.90 ± 0.16	0.57
9R(28)	1083 478	1.12	0.80	0.67		0.95	0.89 ± 0.18	0.57

^a Includes the uncertainty in the ethylene absorption at the 10P(14) CO₂ laser line.

^b Refs. 27, 28, 29

This represents two standard deviations for the CO₂ laser data or about four standard deviations for the AFGL values. Note that FASCOD 2 was adjusted from LOWTRAN 6 recently to agree more closely with the recent measurements using a spectrometer with a resolution of 0.3 cm⁻¹ by Burch and Alt,³³ who heated the mirrors in their white cell to prevent adsorption of water vapor on them, resulting in values of the self-broadening coefficient at 296 K varying from 20% lower than LOWTRAN 6 near 11 μm to 40% lower near 9 μm. Thus the CO₂ laser data for 300 K are nearly consistent with the LOWTRAN 6 values, which were based on the earlier work by Burch.³⁴ Also note that if the respective continuum values are subtracted from the two sets of absorption coefficients in Table III that the number of laser line frequencies for which the two absorption coefficients agree within experimental error jumps from two to seven.

There have also been attempts to measure the water vapor continuum absorption coefficients using broadband techniques with long atmospheric paths. Such work has been reported by Kneizys *et al.*,³⁵ Cutten,³⁶ and Ben-Shalom *et al.*³⁷ Reference 35 seemed to find reasonable agreement with LOWTRAN 6, while Refs. 36 and 37 seemed to find values ~20% or more less than for LOWTRAN 6. While such measurements have the advantage of a large attenuation, they also have a number of difficulties: calibration is difficult; the atmosphere may be inhomogeneous (see, e.g., Ref. 7 for water vapor); other gases, such as carbon dioxide and ozone, interfere; aerosol scattering is difficult to account for^{38,39} and should be based more on analysis of captured aerosols than on visibility; the temperature cannot be controlled; and the spectral resolution makes it more difficult to measure just the continuum.

In our opinion, the strength of the water vapor continuum absorption for the 9–11-μm spectral region is not a fully resolved issue at this time, and there is also some question as to the temperature dependence.⁴⁰ There appears to be good evidence both for values near the present FASCOD 2 values as well as for the older LOWTRAN 6 values. The discrepancy exists mainly between the optoacoustic measurements and the spectroscopic measurements. Because of the consistency

of the independent determination of the optoacoustic measurements, they cannot be lightly rejected. We suggest that it is important to resolve the difference with new measurements and a more careful evaluation of the previous measurements.

III. CO₂ Laser Line Pairs for Remote Measurements of Water Vapor

It is important to evaluate which CO₂ laser line pairs are most useful with CO₂ DIAL lidar for remote measurements of water vapor. The lines listed in Tables III and IV form the starting point for this evaluation. First, those lines for which significant spectral interference from normally occurring molecular species is expected can be eliminated. These include the 9P(10) and 9P(26) lines for which ozone is the interferent¹⁸ and the 9R(30) line for which ammonia is the interferent.²⁴ Second, those lines that are difficult to reach using CO₂ lasers can also be eliminated: the 10P(40) line falls in this category. The remaining line pairs with medium to strong differential absorption coefficients are listed in Table V. Note that because the pairs are formed with small separations between the CO₂ laser lines, the contribution from the water vapor continuum is expected to be nearly the same for both lines of the pair; hence complications arising from the continuum can largely be ignored.

The temperature dependence of the differential absorption coefficients can also be determined from Refs. 12, 14, 15, and 27. Values determined for a few-degree interval at ~300 K are given in Table V. Note that the change in Δα with *T* is ~2%/°C for the 10R(20)/10R(18) laser line pair. Thus an uncertainty in the knowledge of atmospheric temperature by 5°C gives a 10% measurement uncertainty.

Interference due to CO₂ can also be calculated. Values from Ref. 21 for differential absorption coefficients appropriate to the CO₂ line pairs in Table V are given.

With a choice of about five CO₂ laser line pairs with various differential absorption coefficients Δα for measuring atmospheric water vapor concentrations *c*, the appropriate pair can be chosen for Table IV for the expected concentration and the range *l* of the measurement. It was shown in Ref. 39 that the optimum

Table V. CO₂ Laser Line Pairs Useful for Water Vapor Measurements

CO ₂ laser lines		$\Delta\alpha$ for 10 Torr, 300 K (10 ⁻⁶ cm ⁻¹)	Uncertainty (10 ⁻⁶ cm ⁻¹)	Temperature dependence (%/°C)	Differential absorption coefficient for CO ₂ (atm ⁻¹ cm ⁻¹) ^a
Signal	Reference				
10R(20)	10R(18)	10.67	1.68	2.1	-1.5E-4
9R(14)	9R(18)	3.18	0.31	1.9	-3.0E-5
9R(14)	9R(12)	2.65	0.25	2.4	+2.1E-4
10R(12)	10R(10)	1.58	0.22	3.4	+2.6E-4
10R(12)	10R(18)	1.15	0.21	3.7	-1.5E-4

^a Ref. 21.

Table VI. Lidar System Parameters

Transmitters	
Two each hybrid TEA CO ₂ lasers	
Pulse energy:	40-50 mJ
Pulse length:	gain-switched spike - 250-300 ns total, including tail - 1.2 μ s
Delay between firings:	101.6 μ s
Pulse repetition frequency:	15-20 Hz
Divergence:	0.2 mrad
Receiver	
Diameter:	22 cm
Field of view:	0.16 mrad
Local oscillator frequency offset:	30 MHz
Electronics passband:	10 MHz
Filter:	flat phase, 0.4-2.5 MHz
Envelope detection (square root of power)	
Transient digitizer	
Sampling:	5 MHz
Resolution:	10 bit
Accuracy:	7.8 bit

condition is that for which the exponential term $2\Delta\alpha cl$ is equal to unity.

IV. Remote Measurements of Water Vapor Using MAPM

To test the accuracy of the new set of values for the water vapor absorption coefficients and demonstrate the measurement capability of the MAPM, a dual CO₂ laser DIAL lidar system using heterodyne detection (Ref. 40 and Table VI), measurements were made for three days with different atmospheric concentrations of water vapor.

The first day was 12 Nov. 1986. Measurements were made at $\sim 2^\circ$ below the horizon between 1:28 and 2:05 p.m. At 12:00 noon, the ambient temperature at the lidar site was 26.2°C, the relative humidity was 18% (measured using a psychrometer), implying a water vapor partial pressure of 4.6 Torr. At 2:43 p.m., the temperature was 26.8°C, the RH 12%, and the water vapor partial pressure 3.2 Torr. Thus these represent conditions for which the 10R(20)/10R(18) laser line pair is expected to be the most useful. Although considerable effort was expended to align the two laser transmitters so that they would have the same overlap function with the receiver, perfect alignment was not achieved; however, the ratio and the derivative for the 10R(18)/10R(18) laser operating condition can be used to correct other measurements.

DIAL measurements are, of course, based on the Beer-Lambert-Bouguer law:

$$P/P_0 = \exp(-2\Delta\alpha cl), \quad (1)$$

where P is the two-way transmitted power (W);
 P_0 is the incident power (W);
 $\Delta\alpha$ is the differential absorption coefficient
(atm⁻¹ cm⁻¹);
 c is the concentration (atm), and
 l is the path length (m).

Equation (1) can be used to yield concentration values by taking partial derivative of the logarithm of the equation with respect to path length:

$$c = \frac{-1}{\Delta\alpha} \frac{\delta \log(P/P_0)}{\delta l}. \quad (2)$$

Since the signal recorded is proportional to the square root of the backscatter power and since the electronic noise level can be large compared with the signal, a data processing algorithm had to be developed to subtract the background and square the remaining signal. Three approaches were tried on an individual pulse basis after smoothing: (1) subtract the mean prepulse noise level, square the remaining values, and set the squares of negative numbers negative; (2) same as (1) but set the squares of negative numbers negative; (3) subtract the minimum noise level, then square the remaining values. There are problems associated with all three approaches: in (1) setting squares of negative numbers negative may be mathematically unsound, and it reduces the importance of weak signal levels; in (2), a large value for the data beyond the signal return is found; it could be due to a slight base line shifts during the measurements; in (3) weak signals are boosted somewhat in importance because of cross terms with the noise. Of the three approaches, (3) was judged to be the most accurate and was used for the results reported here. In comparison with (1), it gave useful DIAL measurements to a somewhat longer range and with greater accuracy (see Ref. 40).

The data for each pulse were first checked to see that the signal was above a desired minimum value and, if so, smoothed over 210 m, the minimum noise level subtracted, the remaining values squared, and then summed with other returns. The total sum of signals for each laser was then rationed. The derivative of the logarithm of the ratio was then calculated using a parabolic fit to 450 m of data in a running fashion.

Computer plots were made of the logarithm of the signals, the log of the ratio, and the derivative of the log of the ratio. The slope was normalized for a 30-m range element to simplify analysis when the width of the derivative is varied.

Experimental results are shown in Figs. 1-6. Figure 1 shows the squared averaged values, the ratio, and the derivative for 2831 pulse pairs of 10R(18)/10R(18) at 1:50 p.m. The value of the derivative calculated for a 450-m path, but normalized for a 30-m path, from 1.5 to 5 km is 0.004, which represents the offset due to the alignment mismatch. This value should be subtracted from values determined for other line pairs. Figure 2 shows results for 1836 pulse pairs of the 10R(20)/10R(18) laser line pair at 1:38 p.m. The strong absorption by water vapor is quite evident in the averaged lidar signals. The value of the 30-m derivative is -0.018 ± 0.0035 (including 0.004 from Fig. 1 and noting that the sign of the derivative depends on the order of the two laser lines in the ratio) from 1.5 to 5 km, which corresponds to 3.3 ± 0.7 Torr of water vapor. (When the uncertainty of the absorption coefficients is included, the measurement uncertainty increases to 0.8 Torr.) This value is intermediate between the local values measured before and after the lidar measurement. Note that, although the ratio has the same slope over most of its range, the measurement was a true range-resolved measurement of a homogeneous water vapor distribution.

The results in Fig. 3 for 2567 pulse pairs of the 10R(12)/10R(18) line pair at 2:02 p.m. give a derivative of 0.007 (including 0.004 from Fig. 1) ± 0.005 from 1.7 to 6 km. This corresponds to a partial pressure of water vapor of 5.2 ± 4.6 Torr (± 4.7 Torr including absorption coefficient uncertainty), which is close to that measured with the 10R(20)/10R(18) line pair but to a larger range and greater uncertainty or reduced range resolution. If 10,000 pulse pairs had been used, the statistical uncertainty should have dropped to ± 2.3 Torr.

The second measurement day was 19 Nov. 1986, when the water vapor partial pressure, derived using the psychrometer, was 10.2 ± 0.5 Torr. Figure 4 shows results for 1452 pulse pairs of the 10R(20)/10R(18) line pair taken at 5:00 p.m. when the dry bulb temperature was $\sim 15^\circ\text{C}$ and the RH 77%. Note that the signal from the 10R(20) line falls into the noise after 4 km. The ratio is useful only in the region of 1.5-2.4 km because of the high extinction coefficient. Within this region, the ratio is 0.056, corresponding to 11.8 ± 0.8 Torr (± 1.5 including the absorption coefficient uncertainty). The small bump near 3.5 km, attributed to RFI due to a loose SMA connection, caused some inaccuracy in the measurement. The problem was diagnosed and rectified at the end of December.

Figure 5 shows the results for 4397 pulse pairs of the 10R(12)/10R(18) line pair taken at 4:30 p.m. when the temperature was $\sim 16.5^\circ\text{C}$ and the RH 74%. The shape of the ratio before 2.3 km is due to differences in the overlap of the two transmitters with the receiver.

The value of the derivative from 2.3 to 6 km is ~ 0.005 , which corresponds to 14 ± 5 Torr of water vapor.

Figure 6 shows the results using the 9R(14)/9R(18) laser line pair, appropriate for intermediate water vapor partial pressures. During the measurement period on 31 Dec. 1986, the psychrometer measured an ambient temperature of $15-16^\circ\text{C}$ and a water vapor partial pressure of 3.1-3.5 Torr. The visibility was judged to be 10-12 km, affected primarily by haze. The lidar value from 5839 signals from 1.0 to 2.8 km was 5 ± 2 Torr. While the statistical fluctuation was reduced by including more lidar signals in the measurement, the discrepancy between the lidar and the point measurements is puzzling. It may be due to a slight pointing misalignment in changing lines, as discussed above, or to some inaccuracy in the water vapor absorption coefficients, including the temperature correction applied.

The measurement results are summarized in Table VII. The measurements made when the temperature was 26.5°C agree well with the psychrometer measurements, while those made at $15-16.5^\circ\text{C}$ are somewhat higher, although still within experimental error when the uncertainty of the absorption coefficients is included.

In Ref. 40, it was shown that for averaging over 450 m and using 1000 pulse pairs, the standard deviation of the ratio was $\sim 10\%$ and that it improved as $N^{1/2}$, where N is the number of lidar pulse pairs averaged, as long as the atmosphere was relatively stationary and the ratio did not change. These values are generally what is shown in the data in Figs. 1-6 (3-10%). While it would have been desirable to take up to 10,000 pulse pairs for the measurements reported here, the disk capacity was limited to 35,000 pulse pairs, and it would take over an hour to archive the data onto tape; consequently, to make a variety of measurements in a limited amount of time, only 3000-5000 pulse pairs were recorded for each measurement. We are investigating obtaining a reel-to-reel tape drive for data acquisition.

The data presented in this paper are to be considered preliminary in regard to the ultimate performance of MAPM. Already, one significant improvement has been the addition of two mechanical light choppers to limit the local oscillator radiation on the photomixer to one at a time. This improves the SNR by a factor of ~ 2 . Recent measurements indicate that this improvement extends the measurement range out of ~ 8 km for weak absorptions and improves measurement accuracy. Also, the laser prf can be increased to ~ 45 Hz from the 15-20 Hz used for the data reported here. In a full 10,000 pulse pairs are used to acquire the data and improve the measurement accuracy, this takes ~ 4 min. While the ultimate limit to the range resolution is dictated by the gain switched spike (45 m), the transient digitizer (30 m), and the requirement to use at least three range bins, to be ~ 100 m. However, the measurement accuracy would degrade as the path length is reduced, the time-varying concentrations of water vapor would also affect the results.

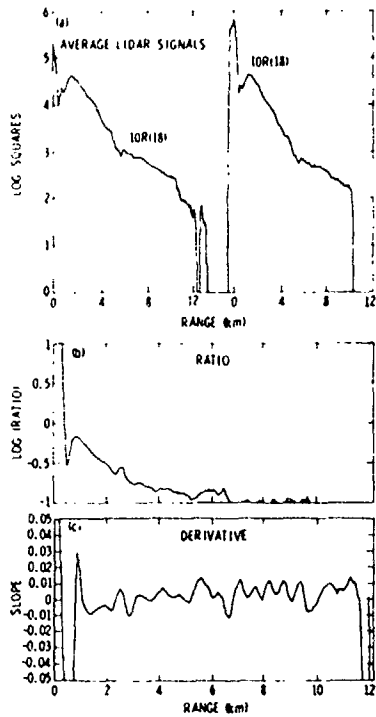


Fig. 1. Averaged signals, ratio, and derivative for the 10R(18)/10R(18) line pair taken at 1:50 p.m. on 12 Nov. 1986.

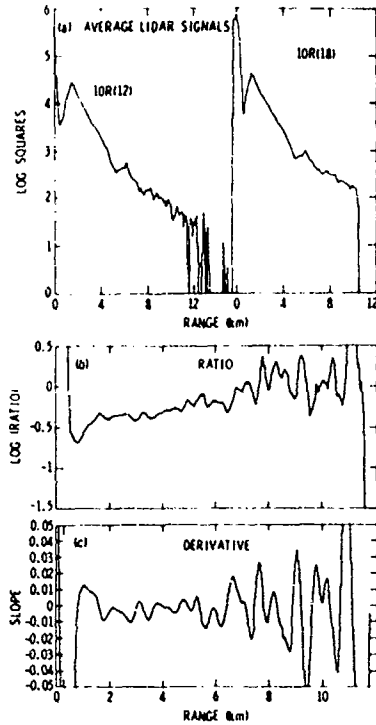


Fig. 3. Same as for Fig. 1 but for the 10R(12)/10R(18) line pair taken at 2:02 p.m. on 12 Nov. 1986.

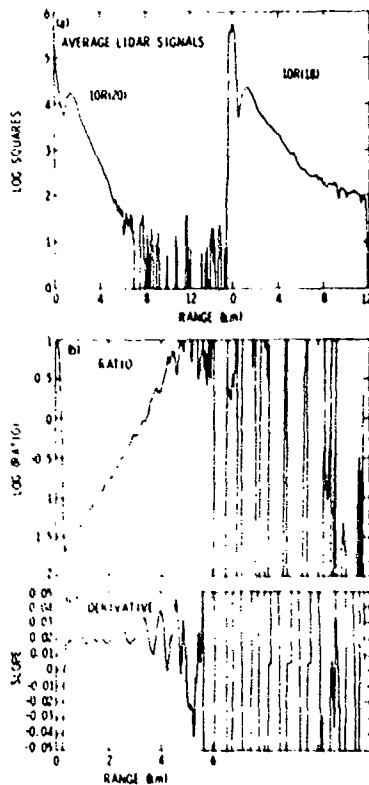


Fig. 2. Same as for Fig. 1 but for the 10R(20)/10R(18) line pair taken at 1:38 p.m. on 12 Nov. 1986.

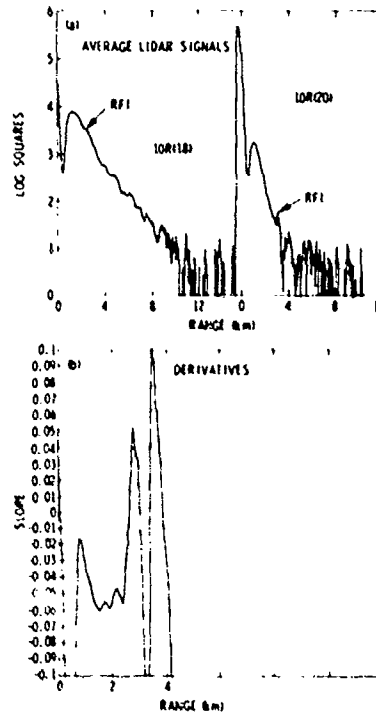


Fig. 4. Averaged signals and derivative for the 10R(20)/10R(18) line pair taken at 5:00 p.m. on 19 Nov. 1986.

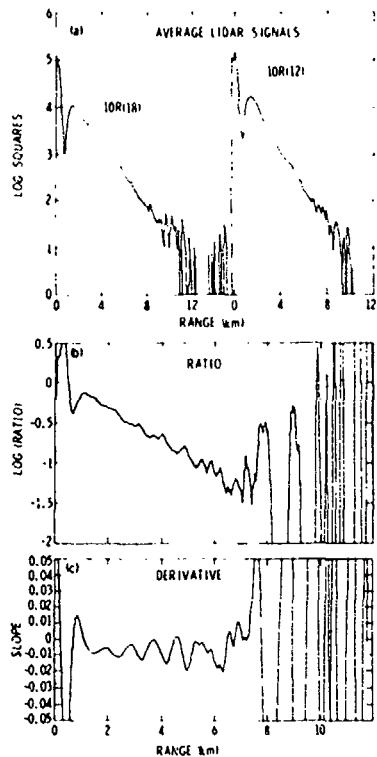


Fig. 5. Same as for Fig. 3, but for data taken at 4:30 p.m. on 19 Nov. 1986.

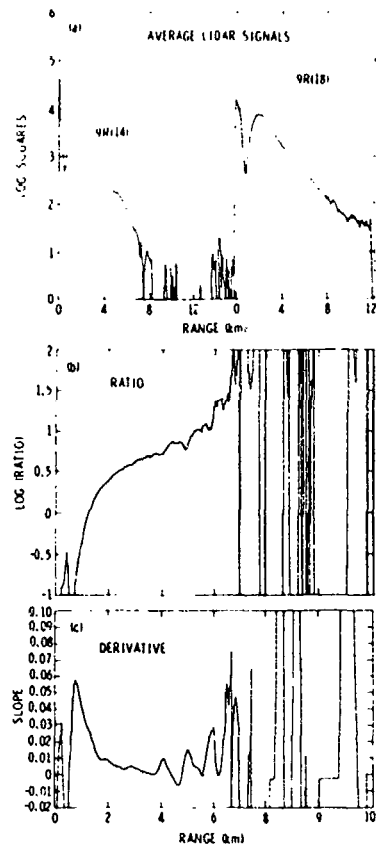


Fig. 6. Averaged signals and derivative for 5839 lidar pulse pairs, the 9R(14)/9R(18) line pair taken at 11:50 a.m. on 31 Dec. 1986.

Table VII. Summary of Water Vapor Measurements

Day	Time	Psychrometer			Δn (10^{-6} cm^{-1})	Number of pulse pairs	MAPM	
		Temperature (°C)	Water vapor concentration (Torr)	CO ₂ laser line pair			Water vapor concentration ^a (Torr)	Measurement range (km)
11/12/86	1:38 p.m.	26.5	3.9 ± 0.7	10R(20)/10R(18)	10.7	1836	3.3 ± 0.8	1.5-5
11/12/86	2:02 p.m.	26.5	3.9 ± 0.7	10R(12)/10R(18)	1.1	2567	5.2 ± 4.7	1.7-6
11/19/86	5:00 p.m.	15	10.2 ± 0.5	10R(20)/10R(18)	8.0	1452	11.8 ± 1.5	1.5-2.4
11/19/86	4:30 p.m.	16.5	10.2 ± 0.5	10R(12)/10R(18)	0.7	4397	14.0 ± 5.0	2.3-6
12/31/86	11:50 a.m.	15.5	3.3 ± 0.2	9R(14)/9R(18)	2.5	5839	5.0 ± 2.0	1.0-4.3

^a This value includes both the lidar random measurement error and absorption coefficient uncertainty.

V. Conclusion

The water vapor absorption coefficients at twenty-eight CO₂ laser line frequencies available in the literature were shown to agree within 1-23% if corrections are made for different assumed values of the ethylene absorption coefficients at the 10P(14) CO₂ laser line. The worst agreements were primarily for those lines where ammonia also absorbs strongly and for the weaker continuum absorptions. The CO₂ laser determined absorption coefficients were compared with values calculated using the AFGL spectral data tapes, and significant differences were found both for the strong water vapor absorption lines as well as for the continu-

um. A number of CO₂ laser line pairs were evaluated for possible use in the remote sensing of water vapor concentrations, and five pairs were assessed as viable. Remote measurements were made using MAPM showing the general suitability of the absorption coefficients and line pairs chosen and the usefulness of a coherent CO₂ DIAL system for such measurements.

The authors would like to thank R. T. Menzies, G. Ancellet, G. L. Ioper (Aerospace Corp.), B. J. Rye (U. Hull), R. M. Hardesty (NOAA), and S. A. Clough (AFGL) for useful discussions. The research described in this paper was carried out by the Jet Propulsion Laboratory, California Institute of Technology,

and was sponsored jointly by the U.S. Air Force and the National Aeronautics and Space Administration. The authors specifically acknowledge the support of the Air Force Engineering and Services Center, Tyndall AFB, FL, and the John F. Kennedy Space Center.

References

1. E. R. Murray, "Remote Measurement of Gases Using Differential Absorption Lidar," *Opt. Eng.* **17**, 30 (1978).
2. K. W. Rothe, "Monitoring of Various Atmospheric Constituents Using a New Chemical Hydrogen/Deuterium Laser and a Pulsed Carbon Dioxide Laser," *Radio Electron. Eng.* **50**, 567 (1990).
3. P. W. Baker, "Atmospheric Water Vapor Differential Absorption Measurements on Vertical Paths with a CO₂ Lidar," *Appl. Opt.* **22**, 2257 (1983).
4. W. Englisch, W. Wiesemann, J. Boscher, and M. Rother, "Laser Remote Sensing Measurements of Atmospheric Species and Natural Target Reflectivities," in *Optical and Laser Remote Sensing*, D. K. Killinger and A. Mooradian, Eds. (Springer-Verlag, Berlin, 1983), p. 38.
5. R. M. Hardesty, "Coherent DIAL Measurement of Range-Resolved Water Vapor Concentration," *Appl. Opt.* **23**, 2545 (1984).
6. S. L. Jain, B. C. Arya, D. R. Nakra, and A. K. Saha, "Differential Absorption Measurements of Atmospheric Minor Constituents with a Laser-Water Vapour," *Ind. J. Radio Space Phys.* **15**, 29 (1986).
7. S. H. Melfi and D. Whiteman, "Observations of Lower-Atmospheric Moisture Structure and its Evolution Using a Raman Lidar," *Bull. Am. Meteorol. Soc.* **66**, 1288 (1985).
8. C. Cahen, G. Megie, and P. Flamant, "Lidar Monitoring of the Water Vapor Cycle in the Troposphere," *J. Appl. Meteorol.* **21**, 1506 (1982).
9. E. V. Browell, "Remote Sensing of Tropospheric Gases and Aerosols With an Airborne DIAL System," in *Optical and Laser Remote Sensing*, D. K. Killinger and A. Mooradian, Eds. (Springer Verlag, Berlin, 1983), p. 138.
10. V. V. Zuev, V. E. Zuev, Yu. S. Makushkin, V. N. Marichev, and A. A. Mitsel, "Laser Sounding of Atmospheric Humidity: Experiment," *Appl. Opt.* **22**, 3742 (1983).
11. M. S. Shumate, R. T. Menzies, J. S. Margolis, and L.-G. Rosengren, "Water Vapor Absorption of Carbon Dioxide Laser Radiation," *Appl. Opt.* **15**, 2480 (1976).
12. R. J. Nordstrom, M. E. Thomas, J. F. Donovan, and D. Gass, "Atmospheric Water Vapor Absorption at 12 CO₂ Laser Frequencies," Final Report 711934-1 by the Ohio State U., ElectroScience Laboratory for the Jet Propulsion Laboratory (Sept. 1979).
13. J. Ryan, M. H. Hubert, and R. A. Crane, "Water-Vapor Absorption at Isotopic CO₂ Laser Wavelengths," *Appl. Opt.* **22**, 711 (1983). Erratum: *Appl. Opt.* **23**, 1302 (1984).
14. G. L. Loper, M. A. O'Neill, and J. A. Gelbwachs, "Water-Vapor Continuum CO₂ Laser Absorption Spectra Between 27°C and 10°C," *Appl. Opt.* **22**, 3701 (1983).
15. J. Hunderling, M. W. Sgrist, and F. K. Kneubuhl, "Laser Photoacoustic Spectroscopy of Water Vapor Continuum and Line Absorption in the 8 to 14 μm Atmospheric Window," *Infrared Phys.* **27**, No. 2, 63 (1987), private communication.
16. J. Nordstrom, M. E. Thomas, J. C. Peterson, E. K. Daman, and R. K. Long, "Effects of Oxygen Addition on Pressure Broadened Water Vapor Absorption in the 10 μm Region," *Appl. Opt.* **17**, 2724 (1978).
17. E. H. Christy and K. H. Faller, in *Second Joint Conference on Sensing of Environmental Pollutants*, Washington, DC, 10-12 Dec. 1975, paper 73.
18. R. R. Patty, G. M. Russwurm, W. A. McClenny, and D. R. Morgan, "CO₂ Laser Absorption Coefficients for Determining Ambient Levels of O₃, NH₃, and C₂H₄," *Appl. Opt.* **13**, 2850 (1974).
19. W. Schnell and G. Fischer, "Carbon Dioxide Laser Absorption Coefficients of Various Air Pollutants," *Appl. Opt.* **14**, 2058 (1975).
20. A. Mayer, J. Comera, H. Charpentier, and C. Jaussaud, "Absorption Coefficients of Various Pollutant Gases at CO₂ Laser Wavelengths; Application to the Remote Sensing of These Pollutants," *Appl. Opt.* **17**, 391 (1978).
21. J. Boscher, G. Schafer, and W. Wiesemann, "Gasfernanalyse mit CO₂-Laser," Report 01 TL 018A-AK/RT/WRT 2077, BF-R-63.616-4 by the Battelle-Institut, e.V., Frankfurt, F.R.G. (Mar. 1979).
22. U. Persson, B. Marthinsson, J. Johansson, and S. T. Eng, "Temperature and Pressure Dependence of NH₃ and C₂H₄ Absorption Cross Sections at CO₂ Laser Wavelengths," *Appl. Opt.* **19**, 1711 (1980).
23. W. Gengchen and K. Qinlin, "Detection of NO_x, C₂H₄ Concentrations by Using CO and CO₂ Lasers," in *Abstracts, Thirteenth International Laser Radar Conference*, Toronto, Canada, NASA Conf. Publ. 2431 (11-15 Aug. 1986), p. 259.
24. K. J. Brewer and C. W. Bruce, "Photoacoustic Spectroscopy of NH₃ at the 9-μm and 10-μm ¹²C¹⁶O₂ Laser Wavelengths," *Appl. Opt.* **17**, 3746 (1978).
25. L. T. Molina and W. B. Grant, "FTIR Spectrometer Determined Absorption Coefficients of Seven Hydrazine Fuel Gases: Implications for Laser Remote Sensing," *Appl. Opt.* **23**, 3893 (1984).
26. J. G. Hawley, R. E. Warren, D. D. Powell, D. E. Cooper, T. F. Gallagher, and B. K. Cantrell, "Remote and *in situ* Detection of Atmospheric Trace Gases - Infrared Spectroscopy for Ammonia," Final Report EA-4370 by SRI International for the Electric Power Research Institute (Dec. 1985).
27. L. S. Rothman *et al.*, "The HITRAN Databases: 1986 Edition," *Appl. Opt.* **26**, 15 Sept. (1987), in press.
28. S. A. Clough, F. X. Kneizys, E. P. Shettle, and G. P. Anderson, "Atmospheric Radiance and Transmittance: FASCOD2," in *Proceedings, Sixth Conference on Atmospheric Radiation*, Williamsburg, VA (American Meteorological Society, 1986).
29. S. A. Clough, AFGL; private communication (1987).
30. L. C. Bradley, K. L. SooHoo, and C. Freed, "Absolute Frequencies of Lasing Transitions in Nine CO₂ Isotopic Species," *IEEE J Quantum Electron* **QE-22**, 234 (1986).
31. S. A. Clough, F. X. Kneizys, R. Davies, R. Gamache, and R. Tipping, "Theoretical Line Shape for H₂O Vapor: Application to the Continuum," in *Atmospheric Water Vapor*, A. Deepak, T. D. Wilkerson, and L. H. Ruhnke, Eds. (Academic, New York, 1980).
32. S. A. Clough, F. X. Kneizys, L. S. Rothman, G. P. Anderson, and E. P. Shettle, "Current Issues in Infrared Atmospheric Transparency," presented at the International Meeting on Atmospheric Transparency for Satellite Applications, sponsored by U. Naples, Capri, Italy (Sept. 1986).
33. D. E. Burch and R. L. Alt, "Continuum Absorption by H₂O in the 700-1200 cm⁻¹ and 2400-2800 cm⁻¹ Windows," Report AFGL-TR 84-0128 to the Air Force Geophysics Laboratory (1984).
34. D. E. Burch, "Continuum Absorption by H₂O," Report AFGL-RT 81-0030 to the Air Force Geophysics Laboratory (1982).
35. F. X. Kneizys *et al.*, "Comparison of 8 to 12 Micrometer and 3 to 5 Micrometer C/F Transmissometer Data with LOWTRAN Calculations," Air Force Geophysical Laboratory Report AFGL-TR 84-0171 (1984).

36. D. R. Cutten, "Atmospheric Broadband Transmission Measurements and Predictions in the 8-13- μ m Window: Influence of Water Continuum Absorption Errors," *Appl. Opt.* **24**, 1085 (1985).
37. A. Ben-Shalom, A. D. Devir, S. G. Lipson, U. P. Oppenheim, and E. Ribak, "Absorption of Infrared Radiation by Atmospheric Water Vapor in the Region 4.3-5.5 and 8-13 Micon." in *Technical Digest, Topical Meeting on Optical Remote Sensing of the Atmosphere* (Optical Society of America, Washington, DC, 1985), paper TuC21.
38. R. G. Isaacs, W.-C. Wang, R. D. Worsham, and S. Goldenberg, "Multiple Scattering LOWTRAN and FASCODE Models," *Appl. Opt.* **26**, 1272 (1987).
39. R. L. Byer and M. Garbuny, "Pollutant Detection by Absorption Using Mie Scattering and Topographic Targets as Retroreflectors," *Appl. Opt.* **12**, 1496 (1973).
40. W. B. Grant, J. R. Bogan, and A. M. Brothers, "DIAL Signal Averaging," submitted to *Appl. Opt.* (1987).

Differential absorption lidar signal averaging

William B. Grant, Alan M. Brothers, and James R. Bogan

This paper presents experimental results using an atmospheric backscatter dual CO₂ laser differential absorption lidar (DIAL). It is shown that DIAL signals can be averaged to obtain an $N^{-1/2}$ dependence decrease in the standard deviation of the ratio of backscattered returns from two lasers, where N is the number of DIAL signals averaged, and that such a lidar system can make measurements of gas concentrations with a precision of 0.7% in absorbance over 75 m in a short measurement time when the signal strength is high. Factors that eventually limit the rate of improvement in the SNR, such as changes in the ratio of the absorption and/or backscatter at the two laser frequencies and background noise are discussed. In addition, it is noted that DIAL measurements made using hard-target backscatter often show departures from $N^{-1/2}$ dependence improvement in the standard deviation, because they are further limited by the combined effects of atmospheric turbulence and speckle, since the relative reproducibility of the speckle pattern on the receiver gives rise to correlations of the lidar signals.

I. Introduction

Two unresolved questions in the lidar field hinge on whether the standard deviation for the ratio (or for the derivative of the ratio's natural log) of the lidar returns at two laser wavelengths for the differential absorption lidar (DIAL) technique (see, e.g., Ref. 1) decreases as $N^{-1/2}$, where N is the number of lidar signals averaged, and, if so, what conditions eventually cause departures from $N^{-1/2}$ dependence. The most comprehensive set of data on this topic has been obtained and analyzed by researchers at the MIT Lincoln Laboratory. In that work, it was shown that backscatter from a stationary hard target exhibits a strong departure from $N^{-1/2}$ even for small N .²⁻¹⁰ However, results using atmospheric backscatter with a UV lidar system indicate that the $N^{-1/2}$ dependence does hold for small N ($N = 64$) when molecular (Rayleigh) scattering is significant,¹¹ and results using a visible wavelength lidar system gave results indicating only slight departures from $N^{-1/2}$, which were attributed by the authors to "fluctuations of backscatter conditions in the atmosphere".¹²

Two single-beam CO₂ coherent lidar systems have also been used previously to address signal averaging

with atmospheric backscatter. Fukuda *et al.*¹³ showed that the inverse relative root variance of the return signal intensity sampled over N pulses (or inverse of the standard deviation) for aerosol backscatter increased as $N^{1/2}$ for values of N up to 50. Hardesty¹⁴ showed that fluctuations in the returns from range elements at 1 and 2 km were highly correlated on a pulse-by-pulse basis (i.e., when the signal was low at one range, it was correspondingly low at the other range). However, it is unclear whether this result is due to fluctuations in laser pulse energy or frequency (which were not monitored) or to atmospheric extinction and backscatter changes.

To investigate the effect of signal averaging on the standard deviation of the DIAL ratio for measurements using atmospheric backscatter more thoroughly, we performed a series of experimental studies using the Mobile Atmospheric Pollutant Mapping System (MAPM), a dual CO₂ laser DIAL system utilizing heterodyne detection that was developed for measuring ambient and anthropogenic molecular trace species and aerosols and has been demonstrated for water vapor measurements.^{15,16} MAPM is perhaps one of the more difficult lidar systems to use for studying the variables affecting DIAL signal averaging, since the backscatter is solely from aerosols, signal fluctuations due to speckle are large, there is significant absorption by molecular species, and the signal quickly falls with range to levels below the electronic noise. Even so, there should be no loss of generality of the results, and the difficulties should help lead to a more complete understanding of the situation. Indeed the authors of Ref. 7 showed that there was no significant difference of the dependence with N for signal averaging between

When this work was done all the authors were with California Institute of Technology, Jet Propulsion Laboratory, 4800 Oak Grove Drive, Pasadena, California 91109. J. R. Bogan is now with University of Oregon, Physics Department, Eugene, Oregon 97403-1274.

Received 14 January 1987, in final form 8 January 1988.

0003-6915/88/101934-05\$02.00/0

© 1988 Optical Society of America

the direct and heterodyne detection cases when a stationary hard target was used to provide the backscatter.

II. CO₂ DIAL System Description

The MAPM CO₂ DIAL system includes two hybrid TEA CO₂ transmitter lasers which generate 10–20-mJ/pulse single longitudinal mode with low N₂ flow, and 30–60 mJ with normal N₂ flow and are typically operated at a 30-Hz prf with a 10-ms delay between the two laser firings. The gain-switched spike has a width of 270 ns FWHM; the tail varies from 230 ns FW with low N₂ flow to 1.5 μ s with normal flow. The transmitted beams have a divergence of 0.2 mrad, while the receiver field of view is 0.16 mrad. For the short-range measurements, a HgCdTe (PV) photomixer 0.15 mm on a side was used; for the long-range measurements, a detector 0.25 mm on a side was used. The beams of the two cw CO₂ lasers that serve as local oscillators are mechanically chopped so that only one beam is incident on the photomixer at a time. (This improves the ratio of the backscattered signal to electronic noise by a factor of 1.4–2.0.) The longitudinal coherence length of the lidar signal was measured to be 40 m, corresponding to the 270-ns gain-switched spike width. For long-range measurements (2–7 km) a signal proportional to the square root of the backscattered power is passed through a flat phase filter (0.4–2.5 MHz) to a transient digitizer, operated at a 5-MHz rate with 10-bit (7.8-bit effective) resolution. For short-range measurements (0.5–2 km), the filter is removed, and the signal is digitized at a 20-MHz rate. Several (typically 1–10) 1024-channel dual-pulse signals are summed in the computer before storing them on the disk to permit several hours of lidar operation before interrupting measurements for data archiving on magnetic tape.

iii. Data Analysis

A region before the lidar signals is used to estimate the electronic noise level, which is typically smoothed by combining several adjacent range bins. The average background level is subtracted from the data, and the remainders are squared. The residual background level is again subtracted to obtain values proportional to backscattered laser power. It is found that when only a small number of lidar signals (1–20) are used in this calculation, the background signal a few kilometers in range is somewhat above zero, possibly because there is a slope to the background, or because it is difficult to estimate properly the background using only a few signals. However, it was thought important to begin the analysis for small N and strong signals where the results would not be significantly affected.

The signals were normalized in one of two ways: for range resolved measurements, the data over most of the signal were used; for column-content measurements (for comparison with the results of Refs. 2–9), the data over a short range near the convergence peak were used. The ratios were formed in subsets of one up to some power of two pulse pairs, which were then

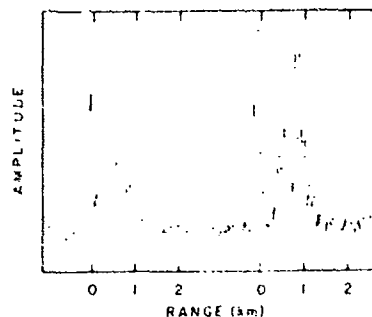


Fig. 1. Lidar signals from one pair of pulses for the lasers tuned to the 10P(14)/10P(20) laser line pair plotted on a linear scale. The peak on the left of each lidar signal is due to RFI from the laser. The transmitters and receiver are converged in the 0.3–1.5-km region, in which a number of peaks due to speckle are evident.

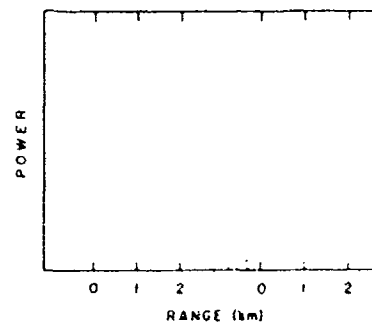


Fig. 2. Average squared lidar signals for 7614 pulse pairs taken as described in Fig. 1 plotted on a logarithmic scale. The extra feature on the left-hand trace from 1.5 to 2.5 km is also due to RFI.

added to form the final ratio for each power of two, and the standard deviation was calculated as a function of range for each power-of-two set. The derivative was calculated for a set of data fit by a quadratic function.

IV. Measurement Results

A number of horizontal DIAL measurements were made to study DIAL signal averaging. Some were made for both lasers tuned to the same line with the time delay between firing the two lasers either 100 μ s or 10 ms. For these cases, it was not expected that the backscatter ratio would change due to aerosol or gas concentration changes, although it might be possible for atmospheric turbulence to have some impact for the longer time delay. Other measurements were made with the lasers tuned to lines appropriate for the measurement of ambient atmospheric gases, such as water vapor, ozone, or ethylene. In these cases it would be possible for changes of concentrations during the measurement to change the ratio and thus affect the results. While not all the data sets exhibited $N^{-0.2}$ dependence for N approaching 1000, most did.

A single pair of lidar signals showing the speckle and electronic noise is shown in Fig. 1, while the average of 7614 lidar signals is shown in Fig. 2. The derivatives and standard deviation of the ratio normalized by the

mean value of the ratio for the data shown in Fig. 2 are shown in Figs. 3 and 4. In this case, the lasers were tuned to the 10P(14)/10P(20) laser line pair appropriate for ethylene. The region from 2 to 3 km for the 10P(14) laser is contaminated by RFI, which apparently originates from one of the pulsed lasers. Since only the data prior to that region are used in the analysis, it has no effect on this discussion. Note that the two averaged lidar signals are very smooth, indicating both a relatively uniform aerosol and gas distribution over 4 min as well as the ability to average out fluctuations due to speckle. The slight slope in the derivative is probably due to transmitter/receiver mismatch for the two lasers, which was not adjusted carefully, rather than the presence of ethylene. The rather uniform fluctuation of the derivative over the 1-km region analyzed is typical of heterodyne-detection lidar performance when the backscattered signal is significantly greater than the electronic noise. Note that the standard deviation of the ratio σ , in Fig. 5 for the data centered at 0.87 km decreases as $N^{-1/2}$ for N out to ~ 2048 , while σ , for the data centered at 1.5 km deviates from the $N^{-1/2}$ dependence after $N = 32$. [The estimation of the standard deviation becomes less certain after N reached one-tenth of the total number of signals averaged (see, e.g., Ref. 17).] The slowdown of the decrease in σ , for N greater than 32 for the latter is probably due to the increased importance of electronic noise in the signal compared to the case at shorter range. If the backscattered signal were considerably higher than was the case for these data (which could have been achieved at the range of 1.5 km by adjusting the transmitter/receiver overlap), the $N^{-1/2}$ dependence would probably have persisted further. The behavior of the latter data set is probably due to the greater impact of electronic noise due to the lower signal level. Note that the alternative explanation of changes in the differential backscatter or absorption is not apparent in most of our data, since such an effect would not always lead to a monotonic increase in with decreasing signal.

While not displayed here, the average fluctuation in the derivative increased from ± 0.007 for 7614 and 2476 pulse pairs, to ± 0.01 for 985 pulse pairs, ± 0.017 for 341 pairs, and ± 0.035 for 109 pairs. This trend indicates that the measurement precision is $\sim 1\%$ differential absorption for 1000 pulse pairs over a 75-m range when the signal is reasonably strong compared with the electronic noise. [This value corresponds to 1.5 ppm-m of ethylene [$\Delta\alpha = 33 \text{ atm}^{-1} \text{ cm}^{-1}$ (Ref. 15)].] These data took 30 s to acquire at 30 Hz but would take only 7 s at 150 Hz, the prf for which the lasers are rated. Steps are being taken to increase the acquisition rate of the data system. Note that measurement accuracy is also affected by other factors such as relative transmitter-receiver overlap for the two beams.

To obtain data that could be compared more directly to the results in Refs. 2-10, we also processed the data to give column content measurements between two ranges, as shown in Fig. 6. A region near 2.2 km was used to normalize the lidar returns, and regions near

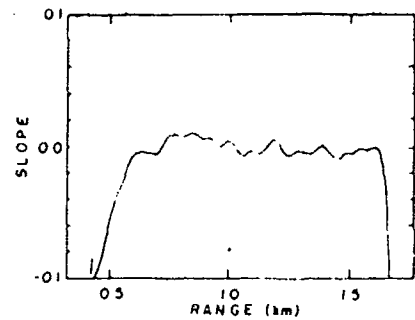


Fig. 3. 75-m derivatives of the logarithm of the ratio of the signals shown in Fig. 2.

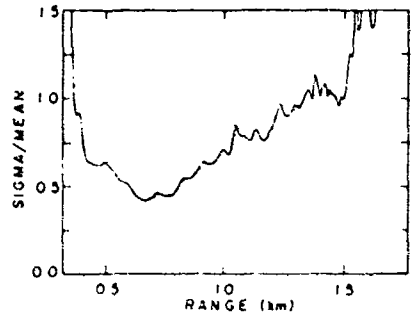


Fig. 4. Standard deviation for the data used in Fig. 2 taken 16 at a time.

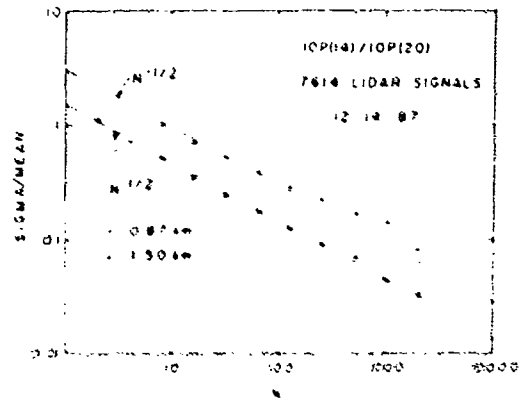


Fig. 5. Standard deviation of the ratio σ , vs N , the number of lidar pulse pairs averaged at a time, for the data shown in Fig. 2. The data were smoothed over 40 m and represent range-resolved calculations.

4.7 and 6.6 km were used as the limit on the range. The data were smoothed over 270 m. Note that the $N^{-1/2}$ dependence is obeyed reasonably well. These results show that there is a fundamental difference between hard-target backscatter and atmospheric backscatter DIAL signal averaging, as suggested by Grant.¹⁹

To illustrate graphically the effect of a changing gas concentration on the measurement results, data for the lasers tuned first to the 10R(18) line, and then to the 10R(12)-10R(18) line pair, were processed together

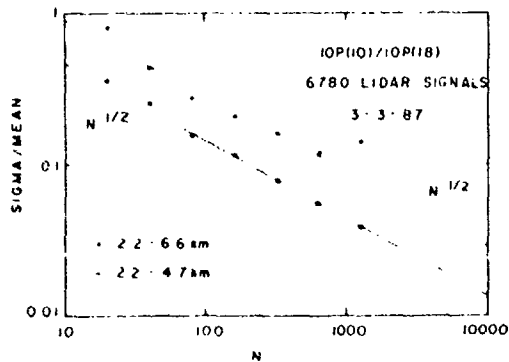


Fig. 6. Standard deviation of the ratio for 6789 pulse pairs taken 3 Mar. 1987 with the lasers tuned to the $10P(10)$ and $10P(18)$ lines. The data were smoothed over 270 m, and the ratios were normalized at a 2.2-km range; thus these data represent column-content calculations.

(Fig. 7). This gives results that are representative of the case where the gas concentration changes abruptly during the course of the measurement. This is admittedly an extreme case but serves to illustrate what could happen if the gas concentration [or alternatively the ratio of the backscatter due to changes in the aerosol/molecular scattering ratio in the UV or visible spectral region (see, e.g., Sasano *et al.*¹⁹ and Browell *et al.*²⁰)] changed somewhat during the measurement interval. Note in Fig. 6 that the departure from $N^{-1/2}$ dependence is immediate and strong.

V. Hard-Target Backscatter

Now let us reexamine the results in the literature for DIAL measurements using hard-target backscatter. In Refs. 2-9, it was shown that there are departures from $N^{-1/2}$ for DIAL signal averaging using stationary hard targets even for small N . The authors originally interpreted the results as being due to turbulence-induced correlation of the returns for the two lidar beams.³ In that work, they used a retroreflector at 2.7 km to provide the return signals and tuned both lasers to the $10P(22)$ line. For a pulse separation of 35 μ s, the signals were very highly correlated (correlation coefficient = 0.868). For a diffuse target the correlation coefficient dropped to 0.593, which is still reasonably high. In a later paper,⁵ it was suggested that over longer time periods gradual changes in the water vapor continuum absorption and aerosol extinction could also contribute to the observed departures from $N^{-1/2}$ behavior. However, since the $10P(28)$ and $10P(22)$ lines are both in spectral regions where water vapor has almost purely continuum absorption with nearly the same absorption coefficient (see, e.g., Ref. 16), it is not clear why water vapor should have an effect in this case. Also, in the MIT LL work the deviations for DIAL data for both lasers tuned to the same line (Ref. 3 for direct detection and Ref. 9, Fig. 6 for coherent detection) were as pronounced as for any of their data for the two lasers tuned to different lines [e.g., Ref. 6, where the $10P(28)$ and $10P(22)$ lines were used].

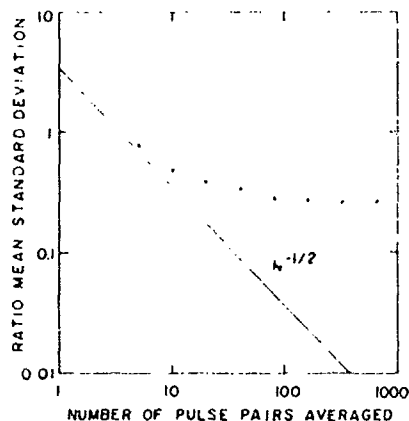


Fig. 7. Standard deviation of the ratio vs N for 5423 sets of data where the $10R(18)/10R(18)$ laser line pair was used for the first half of the data set and the $10R(12)/10R(18)$ pair for the second half.

These results are to be contrasted to our results using atmospheric backscatter, where presumably similar atmospheric changes were occurring and where the $N^{-1/2}$ dependence was typically found for N approaching 1000.

What appears to have occurred during the measurements reported in Refs. 2-9 is that, first, the speckle pattern on the receiver did not change significantly from pulse to pulse and, second, that the changes that did occur were correlated between the two lidar beams because they were fired in a short time compared with index-of-refraction changes in the atmosphere. Indeed, in Ref. 3, it is shown that for returns from a retroreflector, the lidar signals were highly correlated on a short-term (35- μ s) basis and partially correlated for longer times (50 ms). The authors of Refs. 2-9 show that the theory of autocorrelation (correlations between the signals measured for one laser) and covariance (correlations between the signals for the two lasers) describe their experimental results for a fixed hard target.³ The problems with speckle for hard-target backscatter are to be contrasted with the case for atmospheric backscatter: it has been shown experimentally that the aerosol decorrelation time in the 9-11- μ m spectral region is $\sim 1.3 \mu$ s.²¹ Thus, for atmospheric backscatter, the speckle pattern at the receiver for each pulse can be assumed to be totally uncorrelated with those for other lidar pulses. This independence from pulse to pulse is what allows atmospheric backscattered signals to be averaged to reduce the standard deviation with an $N^{-1/2}$ dependence, and the lack of same is what inhibits it in the hard-target backscatter case.

VI. Implications for DIAL Measurements

The data and theory discussed above have a number of implications for the design and utilization of DIAL systems. In general, the data which are averaged should be acquired in a short time compared to changes in concentrations of gases or distribution of aerosols that give differential absorptions or backscat-

ter at the pair of lines used in the measurement. If the concentration is changing rapidly, ratios should be calculated over short periods of time and then combined (see also Rye²² for a discussion of this point). Thus, for example, measurements from aircraft should be analyzed over ground track intervals no longer than the scale of variation in the ratio of backscatter.

For DIAL systems that use hard-target backscatter with direct detection, the lidar system should be designed to collect a large number of speckle lobes on the receiver to minimize the measurement uncertainty due to turbulence and speckle effects (see also a discussion of this point by Grant¹⁸ and Warren²³). In addition, it might be worthwhile to increase the time between pulses at the two wavelengths to a value much larger than 1 ms so that atmospheric turbulence can act differently on the two signals. Also, thought should be given to (a) using targets that have some rotational motion to them, since this will lead to increase the mutual independence of speckle patterns on the receiver²⁴; (b) using a multimode laser²⁵; or (c) scanning the hard target while trying to avoid the problems of differential spectral reflectance.^{26,27}

VII. Summary and Conclusion

It has been demonstrated experimentally that the data from a dual CO₂ DIAL system using atmospheric backscatter can be averaged with an $N^{-1/2}$ reduction in the standard deviation of the ratio for N of several hundred to a thousand for heterodyne detection, furthermore, that such a lidar system can be used to make measurements with a reasonably high precision. Deviations from $N^{-1/2}$ behavior were shown to be due to background noise, changes in the differential backscatter or differential absorption, or, in the case of stationary hard-target backscatter, the combined effects of atmospheric turbulence and speckle.

The author would like to thank R. T. Menzies, D. M. Tratt, R. M. Hardesty (NOAA-WPL, Boulder), D. K. Killinger (U. South Florida), B. J. Rye (U. Hull, U.K.), M. J. T. Milton (National Physical Laboratory, U.K.), and R. M. Schotland (U. Arizona) for helpful discussions. The work was supported by the U.S. Air Force and the National Aeronautics and Space Administration. The author specifically acknowledges support from the Air Force Engineering and Services Center, Tyndall AFB, FL, and the Kennedy Space Center.

References

1. W. B. Grant, "Laser Remote Sensing Techniques," in *Laser Spectroscopy and Its Applications*, L. J. Radziemski, R. W. Solarz, and J. A. Palmer, Eds. (Marcel Dekker, New York, 1987), p. 365.
2. N. Menyuk and D. K. Killinger, "Temporal Correlation Measurements of Pulsed Dual CO₂ Lidar Returns," *Opt. Lett.* **6**, 361 (1981).
3. D. K. Killinger and N. Menyuk, "Effect of Turbulence-Induced Correlation on Laser Remote Sensing Errors," *Appl. Phys. Lett.* **28**, 866 (1981).
4. D. K. Killinger and N. Menyuk, "Remote Probing of the Atmosphere Using a CO₂ DIAL System," *IEEE J. Quantum Electron.* **QE-17**, 1937 (1981).

5. N. Menyuk, D. K. Killinger, and W. E. DeFeo, "Laser Remote Sensing of Hydrazine, MMH, and UDMH Using a Differential-Absorption CO₂ Lidar," *Appl. Opt.* **21**, 2275 (1982).
6. N. Menyuk, D. K. Killinger, and C. R. Menyuk, "Limitations of Signal Averaging due to Temporal Correlation in Laser Remote-Sensing Measurements," *Appl. Opt.* **21**, 3377 (1982).
7. D. K. Killinger, N. Menyuk, and W. E. DeFeo, "Experimental Comparison of Heterodyne and Direct Detection for Pulsed Differential Absorption CO₂ Lidar," *Appl. Opt.* **22**, 682 (1983).
8. N. Menyuk and D. K. Killinger, "Assessment of Relative Error Sources in IR DIAL Measurement Accuracy," *Appl. Opt.* **22**, 2690 (1983).
9. N. Menyuk, D. K. Killinger, and C. R. Menyuk, "Error Reduction in Laser Remote Sensing: Combined Effects of Cross Correlation and Signal Averaging," *Appl. Opt.* **24**, 118 (1985).
10. D. K. Killinger and N. Menyuk, "Laser Remote Sensing of the Atmosphere," *Science* **235**, 57 (1987).
11. M. J. T. Milton and P. T. Woods, "Pulse Averaging Methods for a Laser Remote Monitoring System Using Atmospheric Backscatter," *Appl. Opt.* **26**, 2598 (1987).
12. W. Staehr, W. Lahmann, and C. Weitkamp, "Range-Resolved Differential Absorption Lidar: Optimization of Range and Sensitivity," *Appl. Opt.* **24**, 1950 (1985); and private communication.
13. T. Fukuda, Y. Matsuura, and T. Mori, "Sensitivity of Coherent Range-Resolved Differential Absorption Lidar," *Appl. Opt.* **23**, 2026 (1984).
14. R. M. Hardesty, "Measurement of Range-Resolved Water Vapor Concentration by Coherent CO₂ Differential Absorption Lidar," NOAA Tech. Memo WPL-118, Boulder, CO (Mar. 1984).
15. W. B. Grant, J. S. Margolis, A. M. Brothers, and D. M. Tratt, "CO₂ DIAL Measurements of Water Vapor," *Appl. Opt.* **26**, 3033 (1987).
16. W. B. Grant, "A Critical Evaluation of Water Vapor Absorption Coefficient Measurements in the 840 to 1100 cm⁻¹ Spectral Region," JPL Tech. Report 87-34 (15 Dec. 1987).
17. M. H. DeGroot, *Probability and Statistics* (Addison-Wesley, Reading, MA, 1975), p. 185.
18. W. B. Grant, "He-Ne and cw CO₂ Laser Long-Path Systems for Gas Detection," *Appl. Opt.* **25**, 709 (1986).
19. Y. Sasano, E. V. Browell, and S. Ismail, "Error Caused by Using a Constant Extinction/Backscattering Ratio in the Lidar Solution," *Appl. Opt.* **24**, 3929 (1985).
20. E. V. Browell, S. Ismail, and S. T. Shipley, "Ultraviolet Measurements of O₃ Profiles in Regions of Spatially Inhomogeneous Aerosols," *Appl. Opt.* **24**, 2827 (1985).
21. G. Ancellet and R. T. Menzies, "Atmospheric Correlation-Time Measurements and Effects on Coherent Doppler Lidar," *J. Opt. Soc. Am. A* **4**, 367 (1987).
22. B. J. Rye, "Power Ratio Estimation in Incoherent Backscatter Lidar: Heterodyne Receiver with Square Law Detection," *J. Clim. Appl. Meteorol.* **22**, 1599 (1983).
23. F. R. Warren, "Effect of Pulse-Pair Correlation on Differential Absorption Lidar," *Appl. Opt.* **24**, 3472 (1985).
24. J. H. Shapiro, "Correlation States of Laser Speckle in Heterodyne Detection," *Appl. Opt.* **24**, 1583 (1985).
25. P. H. Flamant, R. T. Menzies, and M. J. Kovacs, "Evidence for Speckle Effects on Pulsed CO₂ Lidar Signal Returns from Remote Targets," *Appl. Opt.* **23**, 1412 (1984).
26. W. B. Grant, "Effect of Differential Spectral Reflectance on DIAL Measurements Using Topographic Targets," *Appl. Opt.* **21**, 7290 (1982).
27. P. Vujkovic Crigin, D. Ignatijevic, I. Mendica, M. Sreckovic, I. Pantano, and P. I. Pippa, "Reflectance Spectra of Terrestrial Surface Materials at CO₂ Laser Wavelengths: Effects on DIAL and Geological Remote Sensing," *Appl. Opt.* **26**, 4723 (1987).